Nanoparticle-based Therapeutic Intervention of cAMP-mediated Immunosuppression in Malignant Melanoma

Dissertation
zur Erlangung des Grades
Doktor der Naturwissenschaften

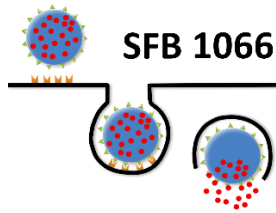am Fachbereich Biologie
der Johannes Gutenberg-Universität Mainz

JG|U

JOHANNES GUTENBERG UNIVERSITÄT MAINZ

Natascha Anna Maria Luther
geboren am 25.07.1987 in Wiesbaden

Mainz, Juli 2018

SFB 1066

JG|U UNIVERSITÄTSmedizin.
MAINZ

Aus der

Hautklinik und Poliklinik

der Universitätsmedizin Mainz

und dem

SFB 1066 - Sonderforschungsbereich

"Nanodimensionale polymer Therapeutika für die Tumortherapie"

der Universitätsmedizin Mainz, des Max-Planck-Institutes für Polymerforschung und der
Johannes Gutenberg-Universität Mainz

Dekan: ███████████████████

1. Berichterstatter: ███████████████

2. Berichterstatter: ███████████████

Tag der mündlichen Prüfung: 17.10.2018

Table of Content

Abstract

Malignant melanoma is a form of skin cancer which, even though it represents its least prevalent form, is accountable for 90% of skin cancer related deaths. While treatment of malignant melanoma up until Stage III promises great success, the same so far does not apply to Stage IV melanoma patients. In recent years, the introduction of novel treatment regiments has raised patients hopes for survival, but limited treatment success requires further development and combination of current and novel strategies.

Modifications in metabolic pathways such as the accumulation of the intracellular second messenger cyclic adenosine monophosphate (cAMP) have been recognized as a hallmark of cancer. In melanoma, elevated intracellular cAMP levels correlate with a greater metastatic potential and are believed to be the cause of regulatory T cell (Treg)-mediated immunosuppression in the tumour. In the present study, it was investigated how a micellar formulation of the adenylyl cylase inhibitor MDL-12, 330A hydrochloride made from the amphiphilic polypeptoid-*block*-polypeptide copolymer polysacrcosine-*block*-polyglutamatic acid benzylester (PSar-b-PGlu(OBn)) can be used to intervene in the formation of cAMP.

The *in vivo* testing of cAMP reduction using the adenylyl cyclase inhibitor MDL-12, 330A hydrochloride showcased its potential as a therapeutic agent by significantly reducing the tumour burden in the context of the murine B16F10-OVA melanoma model. A detailed examination of the tumour immune cell infiltrate following cAMP reduction revealed drastic quantitative and functional changes. Based on these results, a treatment strategy for complete tumour rejection was successfully established, combining cAMP reduction with punctual Treg removal.

In addition, the potential of azide functionalized polysarcosine brushes with polylysine backbone and polysarcosine side chains labelled with the fluorescent dye Alexa Fluor 647 and coupled with antigen and adjuvant could be demonstrated as a protective and therapeutic cancer vaccine. In order to completely eliminate tumour growth in a therapeutic approach, it would be interesting to try to combine it with cAMP reduction.

Zusammenfassung

Das maligne Melanom ist eine Form von Hautkrebs, die, obwohl sie die am wenigsten verbreitete Form ausmacht, für 90% der durch Hautkrebs verursachten Todesfälle ursächlich ist. Während die Behandlung des malignen Melanoms bis zum Stadium III große Erfolge verspricht, gilt dies bisher nicht für Pateinten im Stadium IV. In den letzten Jahren hat die Einführung neuer Behandlungsansätze die Hoffnung vieler Patienten auf ein Überleben geweckt. Begrenzte Behandlungserfolge machen eine Weiterentwicklung und Kombination von aktuell verwendeten und neuen Strategien notwendig.

Veränderungen in Stoffwechselwegen wie zum Beispiel die Anreicherung des intrazellulären Signalbotenstoffes zyklisches Adenosinmonophosphat (cAMP) sind unter anderem ein Kennzeichen von Krebs. In Melanomen korrelieren erhöhte intrazelluläre cAMP Spiegel mit einem größeren metastatischen Potential und sind vermutlich für die durch regulatorische T Zellen (Treg)-vermittelte Immunsuppression im Tumor mit verantwortlich. In der vorliegenden Arbeit wurde untersucht, wie unter Verwendung mizellarer Formulierungen des Adenylylzyklaseinhibitors MDL-12, 330A Hydrochloride bestehend aus dem amphiphilen polypeptoid-*block*-polypeptide Copolymer Polysacrcosine-*Block*-Polyglutaminsäure-benzylester (PSar-b-PGlu(OBn)) in die cAMP-Bildung in Melanomen eingegriffen werden kann.

Die *in vivo* Erprobung der cAMP-Absenkung durch die Verwendung des cAMP Inhibitors MDL-12, 330A Hydrochloride zeigte sein Potenzial als Therapeutikum, indem es im Kontext des murinen B16F10-OVA Melanommodells die Tumorlast signifikant reduzieren konnte. Eine detaillierte Untersuchung des Tumorimmunzellinfiltrates nach cAMP Absenkung zeigte drastische quantitative und funktionelle Veränderungen. Basieren auf diesen Ergebnissen wurde erfolgreich eine Behandlungsstrategie zur kompletten Abstoßung des Tumors etabliert, welche die cAMP Absenkung mit einer punktuellen Entfernung der Tregs verband.

Darüber hinaus konnte das Potential von azid-funktionalisierten Polysarkosinbürsten mit Polylysinrückrat und Polysarkosinseitenketten, die mit dem Fluoreszenzfarbstoff Alexa Fluor 647 markiert und mit Antigen und Adjuvans gekoppelt wurden, als protektiver und therapeutischer Krebsimpfstoff aufgezeigt werden. Um das Tumorwachstum in einem therapeutischen Ansatz vollständig zu eliminieren, wäre es interessant zu versuchen, diesen mit der cAMP-Absenkung zu kombinieren.

1. Introduction

1.1 Melanoma

Malignant melanoma is a form of cutaneous skin cancer which mainly affects Non-Hispanic Caucasians. Even though melanoma represents its least prevalent form, it is accountable for 90% of skin cancer related deaths (Garbe, C. *et al.*, 2016). It develops from melanocytes, pigment producing cells derived from the neural crest, which are located at the bottom of the epidermis and hair follicles (Chichorek, M. *et al.*, 2013). Apart from genetic predispositions the greatest exogenous risk factor is an early and frequent exposure to ultraviolet (UV) radiation (Garbe, C. *et al.*, 2016).

1.1.1 Historical Background

Melanoma were first mentioned in the 5th century by Hippocrates of Cos and later by Rufus of Ephesesus. The first physical evidence originates from metastases in about 2400 year old Pre-Columbian mummies found in Peru (Urteaga, O. & Pack, G.T., 1966; Rebecca, V.W. *et al.*, 2012). From the mid-late 17th century on "fatal black tumours with metastases and black fluid in the body" would frequently get mentioned and referenced in the European medical literature (Rebecca, V.W. *et al.*, 2012). It was, however, not until 1806 that Rene Laennec would coin the term melanose after realizing that melanoma was a distinct disease (Laennec, R.T.H., 1812; Rebecca, V.W. *et al.*, 2012). In 1820 and 1857 Dr. William Norris published his detailed observations on melanosis. He reported that most of his patients were fair skinned, suggested a link between melanoma and environmental factors, described the heritable nature of some melanomas and noted their widespread metastatic potential. He also concluded that any medical intervention would become obsolete the further the disease had progressed (Norris, W., 1820; Norris, W., 1857; Rebecca, V.W. *et al.*, 2012). The pathologist Sir Robert Carswell would later be credited to have identified the disease as melanoma (Carswell, R., 1838; Rebecca, V.W., *et al.*, 2012).

1.1.2 Diagnosis and Staging

The initial diagnosis of melanoma is still today mainly based on a combination of a dermatologists trained eye and dermoscopy (Garbe C. *et al.*, 2016). It has, however, been greatly guided by two independently proposed melanoma classification systems suggested by

Wallace Clark in 1969 (Clark Jr, W.H., 1969) and Alexander Breslow in 1970 (Breslow, A., 1970). The recommendations regarding melanoma staging are continuously updated by the American Joint Commission on Cancer (AJCC) and nowadays also do incorporate genetic data. At present the depth of the tumour (Breslow's depth), a guideline for the recommended excision margin of a tumour, the level of ulceration, the tumour division rate as well as the presence of microsatellites are essentially contributing towards tumour staging (Garbe, C *et al.*, 2016). Clark's level, the level of anatomical invasion, has become less significant and is currently only applied to melanoma with a Breslow depth smaller than 1 mm or an undetermined mitotic rate (Balch, C.M. *et al.*, 2009).

The discovery of a potential lesion immediately leads to its removal and staging. Detection of certain characteristic proteins such as the S-100 protein, HMB45 or Melan-A strongly add towards the diagnosis of melanoma (Garbe, C. *et al.*, 2016). The presence of metastases is evaluated by assessing the levels of lactate dehydrogenase (LDH) (Balch, C.M. *et al.*, 2009), lymph node and sentinel lymph node biopsies and by the different available imaging techniques. The rate of survival for patients with a melanoma up until Stage III are relatively high and is significantly increased by adjuvant Interferon-alpha (IFN-α) therapy. Stage IV melanoma with solitary metastases are often still treated using a curative approach which includes radiation therapy. A palliative approach, systemic therapy, is however chosen as soon as multiple metastases have been detected (Figure 1.1) (Keilholz, U. *et al.*, 2014).
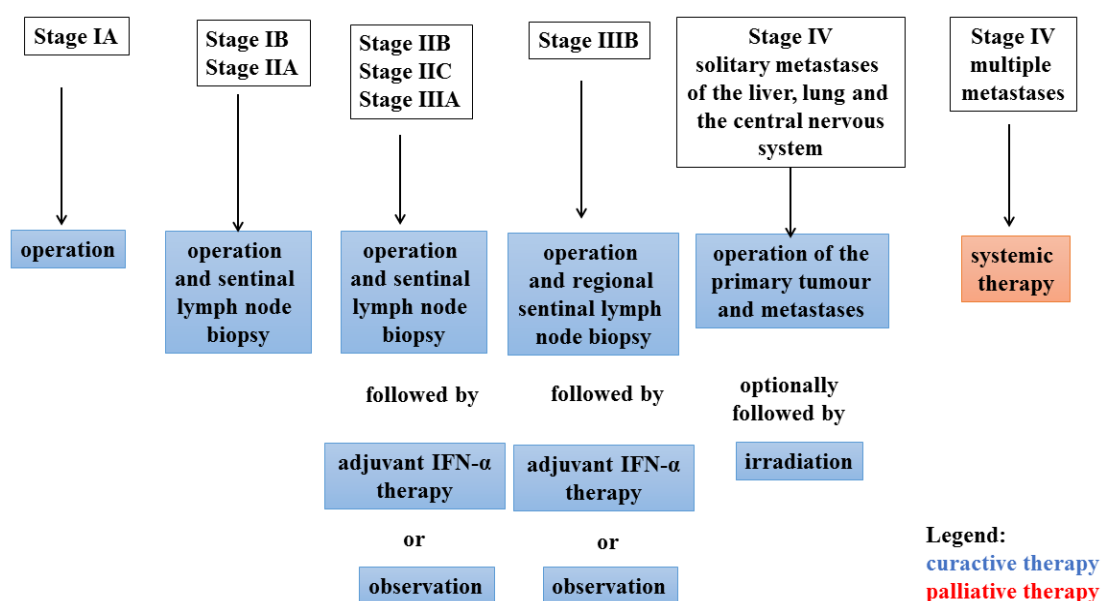
Figure 1.1   Guidelines for the primary therapy of malignant melanoma.
The discovery of a potential lesion during an examination of a dermatologist leads to its immediate removal and staging based on national recommendations, for example by the American Joint Commission on Cancer (AJCC). Based on the staging, guidelines for the treatment of a patient have been suggested. A curative approach is followed up until Stage IIIB which includes operation, lymph node biopsy, adjuvant Interferon-alpha (IFN-α) therapy and observation. Stage IV melanoma patients with solitary metastases are often still treated using a curative approach which includes radiation. A palliative approach, systemic therapy, is chosen as soon as Stage IV melanoma with multiple metastases have been detected. Redrawn from Keilholz, U. *et al.*, 2014.

1.1.3   Systemic Therapy of Stage IV Melanoma Patients

Mandatory molecular analysis must be performed on metastases or if not otherwise feasible the primary tumour of Stage IV melanoma patients considered for systemic therapy. Testing is done regarding the most common mutations in cutaneous melanoma: BRAF V600E or V600K, NRAS, CKIT and NF1. Based on the results of the molecular analysis a seemingly appropriate treatment regimen can be selected (Figure 1.2) (Keilholz, U. *et al.*, 2014). Between 2011 and 2013, the approval and introduction of in total four novel drugs into the clinic, Ipilimumab, Vemurafenib, Dabrafenib and Trametinib, greatly varied the therapeutic options and made it easier to opt for an alternative treatment scheme in case of excessive side effects or resistance. Ipilimumab, a human Immunoglobulin G subclass 1 (IgG1) monoclonal antibody and at present most commonly used medication blocks the cytotoxic lymphocyte associated antigen 4 (CTLA-4). Vemurafenib and Dabrafenib however act against BRAF while Trametinib inhibits MEK1/2. In case of CKIT mutations, tyrosine-kinase inhibitors such as Imatinib are used. NRAS specific inhibitors are currently under development. The first Programmed Death Receptor-1 (PD-1) and Programmed Death Receptor-1 Ligand (PD-1L) antibodies were approved in 2014 and are expected to significantly alter the currently recommended treatment strategies. Nivolumab and Pembrolizumab act by blocking the interaction of PD-1 on immune cells and PD-L1, a ligand commonly expressed on tumours, resulting in increased immune activation including elevated tumour cell killing by cytotoxic T lymphocytes (CTLs) (Stadler, S. *et al.*, 2015). Recently the combination of both Ipilimumab and Nivolumab has been advocated due to reports of favourable response rates regardless of a patient's mutational status (Wolchok, J.D., *et al.*, 2013; Sznol, M. *et al.*, 2014; Stadler, S. *et al.*, 2015).
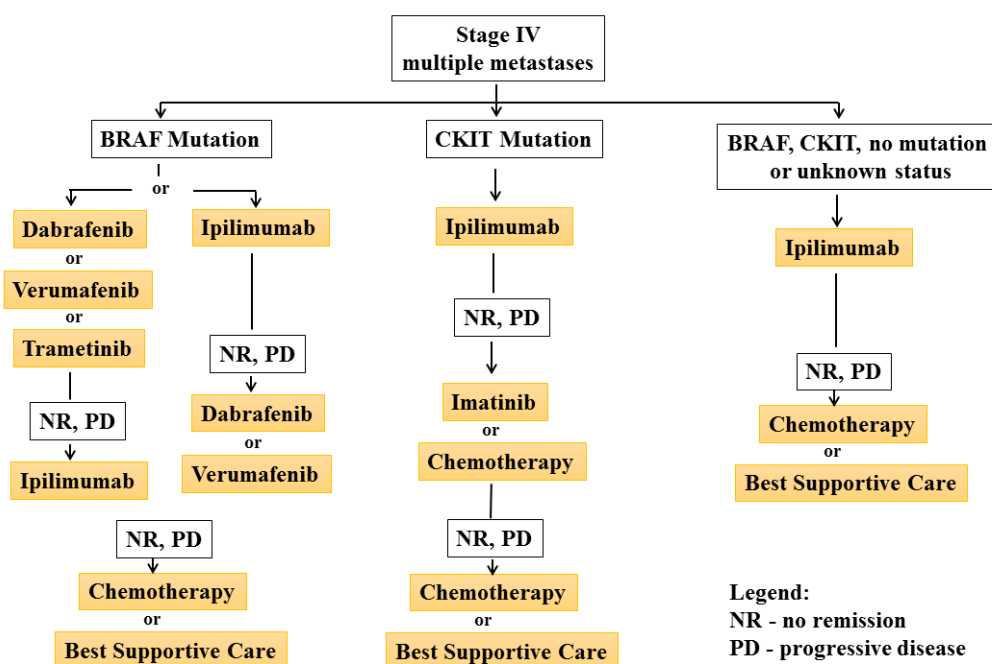
Figure 1.2   Guidelines for the treatment of patients with Stage IV melanoma.

The discovery of a potential lesion during an examination of a dermatologist lead to its immediate removal and staging based on national recommendations, for example by the American Joint Commission on Cancer (AJCC). At present the depth of the tumour (Breslow`s depth), the tumour division rate, the level of ulceration, the presence of microsatellites but also genetic data are considered during staging. A palliative approach, systemic therapy, is chosen as soon as Stage IV melanoma with multiple metastases have been detected. Treatment guidelines have been suggested based on the mutational status and the response to therapy by Stage IV melanoma patient's. Redrawn from Keilholz, U. *et al.*, 2014.

1.1.4   The Future of Systemic Therapy of Stage IV Melanoma Patients

The combination of the currently available therapeutics has been strongly advocated and a great number of trials are ongoing. Novel strategies currently investigated include Indoleamine 2,3-dioxygenase-1 (IDO1) inhibitors as well as Lymphocyte-activation gene-3 (LAG-3) inhibitors. IDO1 is an enzyme responsible for the degradation of tryptophane, an amino acid overexpressed by a great number of tumours, partially responsible for a mindered T cell response. LAG-3 is up-regulated on activated T cells, regulates T cell activation and homeostasis, engages Dendritic Cells (DCs) and influences the secretion of the immunosuppressive cytokines Interleukin 10 (Il-10) and Transforming growth factor beta (TGF-β). Inhibition of any two of these molecules have been suggested to ultimately help to revoke immune suppression. Current and novel strategies must be carefully investigated, and their interactions need to be closely monitored to

ultimately come up with a regimen that promises a long-term response in case of Stage IV melanoma (Koller, K.M. *et al.*, 2016).

1.2 Cyclic Adenosine Monophosphate (cAMP) and Melanoma

1.2.1 cAMP

Cylic adenosine monophosphate (cAMP) is an intracellular second messenger which was first discovered in 1957 by Earl Sutherland and colleagues (Berthet, J. *et al.*, 1957). It is ubiquitously expressed in a wide range of organisms and affects a variety of functions through its five target proteins: protein kinase A (PKA), exchange proteins directly activated by cAMP (EPACs), Popeye domain-containing proteins (POPDCs), cyclic nucleotide receptors involved in sperm function (CRISs) or cyclic nucleotide-gated ion channels (CNGs) (Amunjela, J.N. & Tucker, S.J., 2016). Amongst others these processes include cellular growth, differentiation, proliferation, Ca^{2+}-dependent signalling, reproduction, cardiac function, vision, inflammation, as well as tumour development (Azevedo, M.F. *et al.*, 2014).

The cAMP signalling cascade is initiated by extracellular cues such as hormones or neurotransmitters. It leads to the stimulation of the G_s protein-coupled receptor (G_sPCR) at the plasma membrane or the endosomal compartment and the exchange of guanosine diphosphate (GDP) for guanosine-5'-triphosphate (GTP). Activated G proteins then in turn associate with adenylyl cyclases (ACs) which leads to the conversion of adenosine triphosphate (ATP) to cyclic adenosine monophosphate (cAMP). Upon contact with the appropriate target, cAMP gets degraded by phosphodiesterases (PDE) to 5'adenosine monophosphate-activated protein kinase (5'AMP) (Figure 1.3) (Lefkimmiatis, K. & Zaccolo, M., 2014).

Not only the great number of cAMP targets but also the differential expression and diversity of effector proteins adds towards the complexity of the cAMP signalling cascade (Azevedo, M.F. *et al.*, 2014; Sadana, R. & Dessauer, C.W., 2009). The conversion of ATP to cAMP is regulated by in total ten adenylyl cyclases, nine transmembrane adenylyl cyclases (tAC1-9) and one soluble adenylyl cyclase (sAC10) (Lefkimmiatis, K. & Zaccolo, M., 2014). Furthermore, eight out of a total of eleven phosphodiesterases (PDE), three cAMP selective (PDE4, PDE7 and PDE8) and five cAMP and cyclic guanosine monophosphate (cGMP) responsive (PDE1, PDE2, PDE3, PDE10 and PDE11) phosphodiesterases, are involved in cAMP degradation (Azevedo, M.F. *et al.*, 2014) as well as the creation of signalling compartments as small as 300 nm (Surdo,

N.C., *et al.*, 2017, Musheshe, N. *et al.*, 2017). The contribution of each adenylyl cyclase and phosphodiesterase to individual processes has yet to be determined. So far however, their spatiotemporal distribution across signalling compartments represented by lipid rafts needs to be resolved (Cooper, D.M.F. *et al.*, 2005; Seifert, R. *et al.*, 2012).
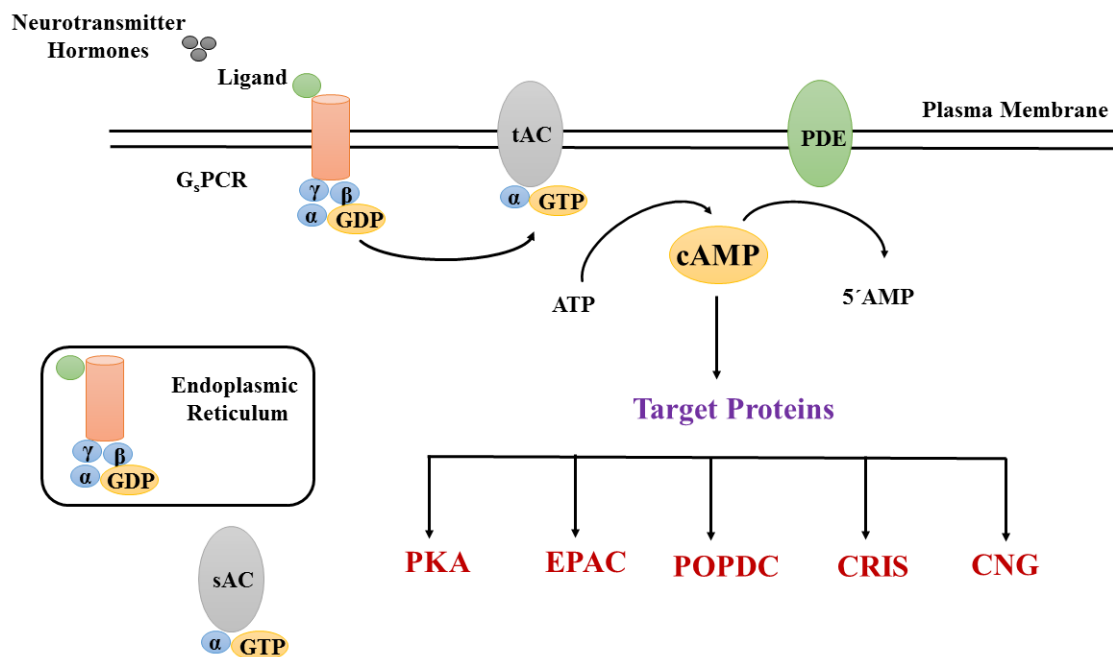
Figure 1.3   The cAMP signalling pathway.
The cAMP signalling pathway is initiated by extracellular cues, for example hormones or neurotransmitters. It leads to the stimulation of the G protein-coupled receptor (G$_s$PCR) at the plasma membrane or the endosomal compartment and the exchange of guanosine diphosphate (GDP) for guanosine-5'-triphosphate (GTP). Activated G proteins associate with transmembrane adenylyl cyclases (tACs) or soluble adenylyl cyclases (sACs) which leads to the conversion of adenosine triphosphate (ATP) to cyclic adenosine monophosphate (cAMP). Phosphodiesterases (PDEs) initiate the degradation of cAMP to 5' adenosine monophosphate-activated protein kinase (5'AMP). cAMP acts upon five effector proteins: protein kinase A (PKA), exchange proteins directly activated by cAMP (EPACs), Popeye domain-containing proteins (POPDCs), cyclic nucleotide receptors involved in sperm function (CRISs) or cyclic nucleotide-gated ion channels (CNGs). Adapted from: Amujela, J.N. & Tucker, S.J., 2016 and Musheshe, N. *et al.*, 2017.

1.2.2   cAMP and the Skin

The skin is one of the largest mammalian organs which protects the remainder of the body from the environment while carrying out important immunological and metabolic functions (Di Meglio, P. *et al.*, 2011). Protection against UV radiation, a major risk factor for melanoma, is modulated by pigmentation and represents one of the most important protective mechanisms

critically dependent on cAMP (Kondo, T. & Hearing, V.J., 2011). Keratinocytes and melanocytes, located at the bottom of the epidermis and hair follicles, together form the so called epidermal melanin unit. Melanocytes, originally derived as melanoblasts from the neural crest, harbour organelles called melanosomes where pigment, also referred to as melanin, is produced. Upon association with keratinocytes, the skins main barrier against environmental damage, differentially shaped melanosomes start to determine skin colour and play a critical role in photoprotection (Slominski, A. *et al.*, 2004, Costin, G.E. & Hearing, V.J. *et al.*, 2007).

While skin colour is primarily determined by a person's genetic traits, the mixture of two chemically distinct forms of melanin, namely the black-to-brown eumelanin and the yellow-to-reddish pheomelanin, are responsible for differential pigmentation (Costin, G.E. & Hearing, V.J. *et al.*, 2007). Melanin synthesis starts when L-Tyrosine is converted to levodopa (L-DOPA) and subsequently to L-Dopaquinone (DOPAquinone) by their oxidation through the tyrosinase enzyme (TYR). At that stage the pathway starts to diverge and tyrosine-realted-protein-1 (TYRP1) as well as tyrosine-related-protein-2 (TYRP2) become the main drivers for the formation of highly polymerized black and brown eumelanin respectively. Glutathion or cystine however become important factors in the synthesis of the photolabile sulfur containing less polymerized yellow-to-reddish pheomelanin. While eumelanin is an effective UV blocker, pheomelanin renders a person susceptible to damage by UV radiation and reactive oxygen species (ROS) (Slominski, A. *et al.*, 2004; Costin, G.E. & Hearing; V.J. *et al.*, 2007; Konto; T. & Hearing, V.J. *et al.*, 2011; Garcia-Borron, J.C. *et al.*, 2014).

Melanin synthesis itself, is mainly driven by the G protein-coupled melanocortin-1 receptor (MC1R), which is primarily expressed in melanocytes but also in keratinocytes, fibroblasts, and immune cells (Nasti, T.H. & Timares, L., 2015). It is stimulated by the α-Melanocyte-stimulating hormone (α-MSH) as well as the adrenocorticotropic hormone (ACTH) which leads to the activation of adenylyl cyclases and the conversion of ATP to cAMP. PKA in turn initiates the binding of the cAMP response element binding protein (CREB) to the cAMP response element (CRE) situated in the microphthalmia-associated transcription factor (MITF) (Rodriguez, C.I. & Setaluri, V., 2014; Nasti, T.H. & Timares, L., 2015; Herraiz, C. *et al.*, 2017). It's up-regulation then leads to eumelanogenesis due to the increase of TYR, TYRP1 and TYRP2 (Garcia-Borron, J.C. *et al.*, 2014). Pheomelanogenesis is a consequence of the inhibition of the MC1R by the agouti protein (Herraiz, C. *et al.*, 2017). MITF is also closely associated to the Ras-Raf-MEK-ERK pathway, which regulates melanogenesis by the down

regulation of the activity of the transcription factor (Figure 1.4) (Chang, T.S., 2012, Nardin; C.A. *et al.*, 2014; Wellbrock, C. & Arozarena, I., 2015).
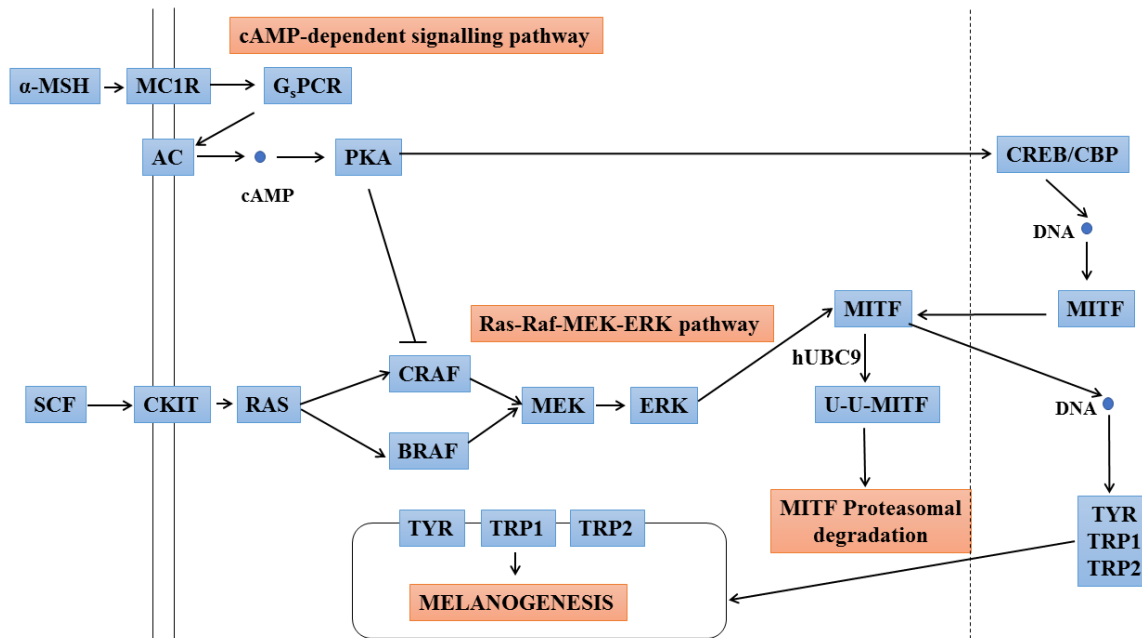
Figure 1.4   Signalling pathways involved in the regulation of melanogenesis.
Melanocortin-1 receptor (MC1R) is a G protein-coupled receptor (G_sPCR) which is stimulated by α-Melanocyte-stimulating hormone (α-MSH). Its activation leads to the stimulation of adenylyl cyclases (ACs) and the conversion of adenosine triphosphate (ATP) to cyclic adenosine monophosphate (cAMP). The cAMP effector protein protein kinase A (PKA) initiates the binding of the cAMP response element binding site (CREB) to the cAMP response element (CRE) situated in the microphthalmia-associated transcription factor (MITF). Its upregulation exerts its effect on the tyrosine enzyme (TYR), the tyrosine-related-protein-1 (TYRP1) and tyrosine-related-protein-2 (TYRP2) and the initiation of melanogenesis. MITF is also closely associated to the Ras-Raf-MEK-ERK pathway, which regulates melanogenesis by the down regulation of the activity of the transcription factor. BRAF: serine/threonine-protein kinase B-Raf; CKIT: mast/stem cell growth factor receptor; CBP: CREB-binding protein; CRAF: RAF proto-oncogene serine/threonine-protein kinase; DNA: deoxyribonucleic acid; ERK: extracellular signal-regulated kinase; hUBC9: ubiquitine-conjugating enzyme UBC9; MEK: mitogen-activated protein kinase kinase; RAS: family of related proteins that belongs to the class of small GTPases, SCF: stem cell factor; U-U-MITF: ubiquinated MITF. Redrawn and adapted from: Chang, T.S., 2012 and Nardin, C.A. *et al.*, 2014.

1.2.3   cAMP and Melanoma

cAMP is a highly complex signalling cascade which has a major significance in skin pigmentation and its protection against UV radiation (Costin, G.E. & Hearing, V.J., 2007).

Disruption of this pathway due to aberrant signalling can easily result in the initiation of melanoma (Rodriguez, C.I. & Setaluri, V., 2014). A link between these two processes was established when it was noted that melanoma do indeed generate elevated intracellular cAMP levels which also correlates with an increased metastatic potential (Shepard, J.R. *et al.*, 1984; Ito, A. *et al.*, 2000; Raskovalova, T. *et al., 2*007; Villares, G.J. *et al.,* 2009). Its repression with the help of the adenylyl cyclase inhibitor MDL-12, 330A hydrochloride has previously been confirmed in the human melanoma cell line MaMel91 (Birke, A. *et al.*, 2014) and was reported to revoke regulatory T cell (Treg) induced immunosuppression (Klein, M. *et al.*, 2012).

The soluble AC10 has been closely linked to hyperproliferative skin disorders which includes skin cancer. It is upregulated in the nuclei of keratinocytes which has previously been linked to activated CREB (Zippin, J.H. *et al.*, 2010, Schmid, A. *et al.*, 2014). Furthermore, it has been noted that upon the acquisition of invasive properties, sAC10 is lost from the nucleus in the context of malignant melanoma (Zippin, J.H. *et al.*, 2004, Schmid, A. *et al.*, 2014). tAC1-9 are indirectly associated with malignant melanoma (Rodriguez, C.I. & Setaluri, V., 2014). While MC1R polymorphisms are essential for the variation of pigmentation (Garcia-Borron, J.C. *et al.*, 2014), unfavourable mutations in MC1R (Scherer, D. & Kumar, R., 2010) or the Ras-Raf-MEK-ERK pathway contribute towards the initiation of melanoma (Wang, A.X. & Qi, X.Y., 2013).

Out of the five cAMP target proteins, only three have been associated with various forms of cancer (Amunjela, J.N. & Tucker, S.J., 2016). While in melanoma cells EPACs have been reported to increase migration (Balijinnyam, E. *et al.*, 2009), they have also been suggested to be involved in transcriptional repression (Lakhter, A.J. & Naidu, S.R., 2017). PKA is an essential element in the regulation of melanogenesis and its crosstalk with the Ras-Raf-MEK-ERK pathway (Rodriguez, C.I. & Setaluri, V., 2014; Nasti, T.H. & Timares, L., 2015; Herraiz, C. *et al.*, 2017; Chang, T.S., 2012, Nardin; C.A. *et al.*, 2014; Wellbrock, C. & Arozarena, I., 2015). Its expression in metastatic melanoma is significantly increased (Mantovani, *et al.*, 2008; Amujela, J.N. & Tucker, S.J., 2016) as it targets the cellular transcription factor CREB (Delghandi, M.P. *et al.*, 2005; Amujela, J.N. & Tucker, S.J., 2016). POPDCs, the most recently uncovered cAMP effector proteins, have been associated with several types of cancer. So far however no specific link to melanoma has been reported (Amujela, J.N. & Tucker, S.J., 2016).

Certain PDEs have also been associated with melanoma development and progression. PDE2 has been suggested to inhibit growth and invasion in melanoma (Hiramoto, K. *et al.*, 2014). In

the human malignant melanoma pseudomyxoma peritonei cell line a point mutation was found in the PDE2A (Morita, H. *et al.*, 2013, Azevedo, M.F. *et al.*, 2014). PDE4 has been suggested to play a major role in melanocyte biology (Rodriguez, C.I. & Setaluri, V., 2014). Various kinds of cancer, which includes melanoma, have however also been found to have homozygous microdeletions associated with elevated PDE4 expression (Lin, D.C. *et al.*, 2013; Azevedo, M.F. *et al.*, 2014; Rodriguez, C.I. & Setaluri, V., 2014). Furthermore, both PDE2 and PDE4 have been linked to immune cell functions. While PDE2 drives the conversion of monocytes to macrophages (Bender, A.T. *et al.*, 2004; Azevedo, M.F. *et al.*, 2014), PDE4 is crucial for the activation of T cells and other inflammatory cells (Abrahamsen, H. *et al.*, 2004; Azevedo, M.F. *et al.*, 2014).

1.3   Nanoparticles in Tumour Therapy

1.3.1   Nanoparticles

Nanoparticles or ultrafine particles have been defined by the International Organization for Standardization (ISO) according to ISO/TS 80004-2:2015. They are identified as having a length range approximately from 1 to 100 nm as well as three external dimensions orthogonal to each other which do not significantly differ in size (ISO, 2015).

Assessments of nanoparticles have furthermore been issued by the Australian National Industrial Chemical Notification and Assessment Scheme (NICAS) (NICAS, 2010), Health Canada (Health Canada, 2011), the United States Food and Drug Administration (US-FDA, 2014) and the Scientific Committee on Emerging and Newly Identified Health Risks (SCENIHR) of the European Commission (SCENIHR, 2010).

1.3.2   Historical Background

Nanoparticles have been used as far back as the 4th century BC for the decoration of a Roman glass cage cup, the Lycurgus Cup, made of dichroic glass (Krukemeyer, M.G. *et al.*, 2015) or as material for the legendary 17th century Damascus sword (Reibold, M *et al.*, 2006; Krukemeyer, M.G. *et al.*, 2015). Only in 1959, following the development of the Ultramicroscope in 1902 by Richard Zsigmond and Henry Siegendorf and the detection of nm sized structures, the invention of the Transmission Electron Microscope (TEM) in 1931 by Max Knoll and Ernst Ruska and the development of the Field-Emission Microscope (FEM) in 1936

by Erwin Müller, the physicist Richard Feynman initiated the though process on nanotechnology (Feynman, R.P., 1960; Krukemeyer, M.G., *et al.*, 2015). Even before Norio Tanigushi had coined the term nanotechnology in 1974 (Tanigushi, N., 1974: Krukemeyer, M.G. *et al.*, 2015), nanoparticles for targeted drug delivery had already been devised in the laboratory of Paul Speiser by the end of the 1960s (Kreuter, J., 2007; Krukemeyer, M.G. *et al.*, 2015).

Direct visualization of nm sized structures became possible when in 1981 the Scanning Tunnelling Microscope (STM) was invented by both Gerd Binning and Heinrich Rohrer. Only a few years later Gerd Binning would in 1986 also devised the Atomic Force Microscope (AFM) (Krukemeyer, M.G. *et al.*, 2015). In the same year, K. Eric Drexler, published the first textbook on nanotechnology (Drexler, K.E., 1986; Krukemeyer, M.G. *et al.*, 2015). The first textbook on nanomedicine was released in 1999 by Robert A. Freitas (Freitas Jr., R.A., 1999; Krukemeyer, M.G. *et al.*, 2015). Since then the continuous refinement of techniques and equipment pertaining to nanotechnology has significantly aided its advance. Nanotechnology does nowadays not only find applications in medicine but also in electronics, transportation, space exploration as well as energy and environmental technology (Nikalje, A.P., 2015).

1.3.3   Nanoparticles and Cancer Therapy

Cancer therapeutics such as for example chemotherapeutics, are extremely aggressive agents that are generally administered systemically in high doses by intravenous injection. Initially elevated drug plasma levels, however, get quickly cleared as a result of drug breakdown and excretion. Nonselective administration as well as high drug dosages cause serious side effects which one hopes to overcome by alternative drug formulations. Nanoparticles represent one strategy with which one aspires to achieve a prolonged and selective delivery of increased dosages of therapeutics. Furthermore, it represents a promising platform to make anticancer drugs with unfavorable physicochemical and biopharmaceutical properties available for therapy (Berciano-Guerrero, M.A. *et al.*, 2014).

Already in 1995, Doxil® (approved and marketed as Caelyx in Europe since 1997), a liposomal formulation of doxorubicine became one of the first nanoparticle-based therapeutics approved by the Food and Drug Administration (FDA) for the treatment of the human immunodeficiency virus (HIV) associated Kaposi's sarcoma. Since then a vast number of different nanoparticle-based formulations for cancer therapy have been approved or are being investigated in

numerous ongoing clinical trials (Ryan, S.M & Brayden, D.J., 2014). These include: liposomes, niosomes, dendrimers, polymeric micelles, polymeric nanoparticles, solid lipids, magnetic nanoparticles, inorganic nanoparticles, quantum dots, carbon nanotubes, human albumin as well as polymersomes (Berciano-Guerrero, M.A. *et al.*, 2014). Next to drug delivery, nanoparticles-based approaches have been investigated as vaccines, adjuvants or for imaging purposes (Bae, K.H., *et al.*, 2011; Zhu, M. *et al.*, 2014; Fang, H.R. & Zhang, L., 2016).

Selective targeting of systemically applied nanoparticles towards tumours is difficult to achieve since their journey through the body can easily be halted by for instance thrombocytes or macrophages and the reticuloendothelial system (RES) (Friberg, S. & Nyström, A.M., 2016). Introduction and retention of nanoparticles at the tumour site has however been suggested to be helped by the controversially discussed enhanced permeation and retention (EPR) effect, a passive enrichment mechanism that exploits the features of tumour tissue. These features include lack of lymph drainage, high vascular density as well as enhanced vascular permeability. Association of nanoparticles with the tumour site is furthermore helped by the functionalization of nanoparticles with site specific receptors (Matsumura, J. & Maeda, H., 1986; Nichols, J.W. & Bae, Y.H., 2014; Danhier, F., 2016; Din, F., *et al.*, 2017.; Tang, J.Q. *et al.*, 2017).

A major problems of cancer therapy is its recurrence and the emergence of drug resistance towards first line therapeutics. Therefore, it is important to tackle problems such as the incomplete elimination or a failed re-education of cancer stem cells (CSCs), which is however extremely difficult due to their flexible phenotype. Furthermore, multidrug resistance (MDR) mechanisms resulting from pathway adaptions such as altered expression of drug efflux pumps, alterations in the ATP-binding cassette transporter (ABC transporter) superfamily, apoptotic processes and events associated with the WNT, NOTCH, HEDGEHOG or NANOG signalling pathways, need to be taken into consideration (Friberg, S. & Nyström, A.M., 2016). Nanoparticles able to encapsulate drugs of diverse physicochemical properties, of differing ratios or with a temporally sequenced release profile have been established and will most likely become increasingly important (Hu, C.M. & Zhang, L., 2012).

Nanoparticle formulations for melanoma therapy have previously and are currently devised, investigated, and tested in numerous pre-clinical and clinical studies. So far, however, no nanoparticle has been approved for the treatment of metastatic melanoma (Berciano-Guerrero, M.A. *et al.*, 2014). Promising approaches include the use and the manipulation of the tumour

environment. Tumour necrosis factor alpha (TNF-α)-enhanced doxorubicin was devised for the enhancement of tumour perfusion leading to improved drug delivery (Curnis, F. *et al.*, 2002; Mundra, V. *et al.*, 2015). Increased expression of the secreted protein acidic and rich in cysteine (SPARC) in human melanoma was to be exploited to increase the accumulation of albumin-bound paclitaxel (PTX) nanoparticles to melanoma (Hersh, E.M. *et al.*, 2015; Mundra, V. *et al.*, 2015). Furthermore, novel targets which convey resistance towards therapy have been uncovered. These include the overexpression of the anti-apoptotic class III ß-tubulin (TUBB3) (Akasaka, K. *et al.*, 2009; Mundra, V. et al., 2015) and the increase of ABCB5$^+$ cells upon therapy (Chartrain, M. *et al.*, 2012; Mundra, V. *et al.*, 2015). In addition, several molecules such as CD20, CD271, CD133 and ABCB5 have been reported as melanoma stem cell markers and may contribute towards specific targeting by nanoparticles (Lee, N., *et al.*, 2016; Mundra, V. *et al.*, 2015).

1.4 Aims and Objectives

cAMP is a ubiquitously expressed second messenger closely linked to molecular events in skin pigmentation. It has however also been associated with melanoma most notably with increased intracellular cAMP levels which correlate with its metastatic potential. Manipulation of the cAMP pathway with the intent of decreasing cAMP to physiological levels in the tumour environment was therefore studied in the context of the transplantable B16F10-OVA murine tumour model.

Possible points of intervention for the manipulation of the cAMP pathway are adenylyl cyclases, phosphodiesterases, and the cAMP effector proteins. The adenylyl cyclase inhibitor MDL-12, 330A hydrochloride was chosen for the intervention with the cAMP pathway due to its ability to non-reversibly inhibit but not completely block all nine transmembrane and the sole soluble adenylyl cyclase.

Since cAMP does not only play a role in skin pigmentation but also in processes such as cardiac function or inflammation it is important to assure a continuous local application of a cAMP pathway modulator. To achieve continuous site directed delivery of MDL-12, 330A hydrochloride but also to further the development and testing of novel nanoparticles, MDL-12, 330A hydrochloride loaded micelles were generated and analysed for their ability to interfere with cAMP production at the tumour site.

The effect of cAMP intervention in the B16F10-OVA melanoma model was investigated. For this purpose, growing tumours were continuously treated with MDL-12, 330A hydrochloride loaded micelles and in addition to the effect on their growth, alterations in the composition and function of the immune cell infiltrate were investigated. Based on these results strategies to abolish tumour growth by combining both cAMP modulation, selective cell depletion as well as other nanoparticle-based systems were though of and tested.

2. Materials

2.1 Laboratory Equipment and Technical Accessories

Apperatus	Designation and Manufacturer
Autoclave	Varioklav Steam Stererlizer (HP Medizintechnik GmbH, Oberschließheim, Germany)
Calipper	DIGITALCALIPER, 0-150 mm (Toko International BV, Zoetermeer, Netherlands)
Cell Harvester	Semiautomatic Cell Harvester Type 11019 (SKATRON Instruments AS, Lier, Norway)
Centifuges	Heraeus Multifuge 3L-R Centrifuge, Heraeus Biofuge Prima R (both ThermoFisher Scientific, Waltham, MA, USA)
Counter	1205 BETAPLATE® Liquid Scintillation Counter (LKB Instruments, Mount Waverly, Victoria, Australia)
Counting Chamber	Neubauer Counting Chamber, improved, depth 0.100 mm (0.0025 mm^2) (LO-Laboroptik, Lancing, GB)
Dissection Kit	Motorenfamilie Medical/Prestige Medical Deluxe Anatomy Dissections Kit (GB Intruments Limited, Kilwinning, Scotland, UK)
Flow Cytometer	BD™ LSR II (BDBiosciences, Becton, Dickinson and Company, Franklin Lakes, NJ, USA)
Freezer	economic-froster (-20 °C freezer) (Robert Bosch GmbH, Gerlingen-Schillerhöhe, Germany) Hera freeze HFU B series, (-80 °C freezer) (ThermoFisher Scientific Inc., Waltham, USA) Arperge 110, (-180 °C freezer) (Air liquide S.A., Paris, France)
Fridge	FKS 1800-20, profi line (Liebherr-International AG, Bulle, Switzerland) Tefcold FSC 1450 (NordCap GmbH & Co. KG, Bremen, Germany)
Ice Machine	Scotsman AF80 Ice Flaker (Hubbard Systems, Ipswich, GB)

Incubator	Heracell 150i CO_2 Incubator Heraeus BB16 Function Line CO_2 Incubator (ThermoFisher Scientific Inc., Waltham, MA, USA)
Magnetic Stirrer	IKAMAG® RCT (Labotec Labortechnik Wiesbaden GmbH, Wiesbaden, Germany)
Magnetic Welding Machine	polystar®601M Magnetic Welding Machine (Allpax GmbH+Co. KG, Papenburg, Germany)
Microplate Reader	ELx808 Absorbance Microplate Reader (BioTek, Winooski, VT, USA)
Microscopes	Laboratory Microscopes Nikon Eclipse TS100 and E100 (both: Nikon, Chiyoda, Tokio, Japan) EVOSfl Fluorescence Microscope from AMG (ThermoFisher Scientific Inc., Waltham, MA, USA)
pH Meter	pH211 Microprocessor pH Meter (Hanna Intruments Inc., Woonsocket, RI, USA)
Pipetts	2, 10, 20, 100, 200 and 1000 µl PIPETMAN (all Gilson Inc., Middleton, WI, USA)
Pipettus	pipetus® junior (Hirschmann Laborgeräte GmbH & Co. KG, Eberstadt, Germany)
Razor	Tondeo Exo-XS, Black Velvet (TONDEO, Solingen, Germany)
Thermomixer	Thermomixer Compact Type 5350 (Eppendorf, Hamburg, Germany)
Vortex Mixer	Vortex Genie 2™ (Bender & Hobein AG, Zürich, Switzerland)
Water Bath	Thermostat 27761 (Eppendorf AG, Hamburg, Germany)
Weighing Scale	MC1 Analytic AC 210 S, BA610 Top-loading Balance (Sartorius, Data Weighing Systems, Elk Grove Village, USA)
Work Bench	HeraSafe KS, KS9 and KS18 (ThermoFisher Scientific Inc., Waltham, MA, USA)

Table 2.1 Laboratory equipment and technical accessories. Model and company purchased from used equipment and technical accessories.

2.2 Consumables

Material	Designation and Manufacturer
Biopsie Punches	Stiefel Biopsy Punch 8 mm (GalaxoSmithKline, Brentford, UK)
Blood Lancet	Solofix® Blood Lancets (B.Braun Melsungen AG, Melsungen, Germany)
Cannulas	BD Microlance™ 3 23G11/4" - Nr.14 0.6x30 mm BD Microlance™ 3 26G1/2" 0.45x13 mm (all BDMedical, Becton Dickinson and Company, Franklin Lankes, NJ, USA)
Cell Culture Flask	Tissue Culture Flask 75 cm^2, Filter Screw Cap (TPP AG, Trasadingen, Switzerland)
Cell Culture Dish	6-well, 24-well, 96-well flat-bottom, 96-well round-bottom, 96-well pointed-bottom sterile tissue culture plates with lid (all Corning, Corning, NY, USA) 96-well round-bottom plate, non-sterile, no lid (Greiner Bio-One GmbH, Frickenhausen, Germany)
Cell Strainer	70 µm Nylon Cell Strainer BD Falcon (Corning, Corning, NY, USA)
Cover Slips	Cover Slips for the Haemocytometer (Menzel Gläser, ThermoFisher Scientific Inc., Waltham, MA, USA)
Cryo Tubes	Nunc™ CryoTube™ Vials, 1.8 ml (ThermoFisher Scientific Inc., Waltham, MA, USA)
FACS-Tubes	5 ml Polystyrene Round-Bottom Tubes, 12 x75 mm style (Corning, Corning, NY, USA)
Falcons	15 ml and 50 ml Falcons (both Greiner Bio-One GmbH, Frickenhausen, Germany)
Gloves	Disposable Gloves, Nitril (VWR International, Radnor, PA, USA)
Petri Dish	Petri Dish, 94x16 mm (Greiner Bio-One GmbH, Frickenhausen, Germany)
Pipette Tips	Pipette Tips 0.1-20 ul (Brand GmbH, Wertheim, Germany) Pipette Tips Gilson®-Style 200 ul, Pipette Tips Gilson®-Style 1000 ul (Greiner Bio-One GmbH, Frickenhausen, Germany)
Recation Tubes	0.5 and 1.5 ml Safe Seal Reaction Tubes (Sarsted, Nürnbrecht, Germany) 2 ml Safe Seal Reaction Tubes (Eppendorf AG, Hamburg, Germany)

Sample Bags	Sample Bag for Betaplate™, maximum membrane size 102x258 mm (PerkinElmer, Inc., Waltham, MA, USA)
Scalpel	Feather Disposable Scalpel (Feather Safety Razor Co., Ltd., Osaka, Japan)
Sheets	Printed Filtermat A, for use with 1205 Betaplate™, glass fibre filter, size 102x258 mm (PerkinElmer, Inc., Waltham, MA, USA)
Syringes	Omnican 0.01-1 ml Syringes 0.3 mm x 12 mm, Injekt®-F Syringe 0.01 ml - 1ml/Luer Solo (both B.Braun Melsungen AG, Melsungen, Germany) 10 ml Syringe BD Discardit™ II, BD Micro-Fine™+Demi U-100 Insulin Syringe 0.3 mm (30G) x 8 mm (both BDMedical, Becton, Dickinson and Company, Franklin Lakes, NJ, USA)

Table 2.2 Consumables. Exact description and company purchased from consumables used.

2.3   Chemicals, Reagents, and Ready-To-Use Reagents

Reagents	Manufacturer
Albumin Fraction V, free from biotine (BSA)	Roth GmbH & Co. KG, Karlsruhe, Germany
Ammonium Chloride (NH_4Cl)	Merck KGaA, Darmstadt, Geramany
Anti-Gr-1 Antibody (Clone: RB6-8C5)	██████████████████████████████ ██████████████████████
Aqua dest. (ddH_2O)	B.Braun Melsungen AG, Melsungen, Germany
BD FACS™ Lysing Solution	BD Biosciences, Becton, Dickinson and Company, Franklin Lakes, USA
BD FACS Flow™	BD Biosciences, Becton, Dickinson and Company, Franklin Lakes, USA
CellTrace™ Carboxyfluorescein Succinimidyl Ester (CFSE) Cell Proliferation Kit	Invitrogen™, ThermoFisher Scientific Inc., Waltham, MA, USA
CellTrace™ Violet Proliferation Kit	Invitrogen™, ThermoFisher Scientific Inc., Waltham, MA, USA
Collagenase Type II	Gibco®, ThermoFisher Scientific Inc., Waltham, MA, USA
Collagenase Typ 4	Worthington Biochemical Cooperation, Lakewood, NJ, USA

Dimethyl Sulfoxide (DMSO) Hybri-Max®	Sigma-Aldrich, St. Louis, MO, USA
Deoxyribonuclease I (DNase I) from bovine pancreas	F. Hoffmann-La Roche AG, Basel, Switzerland
Diphteriatoxin (DT)	Merck KGaA, Darmstadt, Germany
Direct cAMP Enzyme-linked Immunosorbent Assay (ELISA) kit	Enzo Life Sciences, Farmingdale, USA
Dispase II (neutral protease, grade II) from bacillus polymyxa	F. Hoffmann-La Roche AG, Basel, Switzerland
Ethanol 70% denatured	Roth GmbH & Co. KG, Karlsruhe, Germany
Ethylenediaminetetraacetic Acid (EDTA) Disodium Salt Dihydrate ($C_{10}H_{14}N_2O_8Na_2.2H_2O$)	AppliChem GmbH, Darmstadt, Germany
Fetal Claf Serum (FCS)	Gibco®, ThermoFisher Scientific Inc., Waltham, MA, USA
FORENE® 100% (V/V) (Isoflurane)	Abbott Laboratories, Chicago, IL, USA
G418-BC Sulfate	Biochrom, Merck KGaA, Darmstadt, Germany
Hank's Balanced Salt Solution (1x) (HBSS)	Gibco®, ThermoFisher Scientific Inc., Waltham, MA, USA
Heparin-Natrium-25000-ratiopharm®	Ratiopharm GmbH, Ulm, Germany
Human Albumin 20%, salzarm (HSA)	CSL Behring LLC, King of Prussia, PA, USA
Hydrochloric Acid (HCL)	Roth GmbH & Co. KG, Karlsruhe, Germany
MDL-12,330A hydrochloroide	Calbiochem, Merck KGaA, Darmstadt, Germany
Ovalbumin (OVA), Alexa Fluor 647 (AF647) Conjugate	Invitrogen™, ThermoFisher Scientific Inc., Waltham, MA,
Ovalbumin EndoFit™	InvivoGen, San Diego, CA, USA
Penicillin-Streptomycin (10.000 Units Penicillin, 10 mg Streptomycin/ml in 0,9% NaCl)	Sigma-Aldrich, St. Louis, MO, USA
Potassium Hydrogen Carbonate ($KHCO_3$)	Carl Roth, Karlsruhe, Germany
Privigen Infusion Solution (normal Immunoglobulin for humans IVIg 100 mg/ML)	CSL Behring LLC, King of Prussia, PA, USA
Rotizint®eco plus	Roth GmbH & Co. KG, Karlsruhe, Germany
Sodium Chloride (NaCl)	Roth GmbH & Co. KG, Karlsruhe, Germany

Sodium Phosphate Monobasic Dihydrate (NaH$_2$PO$_4$·2H$_2$O)	Merck KGaA, Darmstadt, Germany
Sodium Hydroxide (NaOH)	Roth GmbH & Co. KG, Karlsruhe, Germany
Thymidine, (methyl-^{3}H)-NET027X005MC (^{3}H-Thymidin)	PerkinElmer, Inc., Waltham, MA, USA
Transcription Factor Buffer Set	BDBiosciences, Franklin Lakes, NJ, USA
Triton X-100	Sigma-Aldrich, St. Louis, MO, USA
Trypan Blue Solution (0,4%)	Sigma-Aldrich, St. Louis, MO, USA
Trypsin-Ethylenediaminetetraacetic Acid (Trypsin-ETDA)	Sigma-Aldrich, St. Louis, MO, USA

Table 2.3 Chemicals, reagents, and ready-to-use reagents. Exact description and company purchased from chemicals, reagents and ready-to-use reagents used.

2.4 Antibodies

Antibody	Reactivity	Isotyp	Clone	Conjugate	Manufacturer
CD3	Mouse	Rat IgG2b, kappa	17A2	PE-Cy7	BioLegend, San Diego, CA, USA
CD4	Mouse	Rat IgG2b, kappa	GK1.5	eFluor 450	eBioscience, ThermoFisher Scientific Inc., Waltham, MA, USA
CD4	Mouse	Rat IgG2b, kappa	GK1.5	PE-Cy7	BioLegend, San Diego, CA, USA
CD8a	Mouse	Rat IgG2b, kappa	53-6.7	APC	eBioscience, ThermoFisher ScientificInc., Waltham, MA, USA
CD8a	Mouse	Rat IgG2a, kappa	53-6.7	PerCP	BDBiosciences, Becton, Dickinson and Company, Franklin Lakes, USA

CD11b	Mouse	Rat IgG2b	M1/70	APC	ImmunoTools, Friesoythe, Germany
CD11b	Mouse	Rat IgG2b	M1/70	PE	ImmunoTools, Friesoythe, Germany
CD11c	Mouse	Armenian Hamster IgG	N418	PE-Cy5	BioLegend, San Diego, CA, USA
CD25	Mouse	Rat (OFA) IgG1	PC61	PE-Cy7	BDBiosciences, Becton, Dickinson and Company, Franklin Lakes, USA
CD45	Mouse	Rat IgG2b, kappa	30-F11	APC-eFluor 780	eBioscience, ThermoFisher Scientific Inc., Waltham, MA, USA
CD45R/B220	Mouse/Human	Rat IgG2a, kappa	RA3-6B2	PE-Cy7	BioLegend, San Diego, CA, USA
CD115	Mouse	Rat IgG2a, kappa	AFS98	PE	BioLegend, San Diego, CA, USA
FC Block (CD16/CD32)	Mouse	Rat IgG2a, lambda	93		eBioscience, ThermoFisher Scientific Inc., Waltham, MA, USA
Fixable Viability Dye	Mouse/Human			eFluor506	eBioscience, ThermoFisher Scientific Inc., Waltham, MA, USA
FoxP3	Mouse/Human/Dog	Rat IgG2a, kappa	FJK-16s	PE	eBioscience, ThermoFisher Scientific Inc., Waltham, MA, USA

KLRG-1 (CSF-1R)	Mouse	Syrian hamster IgG	2F1	FITC	BioLegend, San Diego, CA, USA
Ly-6C	Mouse	Rat IgG2c, kappa	HK1.4	PerCP-Cyanine5.5	eBioscience, San Diego, USA
Ly-6C	Mouse	Rat IgG2c, kappa	HK1.4	PE-Cy7	BioLegend, San Diego, CA, USA
Ly-6G	Mouse	Rat IgG2a, kappa	1A8	PB	BioLegend, San Diego, CA, USA
NK1.1	Mouse	Mouse IgG2a, kappa	PK136	PE	eBioscience, ThermoFisher Scientific Inc., Waltham, MA, USA
NK-1.1	Mouse	Mouse IgG2a, kappa	PK136	PE-Cy7	BioLegend, San Diego, CA, USA
TCR beta (TCRβ) chain	Mouse	Armenian Hamster IgG2	H57-597	PE-Cy5	BD Biosciences, Becton, Dickinson and Company, Franklin Lakes, USA

Table 2.4 Antibodies. Antibody, reactivity, isotype, clones, fluorescence, and company purchased of antibodies used.

2.5   Buffers

Buffer	Composition
0.5 M EDTA pH 8.0 (autoclaved after preparation, stored for ≥6 months at 4 °C)	181.1 g $C_{10}H_{14}N_2O_8Na_2.2H_2O$ Ad 1L Aqua dest.
10x PBS pH 6.6 (autoclaved after preparation)	80.4 g NaCl 15.6 g $NaH_2PO_4 \cdot 2H_2O$ Ad 1L Aqua dest.
1xPBS	0.1 L 10xPBS

	Ad 1L Aqua dest.
ACK (Ammonium-Chloride-Potassium)-Buffer pH 7.4	8.29 NH$_4$Cl 1.0 g KHCO$_3$ 200 µl l 0.5 M EDTA Ad 1L Aqua dest.
FACS-Buffer	25 ml HSA 2 ml 0,5 M EDTA 200 µl Privigen Infusion Solution Ad 1L1xPBS
Freezing Media	20 ML FCS 5 ml DMSO
MACS-Buffer	25 ml HSA 6 ml 0.5 M EDTA Ad 1 L 1xPBS
Trypan-Blue	1 ml Trypan Blue Solution (0.4%) 9 ml 1xPBS

Table. 2.5 Buffers. Recipes of buffers used.

2.6   Cell Culture Media

Material	**Manufacturer**
Dulbecco's Modified Medium (DMEM)	Gibco®, ThermoFisher Scientific Inc., Waltham, MA, USA
Iscove`s modified Dulbecco`s Medium (IMDM) with 4 mM L-Glutamine and 25 mM (4-(2-hydroxyethyl)-1-piperazineethanesulfonic acid) HEPES	Lonza Group AG, Basel, Switzerland
Roswell Park Memorial Institute (RPMI)1640	Gibco®, ThermoFisher Scientific Inc., Waltham, MA, USA
RPMI 1640 with 2 mM L-Glutamine	Gibco®, ThermoFisher Scientific Inc., Waltham, MA, USA
X-Vivo 20	Lonza Group AG, Basel, Switzerland

Table 2.6 Cell culture media. Media and company purchased of media commonly used for cell culture.

2.7 Cell Lines

Cell Line	Description	Source
B16F10-OVA	Murine Melanoma Cell Lines	████████████████████
MC-38	Murine Adenocarcinoma Cell Line	████████████████████████ ████████████████████

2.7 Cell lines. Cell Lines and source of cell lines used.

2.8 Experimental Animals

Strain	Source	Official Strain Name	Stock Number
C57BL/6J	Jackson Laboratory, Bar Harbor, ME, USA	C57BL/6J	JAX Stock Number: 000664
Great	Jackson Laboratory, Bar Harbor, ME, USA	B6 129 S4-IFNg	JAX Stock Number: 017581
Nur77	Jackson Laboratory, Bar Harbor, ME, USA	Nur77-EGFP-Cre(tg(Nr4a1-EGFP/cre)820Khog)	JAX Stock Number: 016617
DEREG	Jackson Laboratory, Bar Harbor, ME, USA	C57BL/6-Tg(Foxp3-TR/EGFP)23.2Spae/Mmjax	MMRRC Stock Number: 32050-JAX
OT-I	Jackson Laboratory, Bar Harbor, ME, USA	C57BL76-Tg(TcraTcrb)1100Mjb/J	JAX Stock Number: 003831
OT-II	Jackson Laboratory, Bar Harbor, ME, USA	B6.Cg-g(TcraTcrb)425Cbn/J	JAX Stock Number: 004194

Table 2.8 Experimental animals. Official strain name, company purchased, and stock number of mice used.

2.9   Software

Software	Manufacturer
FlowJo version 7	Tree Star, Inc., Ashland, OR, USA
GraphPad Prism 6	GraphPad Software, Inc., La Jolla, CA, USA
KC Junior	BioTek, Winooski, VT, USA

Table 2.9 Software. Software and manufacturer of software used.

3. Methods

3.1 Cell Biological Methods

3.1.1 Cell Culture

Cell culture was handled under a sterile workbench while using sterile materials. Materials or solutions introduced into the workbench were previously autoclaved or sterilised using 70% ethanol. Cells were cultivated in buffered media and incubated in an incubator at 37 °C and 5% CO_2.

3.1.2 Cell Lines

The ovalbumin (OVA) expressing murine melanoma cell line B16F10-OVA (Fidler, I.J., 1970; Fidler, I.J., 1973a, Fidler, I.J., 1973b; Kedl, R.M. *et al.*, 2001) was provided by ████████, ████████████████ while the murine colon adenocarcinoma cell line MC-38 (Corbett, T.H. *et al.*, 1975) was provided by ██ ████████████████████.

3.1.2.1 B16F10-OVA

The B16 melanoma is a melanin producing murine melanoma cell line characterized by a mixture of spindle-shaped and epithelial-like cells which is most commonly used to model human melanoma and metastasis. In 1954, B16 spontaneously developed in the skin at the base of the ear of a C57BL/6J mouse at the Jackson Laboratory, Bar Harbor, Main (Green, E, 1968; Alvarez, E., 2002, B16-F10 (ATCC® CRL-6475™). It was propagated in mice by subcutaneous transplantation, would kill the host within 3-5 weeks and metastasize into the lung, liver; and spleen (Bertalanffy, F.D. & McAskill, C., 1964).

Isiah J. Fidler experimented with these cells in the 1970s and established the cell lines B16F1 and B16F10. After intravenous injection, pulmonary metastases were continuously passaged in mice (Fidler, I.J., 1970; Fidler, I.J., 1973a; Fidler, I.J., 1973b; Alvarez, E., 2002). Both B16F1 and B16F10 do form metastases in the lung upon intravenous injection, whereby B16F10, the most passaged of these two, is characterized by a significantly higher metastatic potential likely due to subtle cell surface modifications (Raz, A., *et al.*, 1980). While B16F10 exclusively forms metastases in the lung, other sites can also be affected when B16F1 is used. These include the

liver, spleen, adrenal glands, and mesentery lymph nodes (Fidler, I.J. & Nicolson, G.L., 1976). The subcutaneous B16 model is commonly used for the evaluation of potential therapeutic regiments (Overwijk, W.W. & Restifo, N.P., 2001).

B16F10 has been modified by its transfection with ovalbumin (OVA) to generate the B16F10-OVA cell line. The full-length OVA gene with the neomycin-resistance selection gene was therefore placed under the control of the cytomegalovirus long terminal repeat promoter (Kedl, R.M. *et al.*, 2001). OVA is a non-toxic, slightly immunogenic T cell dependent protein which was first isolated in 1889 from the egg white of a chicken's egg. In immunology it is frequently used to study antigen-specific immune responses in mice. B16F10-OVA allows to do so in the context of tumour responses (Hofmeister, F., 1889; Bellone, M. *et al.*, 2000).

3.1.2.2 MC-38

MC-38 is a chemically induced murine colon adenocarcinoma which was established in 1975 in the laboratory of F.M. Schabel Jr., Kettering-Meyer Laboratories, Southern Research Institute, Birmingham, Alabama. It has been provoked by the subcutaneous injection of dimethylhydrazine (DMH) and is syngeneic to C57BL/6 mice. Upon subcutaneous implantation metastases have primarily been noted in the lung while intraperitoneal administration of the tumour cells results in the detection of metastases in the liver (Corbett, T.H. *et al.*, 1975).

3.1.3 Cryo-conservation of Cell Lines

For cryo-conservation, 10×10^6 B16-OVA cells per cryotube, were stored for at least 24 hours in 1 ml freezing medium at -80 °C. For lasting preservation, the cells were transferred into liquid nitrogen tanks at -180 °C.

3.1.4 Defrosting of cryo-conserved Cell Lines

Cryo-conserved B16F10-OVA were thawed for 1 minute in a water bath at 37 °C. Together with 5 ml FCS and 10 ml Iscove's Modified Dulbecco's Medium (IMDM) with 4 mM L-Glutamine and 25 mM 4-(2-hydroxyethyl)-1-piperazineethanesulfonic acid (HEPES) the cells were transferred into a 15 ml falcon and centrifuged for 6 minutes at 360 g and 4 °C. The supernatant was discarded, the cells were suspended in 5 ml medium and centrifuged again at

the same settings. Once more the supernatant was discarded, the cells were suspended in 1 ml medium and then transferred into a 75 cm^2 cell culture flask supplemented with 15 ml of medium. Dead cells were removed the next day by replacing the medium with fresh medium. To start the selection for OVA producing cells the medium of B16F10-OVA was supplemented with 300 µg/ml G418-BC Sulfate.

3.1.5   Maintenance of B16-OVA

B16F10-OVA were cultured in IMDM with 4 mM L-Glutamine and 25 mM HEPES supplemented with 10% fetal calf serum (FCS), 1% penicillum/streptomycin and 300 µg/ml G418-BC Sulfate. The cells were kept in a 75 cm^2 cell culture flasks in an incubator at 37°C in 5% CO_2 and passaged when approximately 70% confluent.

3.1.6   Maintenance of MC-38

MC-38 were cultured in IMDM with 4 mM L-Glutamine and 25 mM HEPES supplemented with 10% FCS and 1% penicillum/streptomycin. The cells were kept in a 75 cm^2 cell culture flasks in an incubator at 37 °C in 5% CO_2 and passaged when approximately 70% confluent.

3.1.7   Passaging of Cell Lines

The medium was removed from the flask and the cells were twice washed with 1x phosphate buffered saline (PBS). 2 ml of trypsin-ethylenediaminetetraacetic acid (Trypsin-EDTA) were then added to the flask which was then incubated for 5 minutes at 37 °C in 5% CO_2. As soon as the cells had detached from the plastic dish, the Trypsin-EDTA was neutralized with 2 ml of media. The suspension was then centrifuged for 6 minutes at 360 g and 4 °C. Following centrifugation, the supernatant was discarded, and the pellet was resuspended in an appropriate amount of medium. The cells were then placed into a new flask at the desired concentration and kept in an incubator at 37 °C in 5% CO_2

3.1.8   Determination of Live Cells

The hemocytometer is a modified and calibrated microscope slide frequently used to estimate the number of cells in a known volume. Louis-Charles Malassez first used it to count blood cells (Malassez, L.C., 1873). Nowadays it is most commonly used in combination with trypan

blue which allows to distinguish viable from non-viable cells. To determine cell numbers cells within a large square of 16 individual squares are counted under a microscope.

The number of viable cells, trypan blue negative, is calculated using the following formula:

Total Cell Number = Cell Number per Big Square x Dilution Factor x Volume x 10^4 (Chamber Constant)

3.1.9   Plating out of Cell Lines

B16F10-OVA or MC-38 were plated out at a concentration of $2x10^6$ cells/per well in a flat-bottom 6-well plate or at $2x10^5$ in a flat-bottom 96-well plate. After shortly centrifuging the cells at 360 g without breaks and 4 °C, the cells were placed in the incubator at 37 °C and 5% CO_2 until they started to attach to the plastic dish.

3.2   *In Vitro* Experiments

3.2.1   Inhibition of cAMP by Adenylyl Cyclase Inhibition

Adenylyl cyclases (AC) are enzymes which catalyse the conversion of ATP into the second messenger cAMP and pyrophosphate. In mammals, there exist in total 10 different adenylyl cyclases, nine transmembrane adenylyl cyclases (tAC1-9) and one soluble adenylyl cyclase (sAC10). They are differently expressed throughout the body, whereby most tissues express multiple adenylyl cyclases (Sadana, R. & Dessauer, C.W., 2009).

Both transmembrane and soluble adenylyl cyclases are homodimers with one polypeptide chain which have two structurally similar catalytic sites, C_1 and C_2, forming a pseudo-heterodimer. Transmembrane adenylyl cyclases also feature two hydrophobic domains each representing six membrane spanning helices which localize these to membranes. G protein-coupled receptors and heterotrimeric G proteins regulate transmembrane adenylyl cyclases, while soluble adenylyl cyclases are directly regulated by Ca^{2+}, the metabolite bicarbonate and variations of ATP levels (Sadana, R. & Dessauer, C.W., *et al.*, 2009; Seifert, R., *et al.*, 2012).

Modulation of cAMP, which includes the inhibition of adenylyl cyclases, is of interest in a great number of research fields. There exists a vast variety of adenylyl cyclase inhibitors which at the catalytic site compete with the ATP substrate, mimic the cAMP·PPi transition state or target

regulatory or yet undefined binding sites. One of the numerous inhibitors is MDL-12, 330A hydrochloride (Seifert, R., *et al.*, 2012).

3.2.1.1 MDL-12, 330A hydrochloride

MDL-12, 330A hydrochloride also known as RMI 12330A or cis-N-(2phenylcyclopentyl) azacyclotridec-1-en-2-amine monohydrochloride is a lactam-imine which was devised at the Merrell Research Centre, Cincinnati, Ohio; USA and first reported on in the late 1970th (Siegel, B.W. & Wiech, N.L., 1976, Guellaen; G. *et al.*, 1977). It is a hydrophobic cell-permeable non-nucleotide-based inhibitor of soluble and transmembrane adenylyl cyclases which is well soluble in organic solutions. Its non-nucleotide-based structure is advantageous since cytotoxic long-term effects due to interference with deoxyribonucleic acid (DNA) synthesis or the purine metabolism can be avoided (Seifert, R. *et al.*, 2012; Emery, A.C. *et al.*, 2013).

Inhibition of both basal as well as stimulated adenylyl cyclases by MDL-12, 330A hydrochloride is immediate and irreversible due to its association with the plasma membrane. It has furthermore been reported to interfere with the glycine transport, calcium related mechanisms and to affect Mg^{2+}-ATPases but not Na^+, and K^+-ATPases and to inhibit phosphodiesterases (Hunt, N.H. & Evans, T. 1980; Grupp, G. *et al.*, 1980; Gadea *et al.*, 1999; Van Rossum *et al.*, 2000). The non-competitive simultaneous inhibition of both adenylyl cyclases and phosphodiesterases is most likely due to a shared site of inhibition. Nevertheless, MDL-12, 330A hydrochloride is still more effective when inhibiting adenylyl cyclases (Lippe, C. & Ardizzone, C., 1991; Seifert, R. *et al.*, 2012).

MDL-12, 330A hydrochloride was purchased from Calbiochem, Merck KGaA, Darmstadt, Germany. A 10 mM stock solution was prepared upon its dissolution in DMSO, aliquoted and stored for up to three months at -20 °C. The proper working of every new charge was checked by incubating B16F10-OVA with lethal and sublethal concentrations of MDL-12, 330A hydrochloride. For short term *in vitro* experiments MDL-12, 330A hydrochloride was used at a final concentration of 10 µM, whereas *in vivo* inoculated tumours were treated with 20 µM or 200 µM MDL-12, 330A hydrochloride/50 µl.

3.2.1.2 MDL-12, 330A hydrochloride loaded Micelles

The amphiphilic peptide-based polypeptoid-*block*-polypeptide copolymer polysacrcosine-*block*-polyglutamatic acid bezylester (PSar-b-PGlu(OBn)) was used for the preparation of empty and MDL-12, 330A hydrochloride loaded micelles. Synthesis and characterization of the polymer as well as the preparation of the micelles was carried out by ██████████████████

██

MDL-12, 330A hydrochloride loaded micelles were prepared by dual centrifugation upon vigorous mixing of the polymer and the drug. Free MDL-12, 330A hydrochloride was separated from the resulting solution by spin filtration. To quantify the amount of MDL-12, 330A hydrochloride encapsulated in the micelles, samples of the filtrate were subjected to High-Performance Liquid Chromatography (HPLC). Portions of the purified micellar solution were lyophilized for the subsequent determination of the total mass concentration. For *in vivo* tracking studies the polymer was coupled with the fluorophore Oregon Green. Upon coupling free fluorophore was removed by dialysis and MDL-12, 330A hydrochloride loaded and empty micelles were prepared. Based on the HPLC quantification of MDL-12, 330A hydrochloride the amount of particle to be used for each individual experiment was determined. The amount of empty particle used was adjusted to MDL-12, 330A hydrochloride loaded particles based on the mass concentration determined for both.

3.2.1.3 Treatment of Cell Lines with free MDL-12, 330A hydrochloride and MDL-12, 330A hydrochloride-loaded Micelles to assess the Effect of the Treatment on Proliferation

When the melanoma cells had started to attach to the plastic dish the appropriate reagents were added to the flat-bottom 96-well plate. They were forced to instantly associate with the cells by a short round of centrifugation at 360 g without breaks at 4 °C. The cells were subsequently incubated at 37 °C and 5% CO_2. At the end of the incubation period, 0.5 µCi/well ^{3}H-Thymidin were added for another 18 hours. By default, DNA synthesis in proliferating cells is demonstrated by the incorporation of ^{3}H-Thymedin during cell division. Autoradiographic methods such as the ß-Counter are then used to measure proliferation.

3.2.1.4 Treatment of Cell Lines with MDL-12, 330A hydrochloride and MDL-12,330A hydrochloride loaded Micelles for the Determination of the intracellular cAMP Content by Enzyme-linked Immunosorbent Assay (ELISA)

As soon as the cells had started to attach to the plastic dish the relevant reagents were added to the flat-bottom 6-well plate. They were forced to immediately associate with the cells by a short round of centrifugation at 360 g without breaks and 4 °C. The cells were then left to incubate at 37 °C and 5% CO_2. At the end of the incubation period the supernatant was removed and discarded. The cells were detached from the cell culture plate using 500 µl of Trypsin-EDTA. It was neutralized with 750 µl of IMDM with 4 mM L-Glutamine and 25mM HEPES and the cell suspension was transferred into a 1.5 ml Eppendorf tube which was then centrifuged for 10 minutes at 360 g and 4 °C. The supernatant was discarded and twice centrifuged to remove the remaining media. The dry pellet was then frozen at -80 °C and stored at these conditions until measured by ELISA (Enzyme-linked Immunosorbent Assay).

3.2.2 Determination of the cAMP content of *In Vitro* and *In Vivo* generated Probes

3.2.2.1 cAMP ELISA

The Direct cAMP ELISA kit from Enzo Life Sciences was used to determine the intracellular cAMP concentration of murine cell lines and tissue. It was carried out according to the manufacturer's instructions.

3.2.2.2 Lysis of *In Vitro* generated Probes for the Determination of the cAMP Content

Cell samples stored at -80 °C were thawed at room temperature. To ensure complete cell lysis, they were resuspended in 150 µl of 0.1 M HCL spiked with 1% Triton X-100, thoroughly vortexed and snap-frozen at -80 °C. Mild thawing at room temperature and rigorous vortexing was followed by numerous freeze-thaw cycles. To remove cellular debris from the probe, it was centrifuged for 10 minutes at 4 °C and 600 g. In total 100 µl of the supernatant were used to determine the cAMP concentration by ELISA. The dilution factor (DF=1.5) was taken into consideration when calculating the probes cAMP content.

3.2.2.3 Lysis of *Ex Vivo* generated Probes for the Determination of the cAMP Content

Tissue samples stored at -80 °C were thawed, shock-frozen in liquid nitrogen and a single cell suspension was prepared upon the disruption of the tissue on a 70 µm cell strainer. The cell strainer was washed with 300 µl of 0.1 M hydrochloric acid (HCL) spiked with 1% Triton X-100 and the cell suspension was transferred into a 1.5 ml Eppendorf tube and frozen at -80 °C. Thawing of the probes at room temperature, rigorous vortexing and several freeze-thaw cycles were followed by the removal of cellular components by centrifugation for 10 minutes at 4 °C and 600 g. 100 µl of the supernatant were used to assay the cAMP content by ELISA. The dilution factor (DF=3) was taken into consideration when calculating the probes cAMP content.

3.3 Handling of Mice used for Animal Experiments

3.3.1 Mouse Strains used for Animal Experiments

All mice were bread and housed in the facilities of the Translational Animal Research Centre (TARC) of the University Medical Centre in Mainz, Mainz, Germany. Animal experiments were carried out with the approval (Tierversuchsnummer: G12-1-087) of the Landesuntersuchungsamt Koblez, Koblenz, Rhineland-Palatinate, Germany and in accordance with the Helsinki Convention for the use and care of animals (WMA, 2016).

3.3.1.1 C57BL/6 (JAX Stock Number: 000664)

C57BL is an inbred laboratory mouse strain established by C.C. Little in 1921. C57BL/6J did separate from the original strain in 1937 while kept at the Jackson Laboratories. It has since been used extensively for the generation of novel mouse strains (Song, H.K. & Hwang, D.Y., 2017).

3.3.1.2 B16 129 S4-IFNg (JAX Stock Number: 017581)

B6 129 S4-IFNg, also referred to as GREAT (interferon-gamma reporter with endogenous polyA transcript) is a homozygous interferon gamma reporter mouse on a C57BL/6 background. When generating the mouse homologous recombination was utilized to introduce an internal ribosome entry site (IRES)-enhanced yellow fluorescent protein (eYFP) amongst the stop codon and the 3' untranslated (UTR)/polyA tail of the ifng gene. The Interferon-gamma (IFN-γ) promoter/enhancer region and the endogenous 3' UTR and polyA tail regulate the

IFNy-IRES-eYFP messenger ribonucleic acid (mRNA) transcription as in the endogenous gene. IFN-γ positive cells can be detected *ex vivo* and *in vivo* by means of Flow Cytometry or Fluorescent Microscopy without the need for prior re-stimulation (Reinhardt, R.L., *et al.*, 2009; Reinhardt, R.L. *et al.*, 2015).

3.3.1.3 Nur77-EGFP-Cre(tg(Nr4a1-EGFP/cre)820Khog) (JAX Stock Number: 016617)

Nur77-EGFP-Cre(tg(Nr4a1-EGFP/cre)820Khog), also called Nur77 is a hemizygous BAC (bacterial artificial chromosome) transgenic reporter mouse on a B6-820 background. An enhanced green fluorescent protein/codon-optimized "humanized" Cre recombinase fusion protein (eGFP-hCre) has been integrated within the BAC transgene and placed under the control of the orphan nuclear receptor Nr4a1 (Nur77) promoter/enhancer region. The observed levels of green fluorescent protein (GFP) follows the endogenous Nur77 expression but is delayed because of the longer half-life of the GFP. Cre recombinase activity is present throughout the hematopoietic cell compartment (Moran, A.E. *et al.*, 2011).

The Nur77 mouse is suitable for studying both the myeloid as well as the lymphoid cell compartment. T and B lymphocytes express low levels of Nur77 which are not affected by inflammatory stimuli but get elevated upon antigen receptor stimulation. Peak expression levels are reached between 12 and 24 hours and mirror the strength of the T cell receptor stimulation. Nur77 expression in mature naïve T cells results from a continuous contact with the Major Histocompatibility Complex (MHC) (Moran, A.E. *et al.*, 2011). Significant levels of Nur77 are detected in Ly6C^{neg} monocytes, also referred to as vascular patrolling monocytes (Hanna, R.N. *et al.*, 2012).

3.3.1.4 C57BL/6-Tg(Foxp3-DTR/EGFP)23.2Spar/Mmjax (MMRRC Stock Number: 32050-JAX)

C57BL/6-Tg(Foxp3-DTR/EGFP)23.2Spar/Mmjax, commonly referred to as DEREG (depletion of regulatory T cells), is a hemizygous BAC transgenic mouse on a C57BL/6 background which expresses a diphtheria toxin receptor (DTR) enhanced green fluorescence protein (eGFP) under the control of the forkhead box P3 (FoxP3) promoter. Mouse Tregs, which are defined by the transcription factor FoxP3, can be temporarily ablated by diphtheria toxin (DT) injection and tracked by the expression of GFP. Upon removal Treg frequencies recover within 6 days (Lahl, K. *et al.*, 2007; Lahl, K. & Sparwasser, T., 2011).

Due to incomplete transgene expression and DT resistant Tregs the depletion efficiency of DREG mice only reaches up to 98%. These remaining Tregs prevent the onset of uncontrolled autoimmunity which makes the model particularly suitable when studying Treg function in adult mice. To avoid DT side effects such as weight loss or proteinuria, DT concentrations need to be carefully adjusted. The advent of anti-DT antibodies should be taken into consideration in long-term depletion regiments (Mayer, C.T. *et al.*, 2014; Wang, J. *et al.*, 2016).

3.3.1.5   C57BL/6-Tg(TcraTcrb)1100Mjb/J (JAX Stock Number: 003831)

C57BL/6-Tg(TcraTcrb)1100Mjb/J, also known as OT-I, is a hemizygous transgenic mouse on a C57BL/6 background. A rearranged T cell receptor, Tcra-v2/Tcrb-V5, specific for the H2K^b/chicken ovalbumin peptide 257-264 (SINFEKEL), was introduced into the genome. OT-I mice are commonly used to examine the response of CD8$^+$ T cells to ovalbumin (Hogquist, K.A., *et al.*, 1994).

3.3.1.6   B6.Cg-Tg(TcraTcrb)425Cbn/J (JAX Stock Number: 004194)

B6.Cg-Tg(TcraTcrb)425Cbn/J, also referred to as OT-II.2, is a homozygous transgenic mouse on a C57BL/6 background. A T cell receptor, Tcr-v2/Tcrb-V5, specific for the H2-Ab1/chicken ovalbumin peptide 323-339, was inserted into the genome. The mice are characterized by a four-fold increase in the CD4$^+$ to CD8$^+$ ratio of peripheral T cells and are used when studying the response of CD4$^+$ T cells to ovalbumin (Barnden, M.J. *et al.*, 1998).

3.3.2   Screening of Nur77 and DEREG Mice

Mice were forcibly sized in a forced grip. Blood samples were obtained from the vena facialis at a point where the orbital vein, the submandibular vein and other veins meet to form the jugular vein. To obtain blood, it was punctured using a blood lancet. Several drops of blood were collected in a 1.5 ml Eppendorf tube supplemented with 50 µl Heparin-Natrium. The probes were stained with antibodies against CD45, CD4 and CD25 for 30 minutes in the dark at room temperature. To lyse the erythrocytes that otherwise would interfere with the flow cytometric measurement, 1 ml of BD Lysing Solution (1ml BD Lysing Solution added to 9 ml ddH$_2$0) was added, resuspended with each probe, and left to incubate for 20 minutes in the dark at room temperature. Up until clear samples were obtained, the probes were washed with 2 ml of FACS-Buffer and centrifuged for 6 minutes at 4 °C and 360 g. The samples were evaluated

using Flow Cytometry whereby Nur77 mice with elevated levels of eGFP expression in the myeloid compartment and DEREG mice with elevated levels of eGFP in the $CD45^+CD4^+CD25^+$ compartment were designated to be Nur77 or DEREG positive.

3.4 Immunological Methods

3.4.1 Isolation of Organs and Preparation of Single Cell Suspensions

CO_2 fumigation was used when killing mice. The mice were opened, different organs were removed, and single cell suspensions were prepared for analysis by Flow Cytometry. When preparing single cell suspensions of organs well supplied with blood, erythrocytes were lysed by ACK (Ammonium-Chloride-Potassium) lysis. While lysing cells, ammonium chloride accumulates inside the cell, which leads to an increase in osmotic pressure and the rupture of the erythrocytes (Bossuyt, X. *et al.*, 1997).

3.4.1.1 Peritoneal Exudate Cells (PECs)

Peritoneal exudate cells (PECs) can be found in the mammalian peritoneal cavity which harbours macrophages, T and B cells. For the extraction of these cells a euthanized mouse was mounted on a dissection pad, sprayed with 70% ethanol and the outer skin of the peritoneum was cut open with the help of forceps and scissors. The skin was gently separated from the inner skin of the peritoneal cavity and a syringe with a 26G needle was carefully inserted into the peritoneum while paying attention to not puncture any organs. 5 ml of ice cold 1x Hank's Balanced Salt Solution (HBSS) were injected into the peritoneal cavity, the peritoneum was massaged to increase the yield of the cells harvested and a syringe with a 23G needle was introduced into the peritoneum to collect as much fluid as possible. The cell suspension was collected in a 15 ml falcon and the cells were pelletized by centrifuging them for 10 minutes at 4 °C and 360 g. If necessary erythrocytes were removed by treating the cells with ACK-Buffer. Therefore, the supernatant was discarded, the cells were mixed and incubated for 2 minutes with 2 ml of ACK-Buffer. FACS-Buffer was then added, the cells were centrifuged for 10 minutes at 4°C and 360 g and it was evaluated weather another round of ACK lysis was necessary.

3.4.1.2 Blood

Blood was extracted from the heart of euthanized mice. The mouse was therefore mounted on a dissection pad. An incision was made a few millimetres above the urinary orifice and was guided down the mid ventral side to the chin. Subsequently the abdominal cavity was opened up to the base of the thorax. Upon lifting the thorax, the sternum and later the diaphragm were cut open and the rib folding's were removed leading to the exposer of the thymus, lungs, and heart. A syringe with 100 µl of the anticoagulating agent Natrium-Heparin was used to puncture the right ventricle of the heart and to carefully remove as much blood as possible. The blood was collected in a 15 ml falcon which was filled with media and centrifuged for 10 minutes at 4 °C and 360 g. After the supernatant had been discarded the blood was mixed with 2 ml of ACK-Buffer and left to incubate for 3 minutes. The addition of FACS-Buffer was followed by one round of centrifugation for 10 minutes at 4 °C and 360 g. This procedure was repeated until only a small pellet of cells was left.

3.4.1.3 Skin

To isolate skin cells, the fur of a euthanized mouse was removed with a razor prior to mounting the mouse on a dissection pad. Millimetres above the urinary orifices an incision was made and guided down the mid ventral side to the chin. Two lateral incisions were then extended towards the extremities of forelimbs and hindlimbs and the skin was separated from the underlying muscular layer. The skin was removed from the mouse, placed on the mounting pad and a skin biopsy stance was used to take about 6 biopsies. These biopsies were then transferred into one well of a flat-bottom 6-well plate with 2 ml of 1xPBS supplemented with 1 mg/ml Dispase II and 50 U/ml desoxyribonuklease I (DNase I). Prior to the start of 45 minutes of incubation at 37 °C forceps and a scalpel were used to place numerous small incisions into each biopsy. To stop the digestion, 1 ml of FCS was added to each well and the biopsies were then carefully dried and subsequently transferred into 2 ml Eppendorf tubes each complemented with 300 µl Dulbecco's Modified Eagle Medium (DMEM) supplemented with 10% FCS, 800 U/ml Collagenase IV and 50 U/ml DNase I. Fine scissors were utilized to cut the samples into small pieces prior to adding another 1.5 ml of DMEM supplemented with 10% FCS, 800 U/ml Collagenase IV and 50 U/ml DNase I. An hour of incubation in a thermoshaker at 37 °C and 900 rpm was followed by the addition of 40 µl of 0.5 M EDTA and 10 more minutes of incubation at identical settings. The samples were then passed through a pre-wetted 70 µm cell strainer into a 50 ml falcon, filled up to 20 ml with 1xHBSS supplemented with 2 mM EDTA

and 0.5% Albumin Fraction V (BSA) and centrifuged for 7 minutes at 4 °C and 350 g. After the removal of the supernatant the samples were discarded and transferred into a pointed-bottom 96-well plate.

3.4.1.4 Bone Marrow

The bone marrow can be found in the hollow cavity of the bones where components of the blood are formed. For bone marrow isolation, the hindlimbs were separated with scissors from a euthanized mouse. Skin, muscles, and connective tissue were removed to expose both the tibia and femur and the end of both bones was cut off. A syringe with a 26G needle and media was used when flushing out the bone marrow from the bones. The bone marrow was collected in a 15 ml falcon, centrifuged for 10 minutes at 4 °C and 360 g and the supernatant was removed. Cells were then resuspended with 2 ml of ACK-Buffer. After 2 minutes of incubation FACS-Buffer was added and the sample was pelletized when centrifuging for 10 minutes at 4 °C and 360 g. The sample was inspected to determine whether further ACK lysis was necessary.

3.4.1.5 Tumour

B16F10-OVA or MC-38 represent experimental murine tumour models which were implanted at the right flank on the back of a mouse and were left to grow until the by the animal protection agency maximally permitted size of 1 cm diameter had been reached. At the end of the experiment the mouse was euthanized, the tumour was carefully removed from the skin using forceps and scissors and cut into small pieces on a petri dish. After transferring the tissue to a 50 ml falcon with 5 ml of dissociation buffer consisting of Roswell Park Memorial Institute (RPMI) 1640 + 2 mM L-Glutamine supplemented with 100 U/ml Collagenase Type II, 100 µg/ml DNase I and 10% FCS it was incubated for 30 minutes at 37 °C and 5% CO_2 while vigorously vortexing it every 5 to 10 minutes. The solution was then passed through a pre-wetted 70 µm cell strainer, the cell strainer was washed with MACS-Buffer and the 50 ml falcon was filled up with MACS-Buffer. Thereafter, the cells were centrifuged for 10 minutes at 4 °C and 360 g, the supernatant was discarded, and the wash step was repeated twice with MACS-Buffer before the cells were once washed with FACS-Buffer. The single cell suspension was transferred into a round-bottom 96-well plate for further analysis.

3.4.1.6 Lymph Nodes

Lymph nodes can be found throughout the body and are part of the lymphatic system. For the extraction of lymph nodes, a euthanized mouse was mounted on a dissecting pad and an incision was made millimetres above the urinary orifices and guided down the mid ventral side to the chin. Two lateral incisions were then extended towards the extremities of forelimbs and hindlimbs, the skin was separated from the underlying muscular layer and pinned on the sides. The inguinal lymph node which is located above the hind paw, slightly above the stomach was removed using bent forceps. Individual lymph nodes were analysed, whereby it was differentiated between the draining lymph node (dLN) and the non-draining lymph node (ndLN). The draining lymph node refers to the lymph node which was removed from the site where a tumour had been grown or an immunisation or vaccination had been performed. Lymph nodes referred to as non-draining lymph nodes were taken from the opposite site where no manipulation had taken place. It was passed through a pre-wetted 70 µm cell strainer with the help of a plunger, transferred to 15 ml falcons, washed with media, and centrifuged for 10 minutes at 4 °C and 360 g. Removal of the supernatant was then followed by the transfer of the cell suspension to a round-bottom 96-well plate.

3.4.1.7 Spleen, Liver, Kidney, Heart, and Lung

The heart and the lung are organs which have essential transport functions. Spleen, liver, and kidney however are mainly involved in the handling and breakdown of substances. To extract these organs, a euthanized mouse was mounted on a dissection pad and an incision that started millimetres above the urinary orifices was guided down the mid ventral side to the chin. Spleen, liver, and kidney were collected upon the opening of the abdominal cavity. To expose and extract the lung and heart, the thorax was lifted, the sternum and the diaphragm were removed as were the rib folding's. A plunger was used to pass the organs through pre-wetted 70 µm cell strainers. The cell strainer was washed with media, the cells were transferred into a 15 ml falcon and pelletized when centrifuging these for 10 minutes at 4 °C and 360 g. Resuspension of the cell pellet in 2 ml of ACK-Buffer was followed by 2 minutes of incubation and the addition of FACS-Buffer. Cells were once again centrifuged for 10 minutes at 4° C and 360 g. This procedure was repeated until most erythrocytes had been removed and the remaining cells were ready to be transferred into a round-bottom 96-well plate.

3.4.2   Flow Cytometry

Flow Cytometry is a laser- or impedance-based technology used for a multiparametric characterisation and/or separation of heterogeneous cell populations which allows for the measurement of cell fluorescence and light scattering (Cheung, K.C., *et al.*, 2010; Jahan-Tigh, R.R. *et al.*, 2012).

Fundamentals in Flow Cytometry started to emerge in 1953 when Wallace H. Coulter had developed the Coulter Counter, an apparatus used for sizing and counting particles suspended in electrolytes (Coulter, W.H., 1957; Valet, G. *et al.*, 2011). The device was later modified by Mack Fulwyler so that by 1965 the first electrostatic cell sorter had been built (Fulwyler, M.J., 1965; Müller, S., 2011). Fluorescence based Flow Cytometry was reported in 1968 by M. Van Dilla (Van Dilla, M.A., 1968; Valet, G. *et al.*, 2011) and Wolfgang Göhde (Dittrich, W. & Göhde, W., 1969; Valet, G. *et al.*, 2011). Fluorescence based cell sorting had been established by 1972 by Leonard Herzenberg (Hulett, H.R. *et al.*, 1969; Valet, G. *et al.*, 2011).

In Flow Cytometry single cell suspensions are introduced into a sheath fluid where a laminar flow is created. The cells individually pass the point of interrogation where monochromatic light from one or more lasers intersects the cells. Optics, filters, and dichroic mirrors direct the emitted light towards photomultiplier tubes (PMT). These detectors then translate the emitted light signals into electronic signals which are stored as measured data (Jahan-Tigh, R.R. *et al.*, 2012).

Optical characteristics deduced from light scattering provide information regarding the size and complexity of a cell. Forward angle light scatters (Forward Scatter) are a measure for the diffraction of light at a flat angle and correlate with cell size. Right angle scatters (Side Scatter) ascertain the refraction at a right angle and provide information regarding the structure and granularity of a cell (Jahan-Tigh, R.R. *et al.*, 2012).

At the same time, fluorescent dyes and fluorescently labelled antibodies are routinely used to deduce further information from a single cell suspension. When passing a laser, fluorescent compounds absorb light energy into a characteristic wavelength range, elevating electrons to a higher energy level. Upon returning to their resting state the fluorescence arises when fluorochromes emit light energy at a higher wavelength (Jahan-Tigh, R.R. *et al.*, 2012).

Since its first description the possibilities of cell analysis by Flow Cytometry have greatly expanded while its principles have not been significantly altered. Due to major advances in hardware technology, software tools and fluorochrome chemistry the number of concurrently measurable parameters has increased from 2 to more than 30 (Chattopadhyay, P.K. & Roeder, M., 2012; Chattopadhyay, P.K. *et al.*, 2014).

3.4.2.1 Surface Staining

For the flow cytometric analysis of various tissue samples, $1x10^6$ cells were used. In case of *in vivo* generated tumours the entire cell suspension was utilized. Cell suspensions to be stained and analyzed were transferred into an either round- or pointed-bottom 96-well plate, pelletized by centrifuging them for 10 minutes at 4 °C and 360 g and washed with 100 µl of FACS-Buffer. To prevent unspecific FC (Fragment, crystallizable) receptor binding during staining, the cells were mixed with 20 µl of CD16/CD32 Monoclonal Antibody and incubated for 15 minutes at 4 °C. Subsequently 20 µl of a mixture of the desired antibodies was added, resuspended with each sample and incubated in the dark for 30 minutes at 4 °C. The optimal concentration of the antibodies used had previously been determined. At the end of the incubation excess unbound antibodies were removed when the cells were washed with 100 µl of cold FACS Buffer while centrifuged for 10 minutes at 4 °C and 360 g. The supernatant was then discarded, the probes were resuspended in 200 µl of cold FACS-Buffer and transferred into FACS tubes. Probes were now ready for the evaluation of surface staining on the BD™ LSR II, Becton Dickinson, Mountain View, CA, USA. To properly adjust the Flow Cytometer in terms of the voltage and compensation both unstained and single stained probes had also been prepared. In case of markers highly expressed on the cell populations the antibodies utilized for the initial staining were used. Otherwise antibodies with an identical fluorescent dye and higher expression levels had to be used.

3.4.2.2 Intranuclear Staining

Prior to intranuclear staining cells were treated with the commercially available Foxp3/Transcription Factor Staining Buffer Set purchased from ThermoFisher Scientific Inc.. Cells which had been washed after surface staining were resuspended in 100 µl of Fixation/Permeabilization solution previously prepared from 1 part of the Fixation/Permeabilization Concentrate and 3 parts of the Fixation/Permeabilization Diluent.

Fixation was performed at 4 °C, lasted for at least 30 minutes and resulted in the opening of the cells nuclear pores. The cells were then twice washed with 100 µl of 1xPermeabilization Buffer (1ml 10xPermeabilization Buffer added to 9 ml ddH$_2$O) while centrifuged for 10 minutes at 4 °C and 550 g. To stain for intranuclear molecules such as cytokines or transcription factors, the supernatant was removed, and the cells were incubated in the dark for 30 minutes at 4 °C with 20 µl of a mixture of the appropriate antibodies previously prepared in 1xPermeabilization Buffer. Once again excess antibodies were removed when washing the cells with 1xPermeabilization Buffer while centrifuging them for 10 minutes at 4 °C and 550 g. After the supernatant had been removed the cells were resuspended in 200 µl of cold FACS-Buffer and transferred into FACS tubes. Probes were now ready for the simultaneous evaluation of the surface and intranuclear staining of the probes on the BD™ LSR II, Becton Dickinson, Mountain View, CA, USA.

3.4.2.3 Evaluation of Flow Cytometry Data

All Flow Cytometric Data were acquired on a BD™ LSR II, Becton Dickinson, Mountain View, CA, USA. Data was analysed with FlowJo® Version 7, Tree Star, Inc., Ashland, OR, USA.

3.4.2.4 Lymphocyte Migration and Proliferation Studies

Carboxyfluorescein succinimidyl ester (CFSE), is a fluorescein based covalent cytoplasmic dye which in Flow Cytometry is excited by the blue laser (excitation/emission: 490/520 nm). At the beginning of the 1990th, Christopher R. Parish and colleagues reported on the dyes usefulness in migration, positioning and cell division studies both *in vitro* and *in vivo*. Since then it has been extensively used in research, mainly to study lymphocyte but also fibroblast and bacterial proliferation (Weston, S.A. & Parish, C.P., 1990; Lyons, A.B. & Parish, C.R.; 1994, Parish, C.R., 1999).

Upon labelling the initially non-fluorescent dye accumulates in a cells cytoplasm where in viable cells cleavage by intracellular esterase's render the dye highly fluorescent. The dye associates with the cell via an amide bond which is formed when its succinimidyle ester moiety covalently binds to intracellular protein amine groups. As labelled cells divide, CFSE is uniformly passed on to the next generation of cells, whereby the fluorescent intensity of every subsequent generation is halved. Considerable levels of cell toxicity when labelling cells at high concentrations represent one major constraint which however can be overcome by using

considerable amounts of buffering proteins during the labelling procedure. The dye has otherwise been very popular since cells can be tracked for several months and up to 11 division steps can be detected (Parish, C.R., 1999, Parish, C.R. *et al.*, 2009; Quah, B.J.C. & Parish, C.R., 2012).

One of the major drawbacks of CFSE is that it is measured on one of the most frequently used channels in Flow Cytometry. Equally powerful dyes with different spectral properties, which also allow the simultaneous tracking of different population, have been welcomed. Such dyes include the red fluorescent Cell Proliferation Dye (CPD) eFluor 670 (excitation/emission: 647/670 nm) and Cell Trace Violet (CTV) (excitation/emission: 405/450 nm). Since their introduction to the market these dyes have become available in a great range of fluorescence's (Parish, C.R., 1999, Quah, B.J.C. & Parish, C.R., 2012).

3.4.2.5   Carboxyfluorescein Succinimidyl Ester (CSFE) Labelling

Spleens were harvested, a single cell suspension was prepared, and the cell number was determined. Cells were washed with warm 1xPBS while centrifuged for 10 minutes at 25 °C and 360 g. $1x10^8$ cells were resuspended in 3 ml of a 1 µM solution of CFSE and left to incubate for 20 minutes at 37°C and 5% CO_2. X-VIVO 20 supplemented with 10% FCS was subsequently added to the cells suspension, it was centrifuged for 10 minutes at 25 °C and 360 g and the supernatant was later discarded. Resuspension of the cell pellet in X-VIVO 20 was followed by 30 minutes of incubation at 37 °C at 5% CO_2. The cell suspension was then centrifuged for 10 minutes at 25 °C and 360 g, the cell pellet was resuspended in an appropriate amount of medium and the cell number was determined and set appropriately. While staining the cells all light sensitive reagents were protected from light. Successful CSFE staining was confirmed by Flow Cytometry.

3.4.2.6   Cell Trace Violet (CTV) Labelling

Spleens were harvested, a single cell suspension was prepared, and the cell number was determined. Cells were washed with warm 1xPBS while centrifuged for 10 minutes at 25 °C and 360 g and resuspended in 1 ml of a 0.5 µM solution of CTV per $1x10^6$ cells. The cells were left to incubate for 20 minutes at 37 °C and 5% CO_2. 4 ml of X-VIVO 20 per 1 ml of CTV were subsequently added to the cell suspension which was then incubated for another 5 minutes at room temperature. The cell suspension was then centrifuged for 10 minutes at 25 °C and 360

g, the supernatant was discarded, and the cell pellet was twice washed with X-VIVO 20 supplemented with 10% FCS and warm 1xPBS. After washing the cell number was determined and set appropriately. To allow for the acetate-hydrolysis the cells were incubated for another 10 minutes at 37 °C. While staining the cells all light sensitive reagents were protected from light. Successful CTV staining was confirmed by Flow Cytometry.

3.5 *In Vivo* Manipulation of Mice

Tumour experiments were carried out using female C57BL/6 or transgenic mice from the Jackson Laboratories, Bar Harbour, Main, USA aged between 4 and 8 weeks. Mice of different groups were age-matched. The animals were anesthetized for a variety of procedures. For anaesthesia they were shortly placed into a sealable container with a small amount of the anaesthetic Isoflurane (Forene) present.

3.5.1 Inoculation of B16F10-OVA

For tumour inoculation B16F10-OVA, under the selective pressure of G418-BC Sulfate, or MC-38 cells were detached from the 75 cm^2 cell culture flask with Trypsin-EDTA, the reaction was neutralized with medium and the cells were transferred into a 15 ml falcon. The cells were washed at least three times with 1xHBSS while centrifuged for 10 minutes at 4°C and 360 g. Determination of the cell number was followed by the adjustment of the cell density to $2x10^5/50$ µl B16F10-OVA or $1x10^6/50$ µl MC-38. The back of the mice was shaved with a razor, the mice were anesthetized, and tumour cells were subcutaneously placed at the right flank of the mouse.

3.5.2 Tumour Growth Curve

Tumour growth progression was assessed three times a week. After subcutaneous injection, tumours became visible at about seven days after inoculation. Measurements of the length and width were taken using a calliper, after any regrown fur had been removed from the back of the mouse. While taking measurements mice were shortly anesthetized. Tumour were only allowed to reach a maximum size of 1 cm. Mice whose tumours had passed that size had to be euthanized. The formula width^2 x length x 0.5 was used to calculate the tumour volume.

3.5.3 Tumour Treatment

3.5.3.1 *In Vivo* Tracking of Nanoparticles and MDL-12, 330A loaded Nanoparticles

To judge the body distribution of MDL-12, 330A loaded and empty micelles, the polymer PSar-b-PGlu(OBn) was coupled with the fluorochrome Oregon Green, and micelles were prepared. Mice were inoculated with tumours which were left to grow for 11 days. Empty or MDL-12, 330A hydrochloride loaded particles were then injected subcutaneously next to the tumour, intravenously via the tail vein or retro-orbitally. One hour or 16 hours after injection the mice were euthanized, and the organs of interest were harvested.

3.5.3.2 *In Vivo* Depletion of FoxP3^{+}Tregs using the DEREG Mouse

DEREG mice were used for the depletion of Treg. Mice were therefore intraperitoneally injected with 0.5 µg of diphtheria toxin (DT) at days 7, 12 and 18 after tumour inoculation.

3.5.3.3 *In Vivo* Depletion of Granulocytes

Granulocytes are continuously produced short lived bone marrow derived cells which are part of the adaptive immune system. To insure effective depletion, depletion antibodies have therefore to be administered on a tight schedule. One day prior to tumour inoculation mice were therefore intraperitoneally injected with 50 µg per mouse of anti-Gr-1 antibody (Clone: RB6-8C5) provided by ███████████████████████████████████████ ███████████████ On the day of tumour inoculation, the injection was repeated. To maintain the depletion, the antibody was from then on injected every second day.

3.5.4 Ovalbumin (OVA) as Model Antigen

Ovalbumin (OVA) is an easily accessible, abundant, and slightly immunogenic T cell dependent protein which was first isolated in 1889 from the egg white of a chicken's egg (Hofmeister, F., 1889). As a model antigen it was essential when the mechanism of antigen recognition, presentation and processing were elucidated (Moore, M.W. *et al.*, 1988; Carbone, F.R. & Bevan, M.J., 1989). Therefore, it has been extensively studied, and a great number of well characterized transgenic OVA mouse model and cell lines do exist (Hogquist, K.A., *et al.*, 1994; Barnden, M.J. *et al.*, 1998; Kedl, R.M. *et al.*, 2001). Nowadays OVA is often transduced in non-immunogenic tumour cell lines to study cancer immunology (Kedl, R.M. *et al.*, 2001),

used as allergen in models of acute allergic pulmonary inflammation (Kumar, R.K., *et al.*, 2008) or to evaluate the potential of novel vaccination strategies (Bellone, M. *et al.*, 2000).

3.5.4.1   Polymer Brushes

Azide functionalized polysarcosine brushes with polylysine backbone (polymerization: 250) and polysarcosine side chains (polymerization: 65) labelled with the fluorescent dye Alexa Fluor 647 were prepared. These brushes were then coupled with either or both the model antigen OVA and the nucleic-acid-based immune modulator cytosine-phosphate-guanine (CpG). Synthesis, characterization, and preparation was carried out by ████████████████████████ ██ ██████████████████████████████

Following the preparation of the polymer brushes, they were labelled with the fluorescent dye Alexa Fluor 647 and later coupled with OVA, CpG or both OVA and CpG. Upon preparation and functionalization of the polymer brushes the free dye or CpG was removed by spin-filtration while unattached OVA was removed by Gel Permeation Chromatography (GPC). Successful elimination and quantification of the dye was determined by Fluorescent Correlation Spectroscopy (FCS) while Polyacrylamide Gel Electrophoresis (PAGE) was employed to confirm that all free OVA or CpG had been removed. A combination of Ultraviolet-Visible Spectroscopy (UV-Vis) and FCS measurement was employed to determine the amount of each component present per brush. Based on the quantification of the different component on the polymer brushes the amount of polymer brushes was calculated based on and normalized to the injection of 10 µg of OVA. For each experiment the amount of soluble OVA used was 10 µg.

3.5.4.2   *In Vivo* Determination of T Cell Responses to OVA-coupled Polymer Brushes

The ability of OVA-coupled polymer brushes to raise OVA-specific T cell responses upon subcutaneous injection was evaluated employing OT-I and OT-II OVA-specific transgenic mice. Therefore, single cell suspensions of spleens of OT-I and OT-II mice were prepared and labelled with 1 µM of CFSE and 0.5 µM of CTV respectively. C57BL/6J mice were then intraperitoneally injected with each $2x10^6$ labelled OT-I and OT-II cells. Thereafter mice were subcutaneously immunized on their right flank with 1xHBSS, OVA, polymer brushes alone or coupled with OVA, CpG or OVA-CpG. Five days later mice were euthanized and the spleens, blood, draining and non-draining lymph nodes were harvested. Single cell suspensions were

prepared, stained with fluorescently labelled antibodies and the level of T cell proliferation was determined by Flow Cytometry.

3.5.4.3 *In Vivo* Tracking of Polymer Brushes

To investigate the handling of the different polymer brushes by mice, the body distribution of Alexa Fluor 647 labelled polymer brushes alone or coupled with OVA, CpG or OVA-CpG as well as commercially available Alexa Fluor 647 labelled OVA was studied. Therefore, OVA, polymer brushes alone and polymer brushes coupled with OVA or OVA-CpG were subcutaneously injected into the right flank of a mouse. Mice were euthanized 1 or 16 hours after injection. The skin, non-draining lymph nodes, draining lymph nodes, blood and spleen were harvested, single cell suspensions were prepared, and fluorescently labelled probes were analysed by Flow Cytometry.

3.5.4.4 Immunization using Polymer Brushes

For the evaluation of polymer brushes as a potential preventative measure against tumours, mice were immunized with polymer brushes alone or coupled with OVA, OVA-CpG and OVA alone. Therefore, mice were subcutaneously injected with the respective agent, on three consecutive weeks. One week later a tumour was inoculated at the site contralateral to the site of immunization, and the growth of the tumours was monitored for two weeks.

3.5.4.5 Therapeutic Treatment using Polymer Brushes

The value of polymer brushes for a potential therapeutic approach was determined. Mice were therefore inoculated with a tumour. At days 3 and 6 after tumour inoculation, OVA alone and polymer brushes with and without OVA or OVA-CpG were injected contralaterally to the tumour. Tumour growth was subsequently monitored.

3.6 Statistical Evaluation

GraphPad Prism® 6, GraPhpad Software, Inc., La Jolla, CA, USA was used for the statistical analysis of all data. Results are shown as mean ±SEM. The unpaired Student *t* test was applied to evaluate differences between 2 study groups. One-way ANOVA with post hoc Tukey

multiple comparisons test was performed when comparing >2 groups. P values of ≤0.05 denote significant changes. *P<0.05, **P<0.01, ***P<0.001, ****P<0.0001.

4. Results

### 4.1 The Effect of MDL-12, 330A hydrochloride Treatment on Tumour Growth

Studying the effect of cAMP inhibition using the adenylyl cyclase inhibitor MDL-12, 330A, both the transplantable murine melanoma model B16F10-OVA as well as the colon adenocarcinoma model MC-38 were employed. Initially, tumour growth dynamics of the B16F10-OVA and the MC-38 model were compared. Therefore, tumours were subcutaneously injected in C57BL/6J and left to grow (Figure 4.1 A). The tumour growth curve and volume of both B16F10-OVA and MC-38 developed evenly and could be in both cases followed for up to 15 days after implantation. Furthermore, mice inoculated with either tumour displayed identical Kaplan-Meier plots (Figure 4.1 B). The cAMP content of the skin as well as B16F10-OVA and MC-38 *in vivo* grown tumours was determined by ELISA. In contrast to both the skin and MC-38, B16F10-OVA did display significantly increased levels of cAMP (Figure 4.1 C).
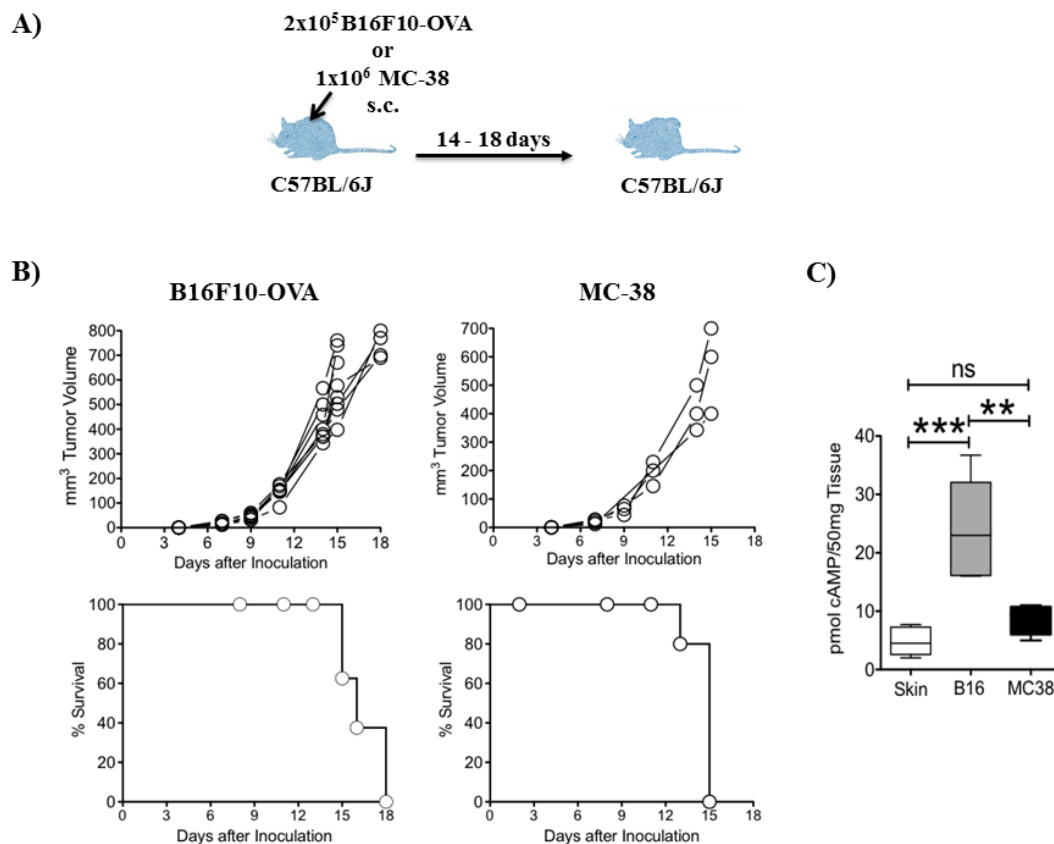
Figure 4.1   Subcutaneous growth and intracellular cAMP levels of B16F10-OVA and MC-38.

A) Schematic representation of the experimental setup. 2×10^5 B16F10-OVA or 1×10^6 MC-38 were subcutaneously (s.c.) injected at the right flank of C57BL/6J. Tumour growth progression was assessed three times a week using a digital calliper. Mice were sacrificed due to poor health or at 1 cm^2 tumour dimensions. **B)** Representative growth curves and Kaplan-Meier plots. **C)** Intracellular cAMP levels at day 14 after tumour implantation. For cAMP measurements, tumours at day 14 after inoculation and skin were excised, weighted, and stored at -80 °C. Upon tissue lysis, a cAMP specific Enzyme-linked Immunosorbant Assay (ELISA) was employed to determine the cAMP content. Results are shown as mean±SEM *P<0.05, **P<0.01, ***P<0.001, ****P<0.0001. ns: not significant.

With the intent of decreasing the extraordinarily high levels of cAMP measured in both *in vivo* and *in vitro* grown B16F10-OVA, B16F10-OVA was treated *in vitro* with subtoxic levels of MDL-12, 330A hydrochloride. Subsequently its effect on the cAMP content and cell proliferation were determined (Figure 4.2 A). MDL-12, 330A hydrochloride, a hydrophobic cell-permeable inhibitor capable of irreversibly blocking all adenylyl cyclases (Figure 4.2 B), was able to drastically lower cAMP levels *in vitro* (Figure 4.2 C) while not impacting on their capacity to proliferate (Figure 4.2. D).
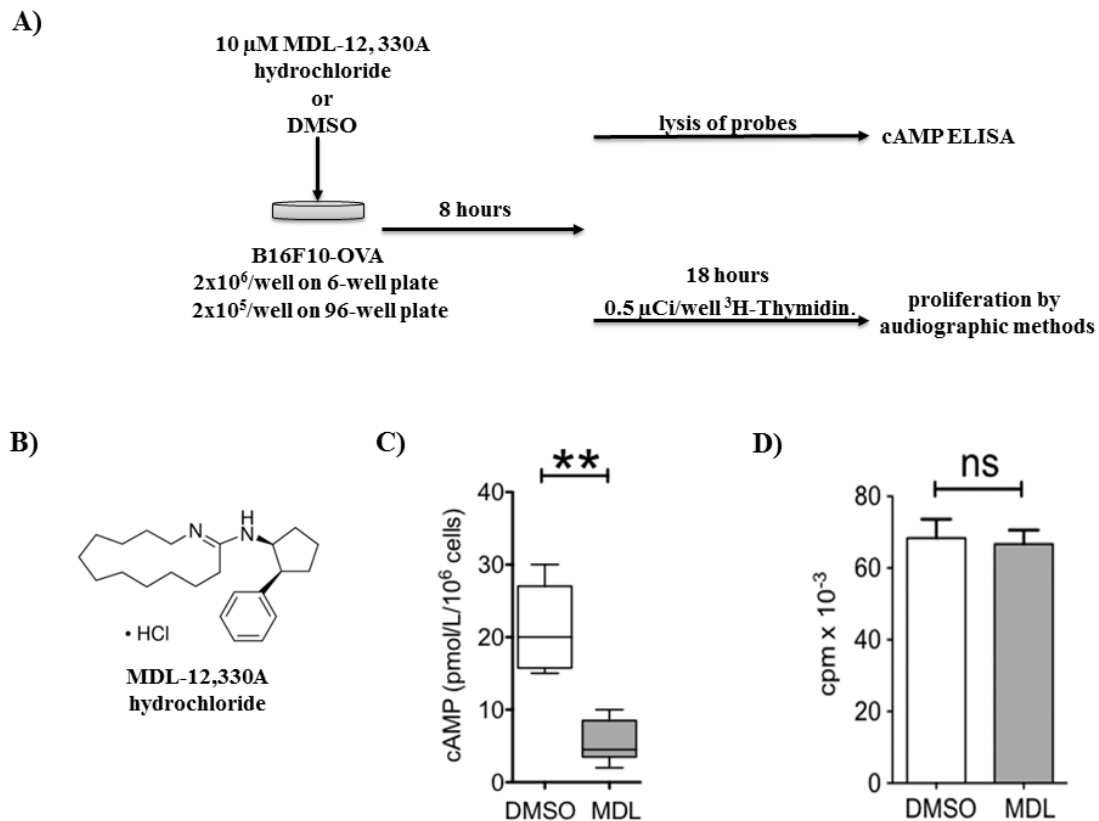
Figure 4.2   MDL-12, 330A hydrochloride reduces the intracellular cAMP content in B16F10-OVA without affecting proliferation.

A) Schematic representation of the experimental setup. B16F10-OVA were plated out at a concentration of $2x10^6$ cells/per well in a 6-well plate or at $2x10^5$ cells per well in a flat-bottom 96-well plate. They were kept at 37 °C and 5% CO_2 until they started to attach to the plastic dish. The cells were then incubated for 8 hours with 10 µM MDL-12, 330A hydrochloride or an equivalent amount of dimethyl sulfoxide (DMSO). To later determine the cells cyclic adenosine monophosphate (cAMP) content by Enzyme-linked Immunosorband Assay (ELISA), the cells were harvested, counted, pelletized, and stored at -80 °C. Proliferation was determined by autoradiographic methods following 18 hours of incubation after the addition of 0.5 µCi/well ^{3}H-Thymidin. **B)** Representation of the structural formula of the adenylyl cyclase inhibitor MDL-12, 330A hydrochloride. **C)** Intracellular cAMP content of B16F10-OVA in presence of MDL-12, 330A hydrochloride or its solvent. **D)** Proliferation of B16F10-OVA in presence of MDL-12, 330A or its solvent DMSO. Results are shown as mean±SEM. *P<0.05, **P<0.01, ***P<0.001, ****P<0.0001. ns: not significant; MDL: MDL-12, 330A hydrochloride.

Having established that *in vitro* subtoxic levels of MDL-12, 330A hydrochloride efficiently interferes with the cAMP pathway while not affecting cellular functions, it was applied towards B16F10-OVA and MC-38 subcutaneously implanted in C57BL/6J (Figure 4.3 A). As melanomas are easily accessible and due to concerns that systemic application of MDL-12, 330A hydrochloride would result in adverse effects elsewhere, peritumoral injection of the inhibitor was chosen as the route of administration. Repeated local injection of MDL-12, 330A hydrochloride at the tumour site resulted in a significantly reduced tumour burden. In contrast, MDL-12, 330A hydrochloride had no effect on MC-38, a tumour virtually devoid of cAMP. As previously established *in vitro*, DMSO, the solvent of the hydrophobic MDL-12, 330A hydrochloride, did not display any unfavourable effects towards cellular functions (Figure 4.3 B).
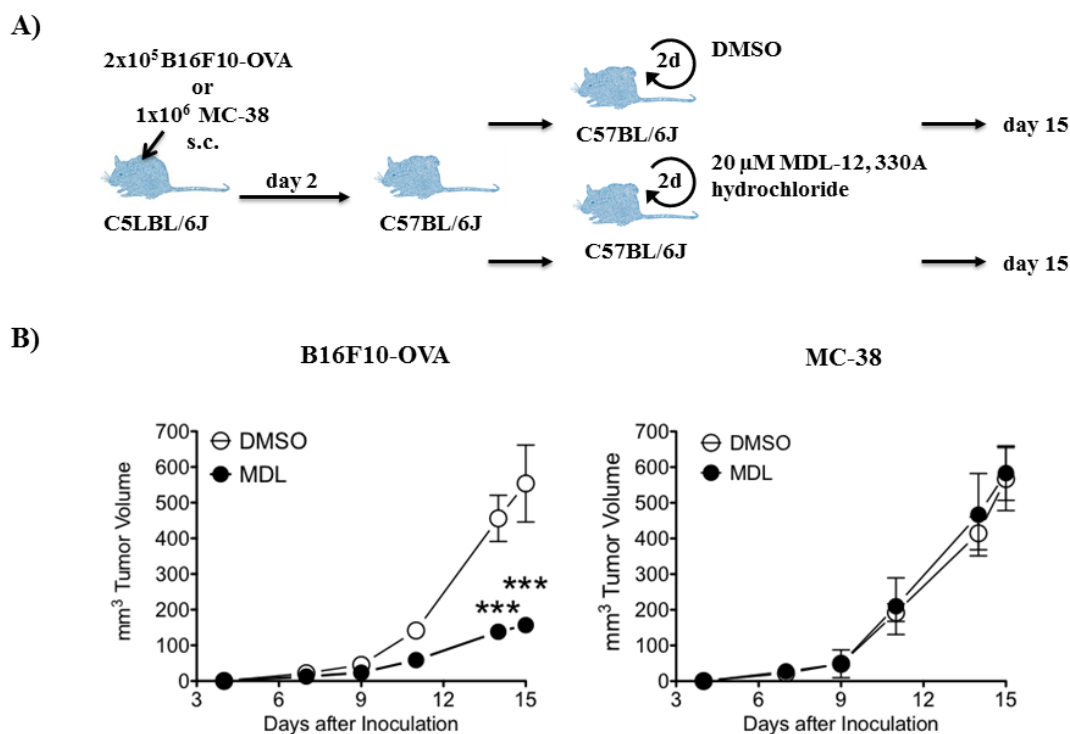
Figure 4.3   Peritumoral MDL-12, 330A hydrochloride injection reduces B16F10-OVA but not MC-38 tumour growth.

A) Schematic representation of the experimental setup. $2x10^5$ B16F10-OVA or $1x10^6$ MC-38 were subcutaneously (s.c.) injected at the right flank of C57BL/6J. Three times a week, tumours were treated with subcutaneous injections of 20 µM MDL-12, 330A hydrochloride/50µl or an equivalent amount of dimethyl sulfoxide (DMSO) at the site of tumour inoculation. Tumour growth progression was assessed at the same time using a digital calliper. Mice were sacrificed due to poor health or upon the tumour reaching 1 cm^2 tumour dimensions. **B)** Tumour growth curves for B16F10-OVA and MC-38 upon treatment with DMSO or MDL-12, 330A hydrochloride. Results are shown as mean±SEM *P<0.05, **P<0.01, ***P<0.001, ****P<0.0001. d: day, days; MDL: MDL-12, 330A hydrochloride.

4.2   *In Vitro* and *In Vivo* testing of novel MDL-12, 330A hydrochloride loaded Micelles

To achieve a controlled and locally restricted release but also to circumvent unfavourable properties of MDL-12, 330A hydrochloride, water soluble drug loaded or empty micelles with a hydrophilic shell and a hydrophobic core were prepared from the polypeptoid-*block*-polypeptide copolymer polysacrcosine-*block*-polyglutamatic acid bezylester (PSar-b-PGlu(OBn)) and the hydrophobic drug (Figure 4.4 A). The inhibitor was passively incorporated when PSar-b-PGlu(OBn) was subjected to dual asymmetric centrifugation in the presence or absence of MDL-12, 330A hydrochloride (Figure 4.4 B). Absence of any non-encapsulated adenylyl cyclase inhibitor was assured by spin filtration while Reverse-Phase High Performance Liquid Chromatography (RP-HPLC) was carried out to determine actual drug loading (Figure 4.4 C). MDL-12, 330A hydrochloride loaded micelles were found to have a 60% loading efficiency, a

reproducible 9% drug load and a hydrodynamic radius of an average diameter of around 76 nm. The hydrodynamic radius of empty micelles was determined to be on average 182 nm. Besides it was shown that loaded and non-loaded micelles could be lyophilized and later be reconstituted with an average shelf life of above 3 months.
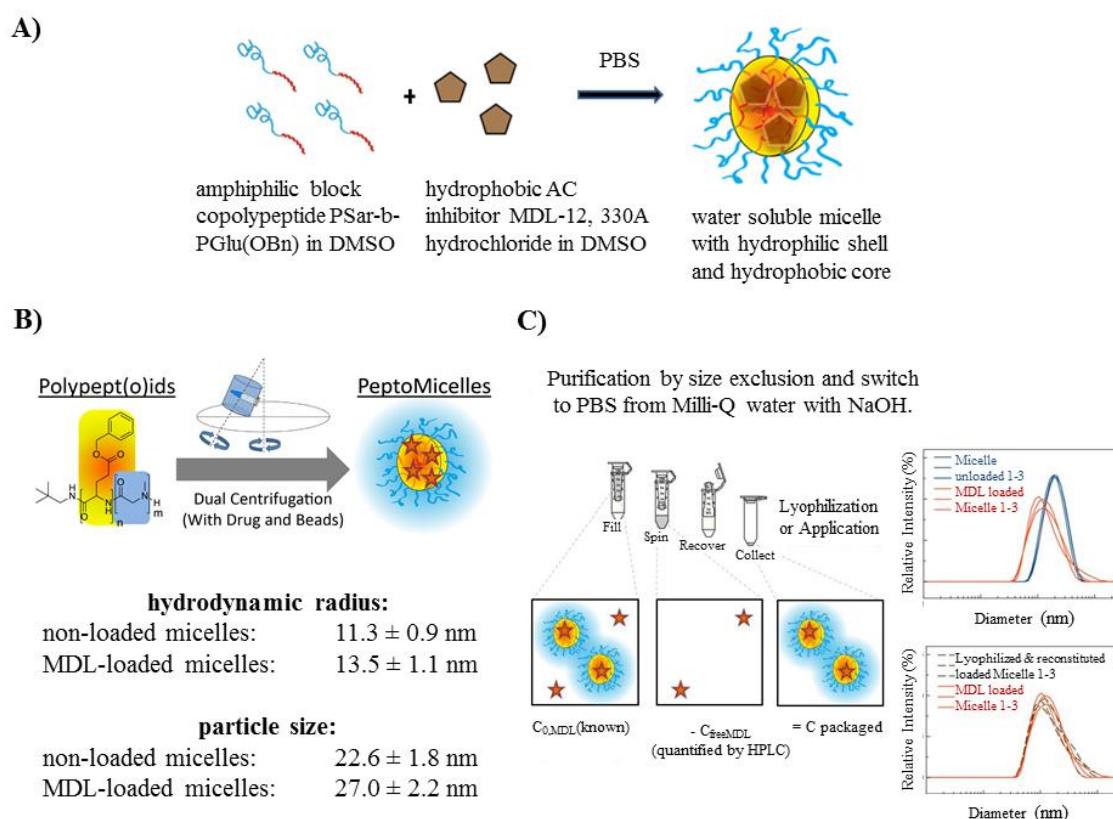
Figure 4.4   Manufacturing and loading of polymer micelles with MDL-12, 330A hydrochloride.

A) Schematic representation of the components of MDL-12, 330A hydrochloride loaded micelles. The amphiphilic peptide based polypeptoid-*block*-polypeptide copolymer polysacrcosine-*block*-polyglutamatic acid bezylester (PSar-b-PGlu(OBn)) and the hydrophilic adenylyl cyclase inhibitor MDL-12, 330A hydrochloride were used for the preparation of empty and MDL-12, 330A hydrochloride loaded micelles. **B)** Schematic representation of the manufacturing of MDL-12, 330A hydrochloride loaded micelles. MDL-12, 330A hydrochloride loaded micelles were prepared by dual centrifugation upon vigorous mixing of the polymer and the drug. **C)** Schematic representation of the purification of micelles and the quantification of its MDL-12, 330A hydrochloride content. Free MDL-12, 330A hydrochloride was separated from the resulting solution by spin filtration. To quantify the amount of MDL-12, 330A hydrochloride encapsulated in the micelles, samples of the filtrate were subjected to Reverse Phase-High-Performance Liquid Chromatography (RP-HPLC). Portions of the purified micellar solution were lyophilized for the determination of the total mass concentration. AC: adenylyl cyclase; C: concentration; DMSO: dimethyl sulfoxide; MDL: MDL-12, 330A hydrochloride; PBS: phosphate buffered saline. Graphic provided by ███

Empty and MDL-12, 330A hydrochloride loaded micelles were tested *in vitro* regarding their ability to properly release the inhibitor and subsequently repress intracellular cAMP levels. Therefore, B16F10-OVA were incubated with toxic and subtoxic levels of MDL-12, 330A hydrochloride loaded micelles and its effect on the intracellular cAMP content and cell viability was determined (Figure 4.5 A). In contrast to empty micelles, cAMP measurements by ELISA revealed a continuous, nearly linear dose dependent decrease of cAMP levels as a result of the cells short incubation with inhibitor loaded micelles (Figure 4.5 B). Upon a prolonged period of incubation cell viability and morphology were inspected. While toxic levels of MDL-12, 330A hydrochloride released from the micelles proved lethal, no adverse effects could be observed upon the cells incubation with empty particles (Figure 4.5 B). *In vitro* testing of the newly prepared micelles revealed that they were able to efficiently released the inhibitor. Components used for particle preparation proved non-toxic and did not interfere with cellular functions. Furthermore, it could be deduced that processes employed during particle preparation did not alter the function of MDL-12, 330A hydrochloride.
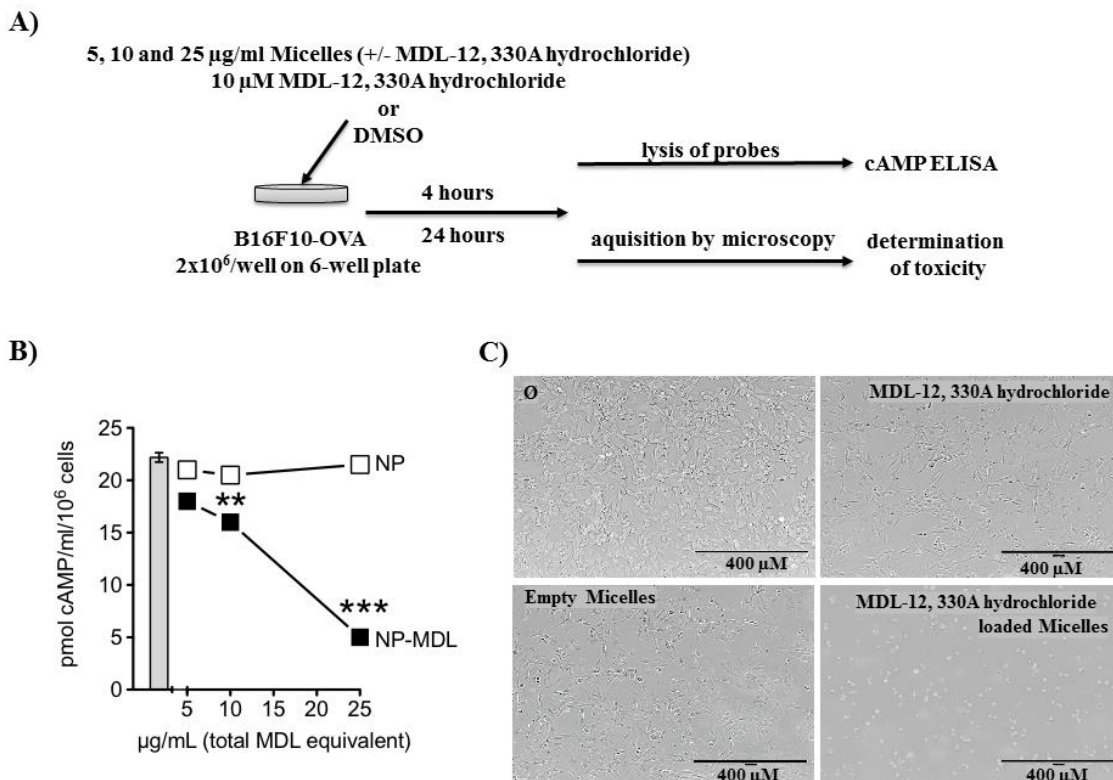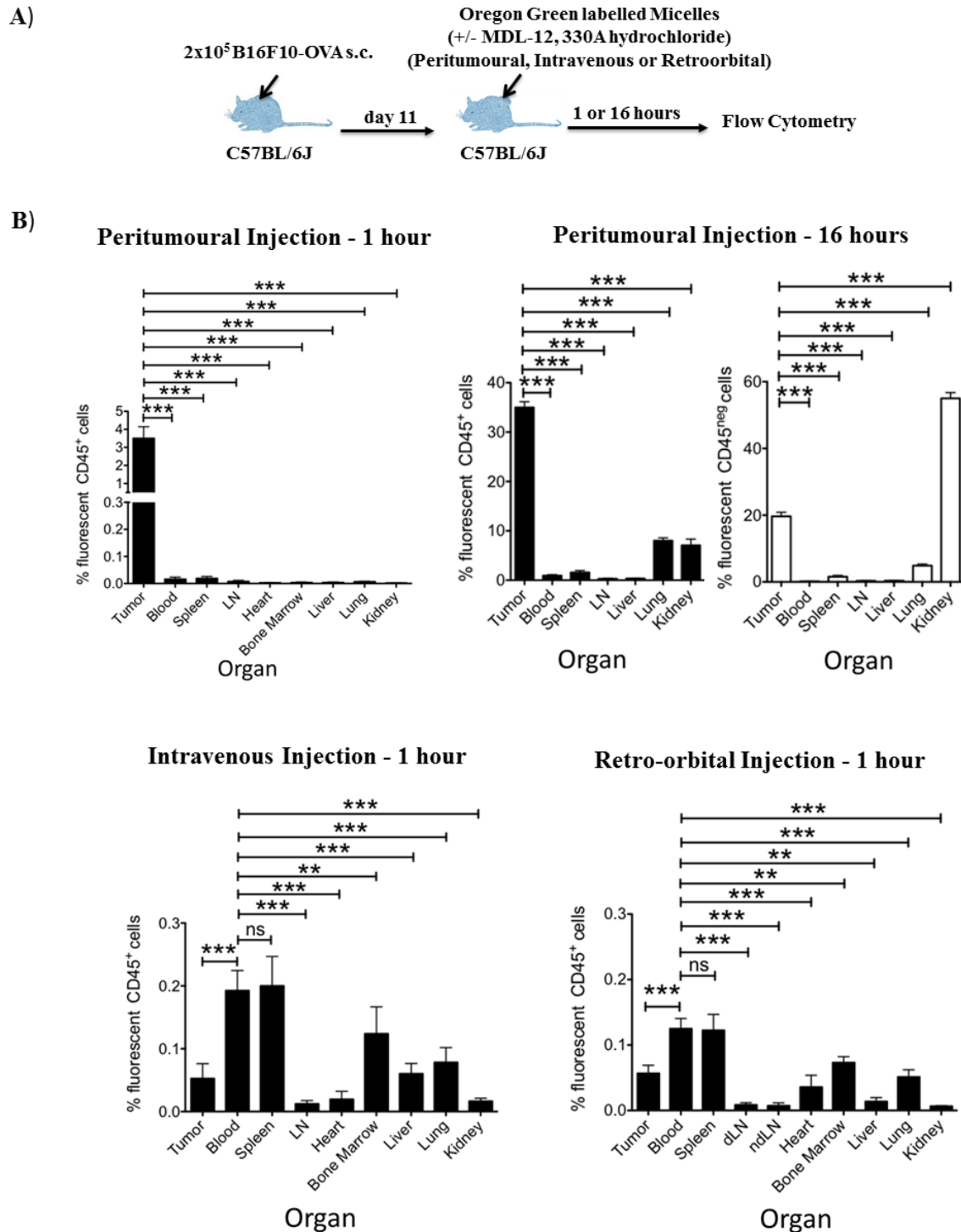
Figure 4.5   MDL-12, 330A hydrochloride loaded micelles repress cAMP production *in vitro*.

A) Schematic representation of the experimental setup. B16F10-OVA were plated out at a concentration of 2×10^6 cells/per well in a flat-bottom 6-well plate and kept at 37 °C and 5% CO^2 until they started to attach to the plastic dish. The cells were incubated for 4 hours with 5, 10 or 25 µg/ml of MDL-12, 330A hydrochloride loaded micelles and the equivalent of empty micelles determined based on their total mass concentration. To later determine the cells cyclic adenosine monophosphate (cAMP) content by Enzyme-linked Immunosorband Assay (ELISA), the cells were harvested, counted, pelletized, and stored at -80 °C. B16F10-OVA were furthermore incubated overnight without any agent, 25 µg/ml of MDL-12, 330A hydrochloride loaded micelles, the equivalent of empty micelles or 10 µM of MDL-12, 330A hydrochloride. Cell viability was determined and documented using the EVOSfl Fluorescence Microscope from AMG. **B)** Graphic representation and statistical evaluation (t-test) of the cAMP ELISA data from B16F10-OVA treated with different concentrations of empty and MDL-12, 330A hydrochloride loaded micelles. **C)** Microscopy images of B16F10-OVA incubated over night with DMSO, MDL-12, 330A hydrochloride, empty micelles and MDL-12, 330A hydrochloride loaded micelles. Results are shown as mean±SEM *$P<0.05$, **$P<0.01$, ***$P<0.001$, ****$P<0.0001$. DMSO: dimethyl sulfoxide; MDL: MDL-12, 330A hydrochloride; NP: nanoparticle; NP-MDL: nanoparticle loaded with MDL-12, 330A hydrochloride.

Since the particles likely redistribution into other tissues it is critical, with regard to its potential application, to be aware of its fate. Its distribution was tracked by flow cytometric analysis of fluorescently labelled empty or MDL-12, 330A hydrochloride loaded micelles at 1 or 16 hours upon peritumoral and at 1 hour after retro-orbital or intravenous application into tumour bearing C57BL/6J (Figure 4. 6A). It became apparent that regardless of the route chosen for systemic venous administration, MDL-12, 330A hydrochloride loaded or empty micelles in case of the heart, liver, kidney, lung, PECs, draining or non-draining lymph node associated with much less than 0.1% of viable CD45$^+$ cells. This was different for the blood, spleen, bone marrow and tumour where more than 0.1% of viable CD45$^+$ cells associated with the micellar formulation. In case of all organs investigated, empty and loaded micelles did however not significantly associate with viable CD45$^-$ cell. Upon peritumoral injection of the fluorescently labelled empty or inhibitor loaded micelles, at 1 hour at the tumour site, non to negligible amounts of particles had associated with viable CD45$^-$ or CD45$^+$ cells in the blood, heart, liver, kidney, spleen, bone marrow, PECs, lung as well as the draining and non-draining lymph node. In the tumour however less than 0.01% of viable CD45$^+$ cells and about 1% of CD45$^-$ cells did associate with the micelles. At a later timepoint, 16 hours after peritumoral injection of micelles, the number of micelles associated to viable CD45$^+$ and CD45$^-$ had significantly increased at the tumour site. In contrast to all other organs, increased association of viable CD45$^+$ cells with micelles was also the case for the lung and the kidney, whereby the overall increase of micelles associated to the kidney was most prominent (Figure 4.6 B). As systemic venous application of MDL-12, 330A hydrochloride loaded or empty micelles did not result in its preferential

accumulation at the tumour site it was deemed unfavourable for the intended application. Instead peritumoral injection seems favourable due to it amassing at the tumour site over time and its redistribution towards the kidney, implying the particles route of excretion.

Figure 4.6   **Body distribution of MDL-12, 330A hydrochloride loaded micelles and empty micelles following peritumoral, intravenous or retro-orbital injection.**

A) Schematic representation of the experimental setup. $2x10^5$ B16F10-OVA were subcutaneously (s.c.) injected at the right flank of C57BL/6J and left to grow for 11 days. Empty and MDL-12, 330A loaded micelles coupled with the fluorophore Oregon Green had been prepared and were subcutaneously injected at the tumour site, intravenously or retro-orbitally. 20 µM of MDL-12, 330A hydrochloride loaded micelles/50 µl and the equivalent of an empty micelle based on the particles mass concentration were used for the experiments. Upon injection of the particle, 1 or 16 hours were allowed to pass until the mice were euthanized and the blood, heart, liver, kidney, spleen, bone marrow, peritoneal exudate cells (PECs), lung, tumour, draining lymph node (dLN) and non-draining lymph node (ndLN) were harvested. Single cell suspensions were prepared and labelled with fluorescently labelled antibodies against CD45 and acquired by Flow Cytometry. Dead cells were excluded using Fixable Viability Dye. **B)** Graphic representation and statistical evaluation (t-test) of the association of Oregon Green labelled empty and MDL-12, 330A loaded micelles after 1 or 16 hours upon peritumoral, intravenous or retro-orbital injection. Results are shown as mean±SEM *P<0.05, **P<0.01, ***P<0.001, ****P<0.0001. LN: lymph node; ns: not significant.

Now that peritumoral application of MDL-12, 330A hydrochloride loaded micelles made from PSar-b-PGlu(OBn) was deemed favourable and since in case of melanoma this route of application is feasible, peritumoral injection of empty or drug loaded micelles was applied towards an earlier defined *in vivo* experimental regiment of tumour reduction in the context of B16F10-OVA (Figure 4.7 A). As previously established, treatment of B16F10-OVA with MDL-12, 330A hydrochloride did result in significantly reduced tumour volumes when compared to tumours treated with its polar solvent DMSO. No significant difference in terms of reduced tumour volume or survival when comparing tumour volume upon treatment with free or encapsulated MDL-12, 330A hydrochloride could however be observed. While encapsulation of MDL-12, 330A hydrochloride did not improve tumour reduction, treatment of tumours with empty micelles did however also not seem to cause any adverse or toxic side effects (Figure 4.7 B; Figure 4.7 C).
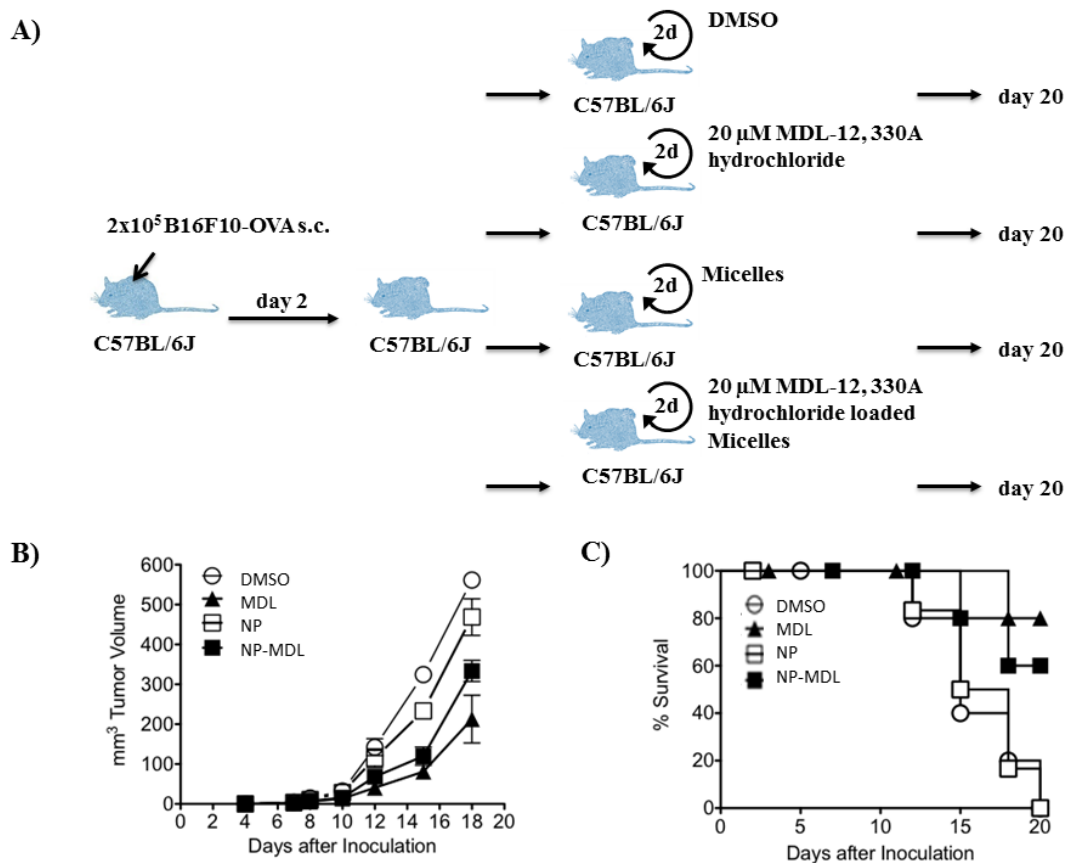
Figure 4.7   B16F10-OVA growth curve upon treatment with MDL-12, 330A hydrochloride loaded or empty micelles.
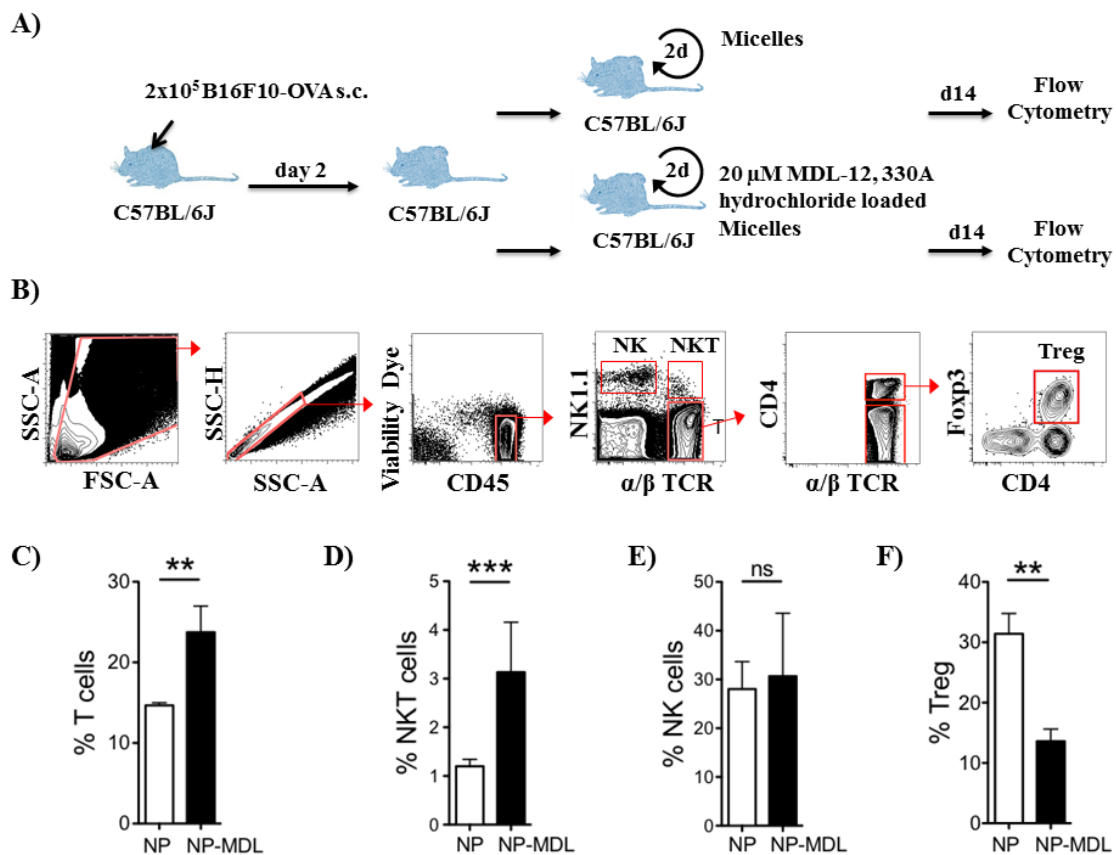
A) Schematic representation of the experimental setup. $2x10^5$ B16F10-OVA were subcutaneously (s.c.) injected at the right flank of C57BL/6J. Three times a week, tumours were treated with subcutaneous injections at the site of tumour inoculation of 20 µM MDL-12,330A hydrochloride /50µl, an equivalent amount of dimethyl sulfoxide (DMSO), 20 µM of MDL-12, 330A hydrochloride loaded micelles/50 µl and the equivalent of an empty micelle based on the particles mass concentration. **B)** Tumour growth curve of B16F10-OVA upon treatment with DMSO, MDL-12, 330A hydrochloride, empty and MDL-12, 330A hydrochloride loaded micelles. Tumour growth progression was assessed at the same time using a digital calliper. Mice were sacrificed due to poor health or upon the tumour reaching or passing the maximum tumour dimensions of 1 cm^2 **C)** Kaplan-Meier plots for mice with B16F10-OVA tumours treated with DMSO, MDL-12, 330A hydrochloride, empty and MDL-12, 330A hydrochloride loaded micelles. Results are shown as mean±SEM *P<0.05, **P<0.01, ***P<0.001, ****P<0.0001. d: day, days; MDL: MDL-12, 330A hydrochloride; NP: nanoparticle; NP-MDL: nanoparticle loaded with MDL-12, 330A hydrochloride.

4.3   Effect of MDL-12, 330A hydrochloride loaded Micelles on the Immune Cell Content of B16F10-OVA

In vivo treatment of the murine melanoma B16F10-OVA with the adenylyl cyclase inhibitor MDL-12, 330A hydrochloride resulted in a significant decrease of the tumour growth rate and supposedly a reduction of the tumours cAMP content. To elucidate mechanisms which could explain or add towards an understanding of these observations the immune cell content of an

end stage B16F10-OVA melanoma was systematically investigated upon its treatment with empty or MDL-12, 330A hydrochloride loaded micelles (Figure 4.8 A, Figure 4.9 A, Figure 4.10 A, Figure 4.11 A).

Flow Cytometric analysis of the immune cell content of murine end stage B16F10-OVA treated with MDL-12, 330A hydrochloride loaded or empty micelles regarding the composition of the T cell compartment revealed that inhibition of the adenylyl cyclases resulted in a significant increase of T cells (viable $CD45^+NK1.1^-TCRß^+$) (Figure 4.8 C) and Natural Killer T (NKT) (viable $CD45^+TCRß^+NK1.1^+$) (Figure 4.8 D) cells into the tumour. No numerical changes in terms of Natural Killer (NK) (viable $CD45^+NK1.1^+$) cells could be observed in MDL-12, 330A hydrochloride treated when compared to untreated tumours (Figure 4.8 E). In contrast to the prominent increase in T and NKT cells, a significant decrease of Tregs (viable $CD45^+NK1.1^-$ $TCRß^+CD4^+Foxp3^+$) was noted in the tumour tissue when treated with MDL-12, 330A hydrochloride loaded micelles (Figure 4.8 F).

Figure 4.8   Local micelle-based cAMP repression alters the tumour immune cell infiltrate (I).

A) Schematic representation of the experimental setup. 2×10^5 B16F10-OVA were subcutaneously (s.c.) injected at the right flank of C57BL/6J. Three times a week, tumours were treated with subcutaneous injections at the site of tumour inoculation of 20 µM of MDL-12, 330A hydrochloride loaded micelles/50 µl or the equivalent of an empty micelle based on the particles mass concentration. Mice were sacrificed 14 days after tumour inoculation and tumours were harvested. Single cell suspensions were stained with fluorescently labelled antibodies against CD45, the beta chain of the alpha/beta T cell receptor (TCR β), NK1.1, CD4 and the transcription factor forkhead box P3 (Foxp3). The number of T (CD45$^+$NK1.1$^-$TCRβ$^+$), Natural Killer T (NKT) (CD45$^+$TCRβ$^+$NK1.1$^+$), Natural Killer (NK) (CD45+NK1.1+) and regulatory T (Treg) (CD45$^+$NK1.1$^-$TCRβ$^+$CD4$^+$Foxp3$^+$) cells were determined by Flow Cytometry. Dead cells were excluded using Fixable Viability Dye. **B)** Gating strategy for different subsets of the T cell compartment. Graphic representation and statistical evaluation (t-test) of **C)** T cells, **D)** NKT cells, **E)** NK cells, **F)** Tregs in the tumour with and without treatment with MDL-12, 330A hydrochloride. Results are shown as mean±SEM $*P<0.05$, $**P<0.01$, $***P<0.001$, $****P<0.0001$. d: say, days; FSC-A: Forward Scatter Area; NP: nanoparticle; NP-MDL: nanoparticle loaded with MDL-12, 330A hydrochloride; ns: not significant; SSC-A: Side Scatter Area; SSC-H: Side Scatter Hight.

The functional state of CD4$^+$ (viable CD45$^+$NK1.1$^-$TCRß$^+$CD4$^+$) and CD8$^+$ (viable CD45$^+$NK1.1$^-$TCRß$^+$CD8$^+$) cells upon treatment of B16F10-OVA with MDL-12, 330A hydrochloride loaded and empty micelles was investigated by assessing the production of IFN-γ and Killer cell lectin-like receptor subfamily G member 1 (KLRG-1) (Figure 4.9 A). While the treatment did not affect the IFN-γ production in CD4$^+$ cells, it was significantly decreased in CD8$^+$ cells (Figure 4.9 B). The expression of KLRG-1 was however greatly reduced in both the CD4$^+$ and CD8$^+$ compartment when treated with MDL-12, 330A hydrochloride (Figure 4.9 C).
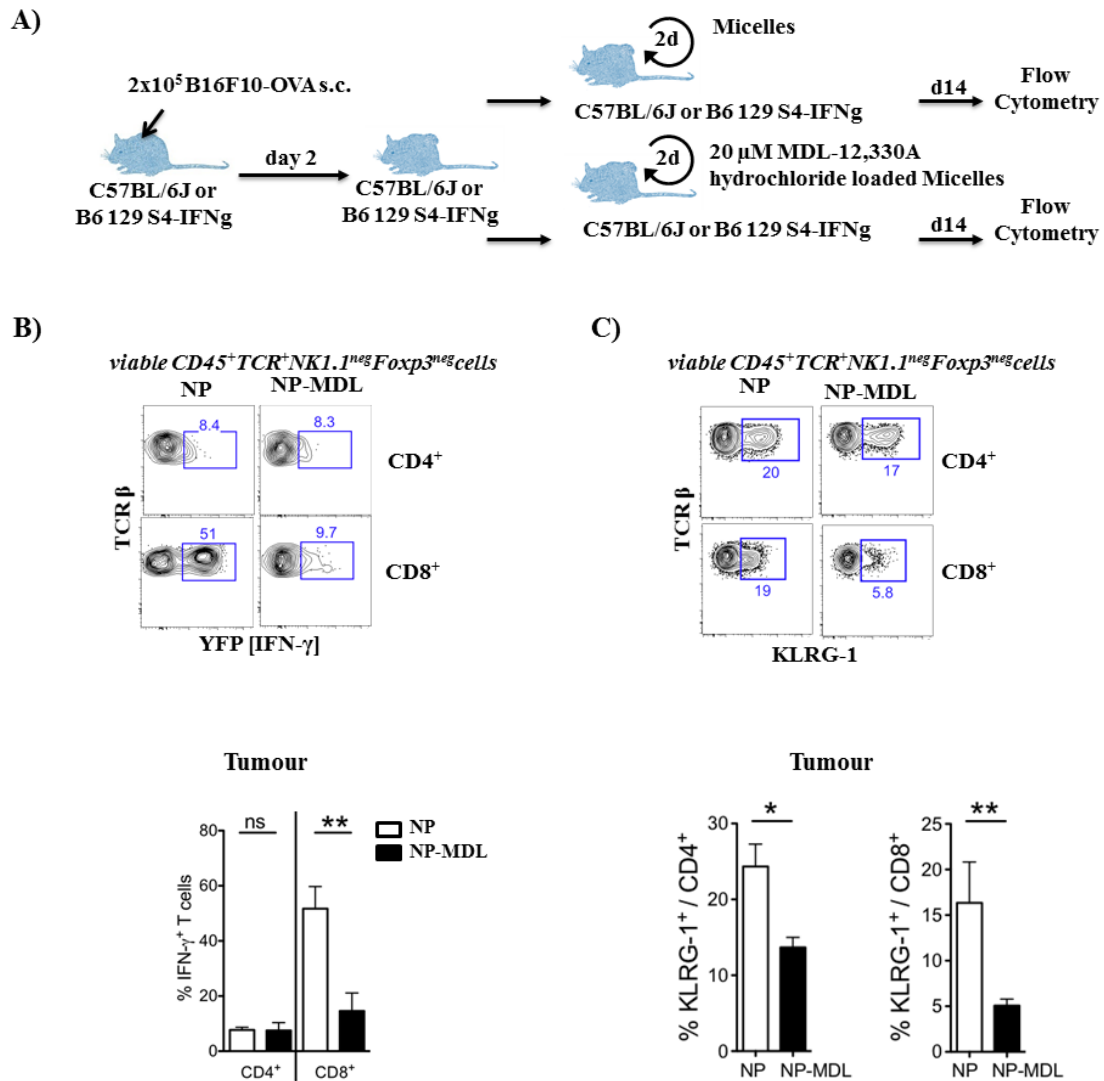
Figure 4.9 **Local micelle-based cAMP repression alters the tumour immune cell infiltrate (II).**

A) Schematic representation and experimental setup. 2×10^5 B16F10-OVA were subcutaneously injected at the right flank of B6 129 S4-IFNg or C57BL/6J. Three times a week, tumours were treated with subcutaneous (s.c.) injections at the site of tumour inoculation of 20 µM of MDL-12, 330A hydrochloride loaded micelles/50 µl or the equivalent of an empty micelle based on the particles mass concentration. Mice were sacrificed 14 days after tumour inoculation and tumours were harvested. Single cell suspensions were stained with fluorescently labelled antibodies against CD45, the beta chain of the alpha/beta T cell receptor (TCRβ), NK1.1, CD4, the transcription factor forkhead box P3 (Foxp3) and Killer cell lectin-like receptor subfamily G member 1 (KLRG-1). The number of Interferon -gamma (IFN-γ) producing CD4 (CD45+NK1.1-TCRβ+CD4+Foxp3-IFN-γ+), IFN-γ producing CD8+ (CD45+NK1.1-TCRβ+CD4-Foxp3-IFN-γ+), KLRG-1+CD4+ (CD45+NK1.1-TCRβ+CD4+Foxp3-KLRG-1+) and KLRG-1+CD8+ (CD45+NK1.1-TCRβ+CD4-KLRG-1+) cells were determined by Flow Cytometry. Dead cells were excluded using Fixable Viability Dye. **B)** Representative contour plots, graphic representation, and statistical evaluation (t-test) of data from the analysis of B16F10-OVA tumours treated with empty and MDL-12, 330A hydrochloride loaded micelles regarding IFN-γ producing and **C)** KLRG-1 expressing CD4+ and CD8+ T cells. Results are shown as mean±SEM. *P<0.05, **P<0.01, ***P<0.001, ****P<0.0001. d: day, days; neg: negative; NP: nanoparticle; NP-MDL: nanoparticle loaded with MDL-12, 330A hydrochloride ns: not significant; YFP: yellow fluorescent protein.

Next to the T cell compartment, it was probed weather upon treatment of B16F10-OVA with MDL-12, 330A hydrochloride loaded or empty micelles, there were apparent changes in the myeloid compartment. Flow cytometric analysis of the CD45$^+$Lin(CD3, CD45R/B220, NK1.1)$^-$ CD11c$^-$CD11b$^+$Ly6G$^+$ (Figure 4.10 B) revealed that upon tumour treatment the number of neutrophils/granulocytes significantly decreased (Figure 4.10 C).
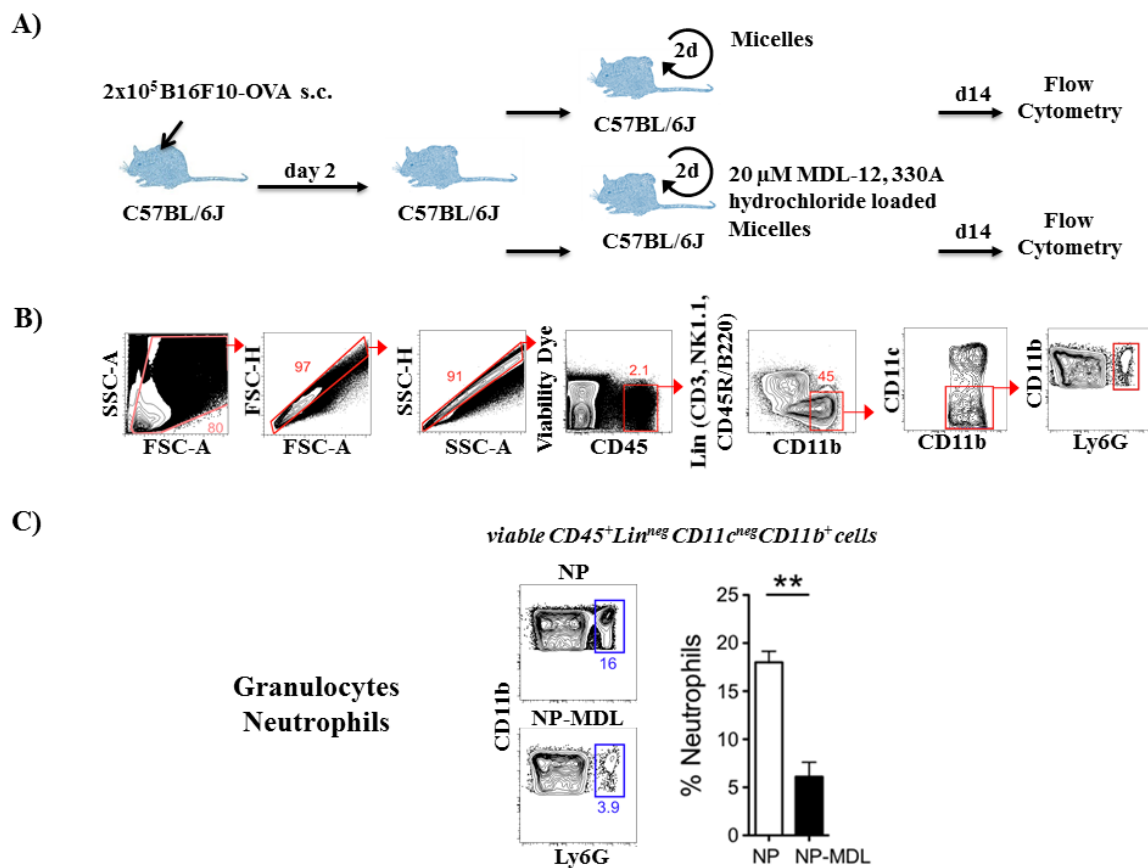
Figure 4.10   Local micelle-based cAMP repression alters the tumour immune cell infiltrate (III).

A) Schematic representation of the experimental setup. 2x10^5 B16F10-OVA were subcutaneously (s.c.) injected at the right flank of C57BL/6J. Three times a week, tumours were treated with subcutaneous injections at the site of tumour inoculation of 20 µM of MDL-12, 330A hydrochloride loaded micelles/50 µl or the equivalent of an empty micelle based on the particles mass concentration. Mice were sacrificed 14 days after tumour inoculation and tumours were harvested. Single cell suspensions were stained with fluorescently labelled antibodies against CD45, CD11b, CD11c, Ly6G and the lineage markers CD3, CD45R/B220 and NK1.1. The number of granulocytes/neutrophils (CD45$^+$Lin (CD3, CD45R/B220, NK1.1)$^-$CD11c$^-$CD11b$^+$Ly6G$^+$) was determined by Flow Cytometry. Dead cells were excluded using Fixable Viability Dye. **B)** Gating strategy for the evaluation of granulocytes/neutrophils. **C)** Representative contour plots, graphic representation, and statistical evaluation (t-test) of data from the analysis of B16F10-OVA treated with empty and MDL-12, 330A hydrochloride loaded micelles regarding granulocytes/neutrophils. Results are shown as mean±SEM. *P<0.05, **P<0.01, ***P<0.001,

****P<0.0001. d; day, days; FSC-A: Forward Scatter Area; FSC-H: Forward Scatter Hight; Lin: lineage; neg: negative; NP: nanoparticle; NP-MDL: nanoparticle loaded with MDL-12, 330A hydrochloride, SSC-A: Side Scatter Area; SSC-H: Side Scatter Hight; MDL: MDL-12.

Furthermore, the functional state of these myeloid tumour infiltrating lymphocytes (TILs) was determined by studying the endogenous expression of the GFP-tagged orphan nuclear receptor Nr4a1 (Nur77) using the Nur77 mouse. With the help of the differential expression of both Nur77 and Ly6C, it is thus possible to distinguish between patrolling (Ly6C^{low}Nur77$^+$) and inflammatory (Ly6C^{high}Nur77) monocytes (Moran, A.E. *et al.*, 2011; Hanna, R.N. *et al.*, 2012). Treatment of B16F10-OVA with MDL-12, 330A hydrochloride resulted in a shift from the number of patrolling monocytes (CD45$^+$Lin(CD3, CD45R/B220, NK1.1, Ly6G)$^-$ CD11b$^+$CD115$^+$Ly6C^{low}Nur77l$^+$) in untreated tumours to an increase in the number of inflammatory monocytes (CD45$^+$Lin (CD3, CD45R/B220, NK1.1, Ly6G)$^-$ CD11b$^+$CD115$^+$Ly6C^{high}Nur77l$^-$) (Figure 4.11 B, Figure 4. 11 C).
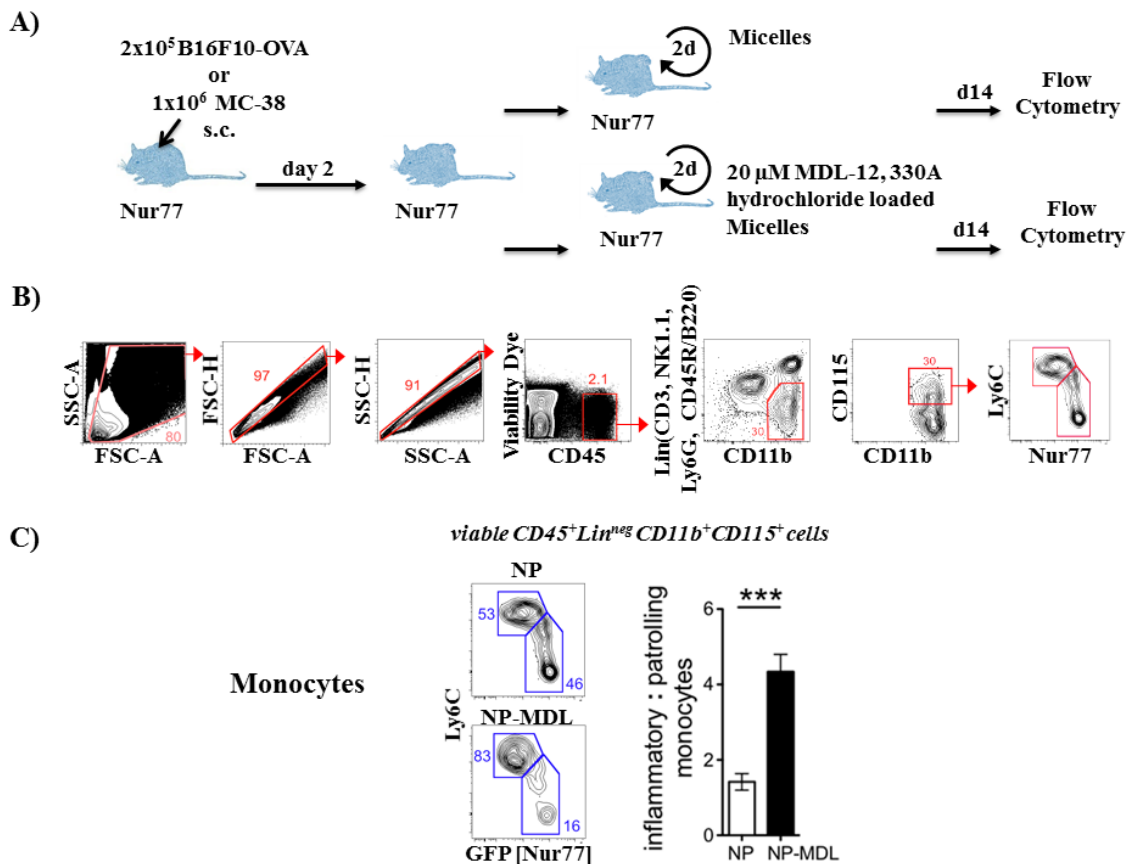
Figure 4.11   Local micelle-based cAMP repression alters the tumour immune cell infiltrate (IV).

A) Schematic representation of the experimental setup. $2x10^5$ B16F10-OVA were subcutaneously (s.c.) injected at the right flank of Nur77. Three times a week, tumours were treated with subcutaneous injections at the site of tumour inoculation of 20 µM of MDL-12,330A hydrochloride loaded micelles/50 µl or the equivalent of an empty micelle based on the particles mass concentration. Mice were sacrificed 14 days after tumour inoculation and tumours were harvested. Single cell suspensions were prepared and stained with fluorescently labelled antibodies against CD45, CD11b, CD115 and the lineage markers CD3, CD45R/B220, NK1.1 and Ly6G. The number of inflammatory (CD45$^+$Lin (CD3, CD45R/B220, NK1.1, Ly6G)$^-$CD11b$^+$CD115$^+$Nur77^{high}) and patrolling CD45$^+$Lin (CD3, CD45R/B220, NK1.1, Ly6G)$^-$CD11b$^+$CD115$^+$Nur77^{low}) monocytes was determined by Flow Cytometry and their ratio was calculated. Dead cells were excluded using Fixable Viability Dye. **B)** Gating strategy for the evaluation of inflammatory and patrolling monocytes. **C)** Representative contour plots, graphic representation, and statistical evaluation (t-test) of data from the analysis of B16F10-OVA tumours treated with empty and MDL-12, hydrochloride loaded micelles regarding inflammatory and patrolling monocytes. Results are shown as mean±SEM. *$P<0.05$, **$P<0.01$, ***$P<0.001$, ****$P<0.0001$. d: day, days; FSC-A: Forward Scatter Area; FSC-H: Forward Scatter Hight; GFP: green fluorescent protein; Lin: lineage; neg: negative; NP: nanoparticle; NP-MDL: nanoparticle loaded with MDL-12, 330A hydrochloride; SSC-A: Side Scatter Area; SSC-H: Side Scatter Hight.

4.4   Combining MDL-12, 330A hydrochloride and Cell Depletion Strategies for Melanoma Therapy

The current trend in tumour therapy towards the combination of successfully tested treatment approaches has been strongly advocated and already proven beneficial (Koller, K.M. *et al.*, 2016). Drastic changes in the immune cell compartment upon *in vivo* cAMP interference in the context of the B16F10-OVA tumour model regarding granulocytes/neutrophils (Figure 4.10 C) as well as reports indicating a reduction of the tumour burden upon the depletion of the myeloid compartment (Jablonska, J. *et al.*, 2010) initiated efforts to test the combination of both cAMP reduction and granulocyte depletion (Figure 4. 12 A). Granulocyte depletion alone and its combination with cAMP interference did result in a reduction of the tumour size compared to the sole treatment of the tumour with DMSO, the decrease in tumour size did however equal its reduction upon administration of MDL-12, 330A hydrochloride only (Figure 4.12 B).

A)

B)
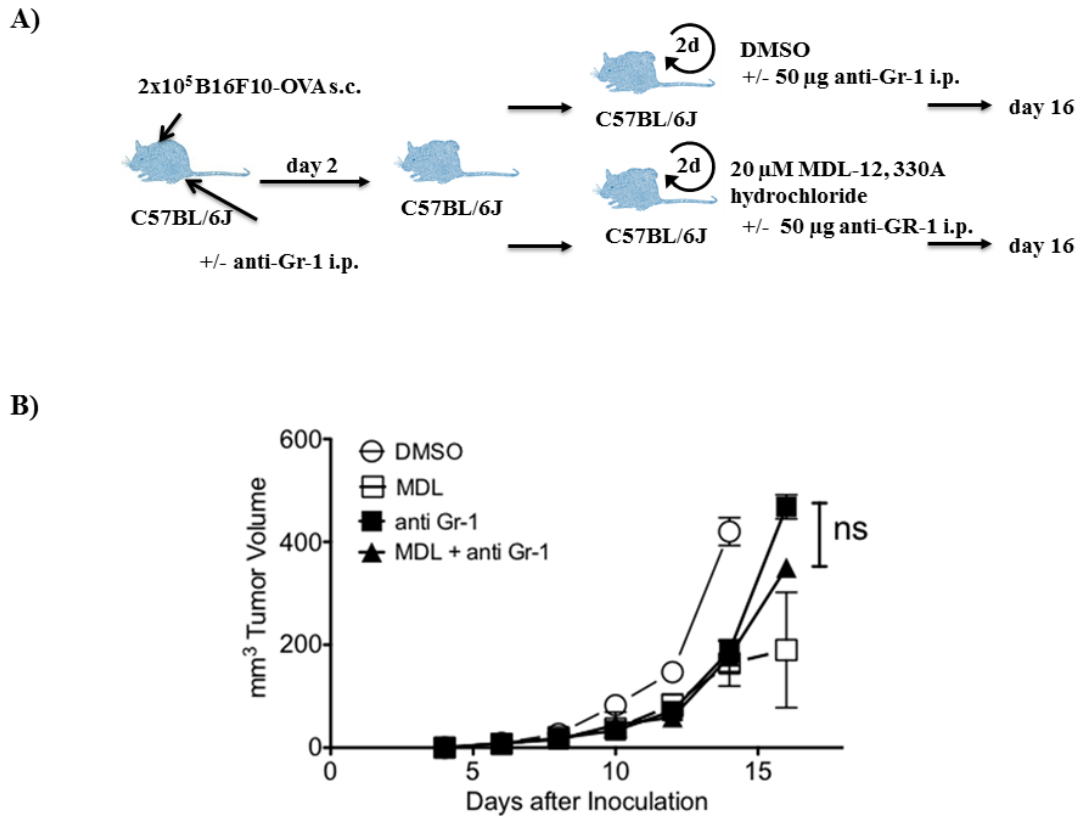
Figure 4.12 **The effect of continuous granulocyte depletion on the treatment of B16F10-OVA with MDL-12, 330A hydrochloride.**

A) Schematic representation of the experimental setup. $2x10^5$ B16F10-OVA were subcutaneously (s.c.) injected at the right flank of C57BL/6J. One day prior to the implantation of B16F10-OVA, the day of the implantation and from then on, every second day until the experiment ended the animals were intraperitoneally (i.p.) injected with $50\,\mu g$ of anti-Gr-1 antibody (Clone: RB6-8C5 (Ly-6G/Ly6-C). At the same time, tumours were treated with subcutaneous injections of $20\,\mu M$ of MDL-12, 330A hydrochloride/$50\,\mu l$ or the equivalent of dimethyl sulfoxide (DMSO)/$50\mu l$ at the site of tumour inoculation. Tumour growth progression was concurrently assessed using a digital calliper. Mice were sacrificed due to poor health or upon the tumour reaching or passing the maximum tumour dimensions of $1\,cm^2$. The treatment was controlled with the individual treatment of groups of mice with MDL-12A, hydrochloride, its equivalent of DMSO or the depletion of granulocytes. **B)** Tumour growth curve of B16F10-OVA upon anti-Gr-1 antibody depletion and treatment with either DMSO or MDL-12, 330A hydrochloride. d: day, days; MDL: MDL-12,330A hydrochloride. ns: not significant.

The drastic reduction of the number of Treg in the tumour microenvironment upon cAMP interference (Figure 4.8 H), the presumably resulting resolution of immunosuppression as well as studies pointing towards the initiation of a beneficial anti-tumour response due to transient Treg depletion (Klages, K. *et al.*, 2010) prompted the efforts to combine cAMP interference and Treg depletion with the intent to fully abolish tumour growth. DEREG, a transgenic mouse model which under the control of the FoxP3 locus, a transcription factor defining mouse Treg, expresses both a diphtheria toxin receptor and an eGFP protein, were used for this study. Intraperitoneal injection of diphtheria toxin (DT) thus allows for the temporary removal of

Tregs while the eGFP is frequently used for tracking their presence (Figure 4.13 A) (Lahl, K. *et al.*, 2007; Lahl, K. & Sparwasser, T., 2011). As previously established by intranuclear antibody staining of the transcription factor FoxP3 (Figure 4.8 H), the observation that as a result of MDL-12, 330A hydrochloride treatment of B16F10-OVA, the number of Tregs (viableCD45$^+$NK1.1$^-$TCRß$^+$CD4$^+$Foxp3$^+$/Dereg$^+$) was drastically reduced, could be corroborated when using DEREG mice (Figure 4.13 B).

Effectiveness of the combination of cAMP interference and punctual Treg depletion to reach lasting tumour removal was tested. The timepoints for Treg removal, days 7, 12 and 18 after tumour implantation, were carefully chosen based on previously reported effects of Treg ablation on tumour growth. While Treg depletion shortly after tumour implantation results in the cessation of tumour growth, Treg ablation at later timepoints does not alter tumour development (Klages, K. *et al.*, 2010). To avoid that favourable effects of cAMP interference and Treg depletion could be ascribed to an untimely depletion of Tregs, intermediate timepoints for DT injections were chosen (Figure 4. 13 C). Combing cAMP interference using MDL-12, 330A hydrochloride with punctual Treg removal as well as Treg depletion alone resulted in a significant decrease of tumour growth compared to tumour treatment with just MDL-12, 330A hydrochloride. While for both treatment strategies the tumour growth was initially halted it would vanish completely when cAMP interference and Treg depletion were combined. In case of Treg depletion only it would later start to re-emerge (Figure 4.13 D). When looking at the Kaplan-Meier plot, it becomes apparent that the combination of Treg ablation and cAMP interference was much more effective than Treg depletion alone. While at day 36 after initial tumour inoculation all mice had died upon Treg removal, none of the mice treated with both MDL-12, 330A hydrochloride and DT had succumbed to the tumour (Figure 4.13 E) consequently also highlighting the superiority of this treatment approach. The surviving mice were subjected to a challenge with B16F10-OVA. While in a control group the tumours did grow out as expected, no tumour growth could be detected in the mice previously subjected to the novel combination of therapeutic approaches implying a state of systemic immunity (Figure 4.13 F).
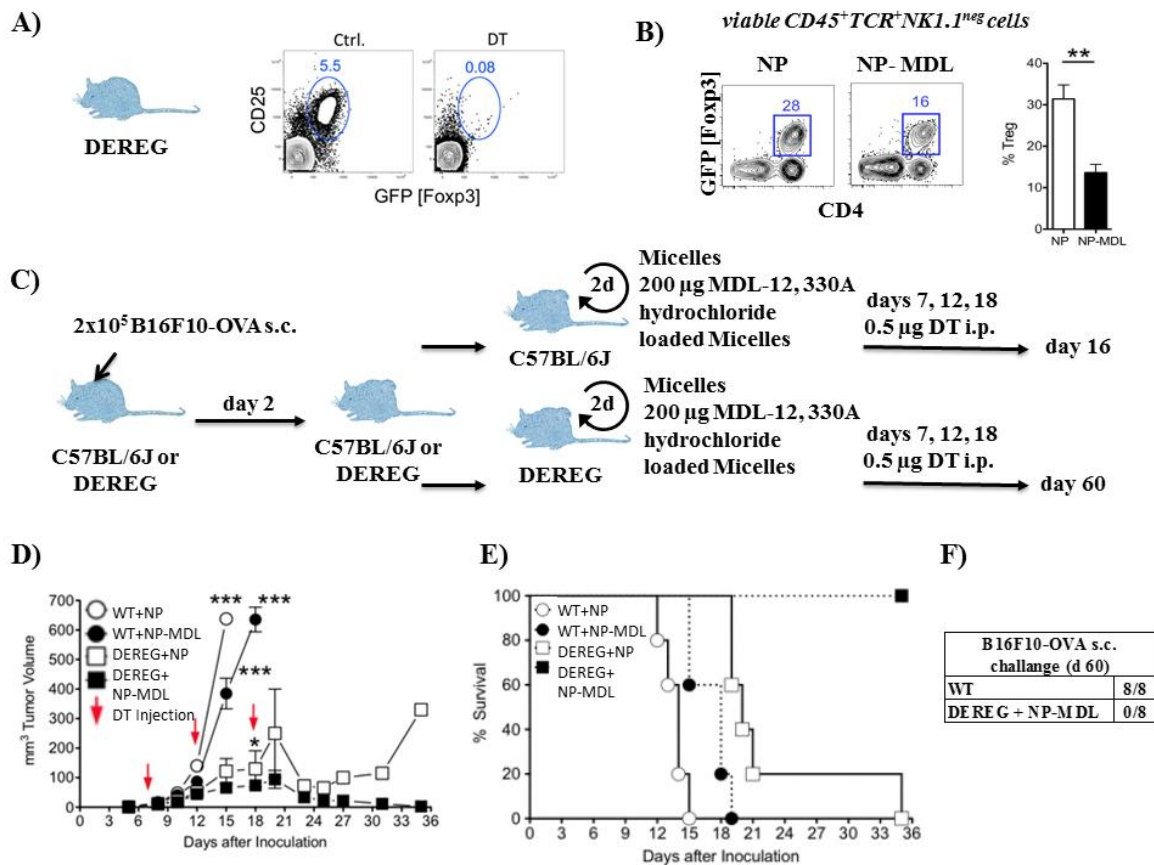
Figure 4.13 Combination of tumour treatment with MDL-12, 330A hydrochloride loaded micelles with ablation of regulatory T cells.

A) Representative contour plot of regulatory T cells (Tregs) in the blood from a DEREG (depletion of regulatory T cells) mouse prior to and after several diphtheria toxin (DT) injections. **B)** Representative contour plots, graphic representation, and statistical evaluation (t-test) of data from the analysis of B16F10-OVA tumours in DEREG treated with empty or MDL-12, hydrochloride loadedmicelles regarding regulatory T cells. **C)** Schematic representation of the experimental setup. $2x10^5$ B16F10-OVA were subcutaneously (s.c.) injected at the right flank of C57BL/6J or DEREG. Three times a week, tumours were treated with subcutaneous injections at the site of tumour inoculation of 20 µM of MDL-12, 330A hydrochloride loaded micelles/50 µl and the equivalent of an empty micelle based on the particles mass concentration. To ablate Tregs, mice were intraperitoneally (i.p.) injected with 0.5 µg of DT at days 7, 12 and 18 after tumour inoculation. Tumour growth progression was assessed using a digital calliper. Mice were sacrificed due to poor health or upon the tumour reaching or passing the maximum tumour dimensions of 1 cm^2. The treatment was controlled with the individual treatment of groups of mice with MDL-12, 330A hydrochloride, its equivalent of dimethyl sulfoxide (DMSO) or the depletion of Tregs. Animals which had survived the treatment regimen past day 35 were subcutaneously injected with $2x10^5$ B16F10-OVA at their left flank. Tumour growth was assessed until 60 days after the initial tumour inoculation. **D)** Tumour growth curve in C57BL/6J and DEREG mice upon treatment of B16F10-OVA with empty and MDL-12, 330A loaded micelles and depletion of Tregs. **E)** Kaplan-Meier plot for C57BL/6J and DEREG mice upon treatment of B16F10-OVA with empty and MDL-12, 330A loaded micelles and depletion of Tregs. Results are shown as mean±SEM. *P<0.05, **P<0.01, ***P<0.001, ****P<0.0001. Ctrl: control; d: day, days; GFP: green fluorescent protein; NP: nanoparticle; NP-MDL: nanoparticle loaded with MDL-12, 330A hydrochloride; WT: C57BL/6J also referred to as wild type.

4.5 *In Vivo* testing and Protective and Therapeutic Intervention of B16F10-OVA with Polymer Brushes

Another therapeutic strategy successfully ventured in the fight against cancer are protective and therapeutic vaccination strategies. In contrast to traditional vaccine where the use of soluble antigens frequently leads to the favouring of the CD4^{+} T cell response, it is essential to promote the CD8^{+} T cell response in the context of cancer vaccines (Fan, Y. & Moon, J.J., 2015). Nanoparticle-based systems have recently been developed to improve the efficacy of protective and therapeutic tumour vaccination strategies (Zhao, L. *et al.*, 2014).

In the present study azide functionalized polysarcosine brushes with polylysine backbone and polysarcosine side chains labelled with the fluorescent dye Alexa Fluor 647 and coupled with either or both the antigen OVA or the nucleic-acid-based immune modulator CpG were tested as a potential tumor vaccine in the context of the B16F10-OVA melanoma model. The brushes were therefore labelled with the fluorescent dye Alexa Fluor 647 and functionalized with the model antigen OVA and the nucleic-acid-based immune modulator CpG (Figure 4.14 A). Following the preparation of the brushes, free dye or CpG was gotten rid of by spin-filtration, while unattached OVA was removed by means of Gel Permeation Chromatography (GPC) (Figure 4.14 B). To confirm that all free dye had been successfully eliminated and to determine the amount of dye per brush present, Fluorescent Correlation Spectroscopy (FCS) was performed (Figure 4.14 C), while Polyacrylamide Gel Electrophoresis (PAGE) was used to confirm that all free OVA or CpG had been removed (Figure 4.14 D, Figure 4.14. E). A combination of Ultraviolet-Visible Spectroscopy (UV-Vis) (Figure 4.14 F) and FCS measurements was employed to determine the number of each component per brush (Figure 4. 14 G).
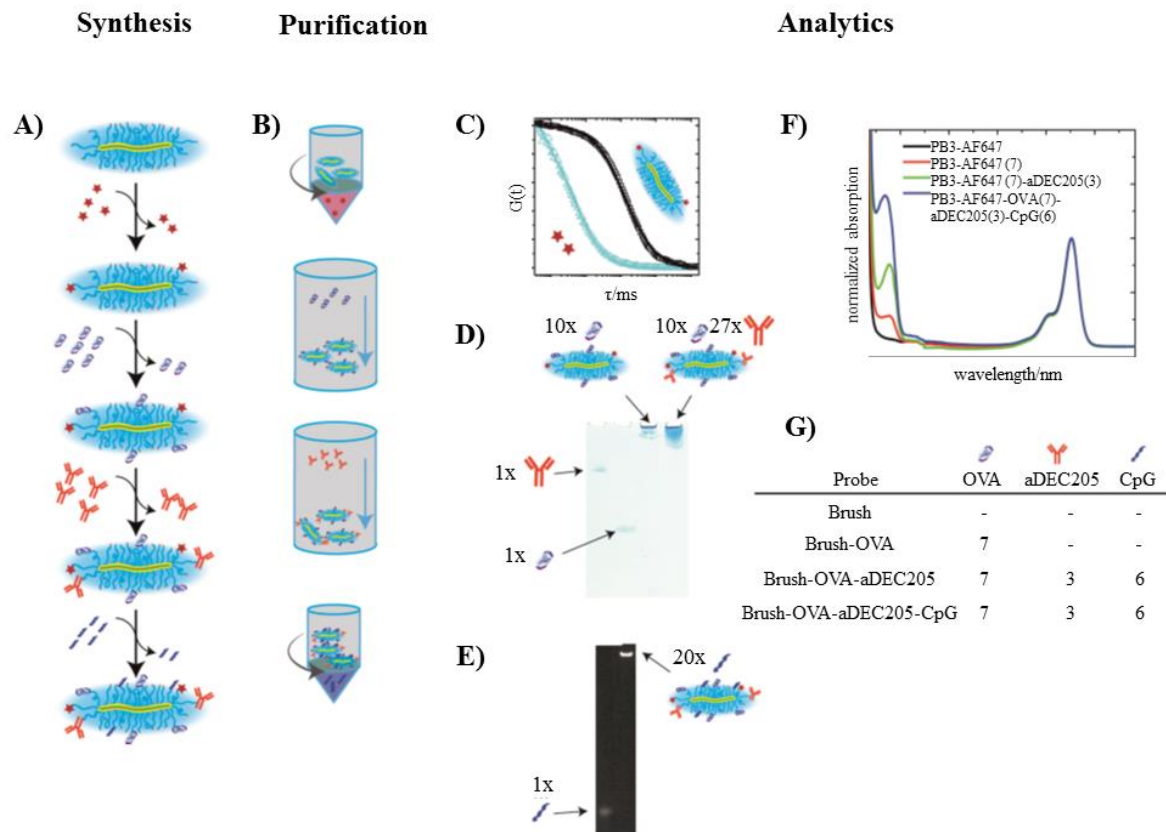
Figure 4.14   The making of polymer brushes.
Example of the synthesis of Polymer Brushes. Purification and characterization of an ovalbumine (OVA) - anti-DEC205 (aDEC205) - cytosin-phosphate-guanine (CpG) polymer brush conjugate starting from polymer brush 1. **A)** Stepwise synthesis of the conjugates. **B)** Purification: separation of free fluorescence and CpG by means of spin filtration. Separation of OVA and antibody by means of Gel Permeation Chromatography (GPC). **C)** Fluorescence Correlation Spectroscopy (FCS) of the dye labelled brushes determining the amount of dye per brush as well as the absence of free dye. **D)** Polyacrylamide gel electrophoresis (PAGE) bands: 1= aDEC205- dibenzocyclooctyne (DBCO) (0.3 µg), 2= OVA-DBCO (0.5 µg), 3= Brush-OVA (5 µg OVA), 4= Brush-OVA-aDEC205 (5 µg OVA, 8 µg aDEC205). **E)** PAGE bands: 1= CpG-DBCO (50 ng), 2= Brush-OVA-aDEC205-CpG (1000 ng). **F)** Ultraviolet-Visible Spectroscopy (UV-VIS) spectrum of the brush and conjugates normalized to the absorption of the dye. **G)** Quantification of OVA, aDEC205 and CpG per brush. Data is calculated from the amount of dye per brush determined over FCS and the UV-Vis spectra. Graphic provided ███████

To elucidate the differences between the *in vivo* handling of soluble Alexa Fluor 647 labelled OVA in comparison to Alexa Fluor 647 labelled brushes alone or coupled with OVA, CpG or OVA-CpG, their body distribution upon subcutaneous injection was examined at 1 or 16 hours after their initial administration into C57BL/6J. Body distribution was assessed by flow cytometric analysis of the skin, blood, spleen, draining lymph node and non-draining lymph

node (Figure 4.15 A). Alexa Fluor 647 labelled OVA or polymer brushes associated with $CD45^+$ cells were identified in the different organs by gating for $ViabelCD45^+AF647^+$ cells (Figure 4.15 B). The body distribution of each of the Alexa Fluor 647 labelled polymer brush alone or coupled with OVA, CpG or OVA-CpG has been summarized in one graph since no significant differences in terms of distribution were observed 1 or 16 hours after subcutaneous administration. While 1 hour after injection the polymer brushes did mainly associate with $CD45^+$ cells in the skin, soluble OVA was detected not only in the skin but also in the draining and non-draining lymph node. After 16 hours the brushes were still present in the skin but had distributed to the draining lymph node and the spleen. At that stage the soluble OVA had completely vanished from the organism (Figure 4. 16 C). These results indicate that the intermediate sized polymer brushes with a hydrodynamic radius of 21 nm prevent a fast redistribution of the antigen and adjuvant but instead anchor these in the skin allowing them to efficiently drain to close by lymph nodes and for a prolonged exposition to antigen presenting cells (APCs) (Fan, Y. & Moon, J.J., 2015). Although it is not expected that significant alterations in the outcome would occur, it should be kept in mind that in case of the polymer brushes the fluorescent labelling was at the backbone of the brushes, whereas the soluble OVA was directly labelled with the fluorescent dye.
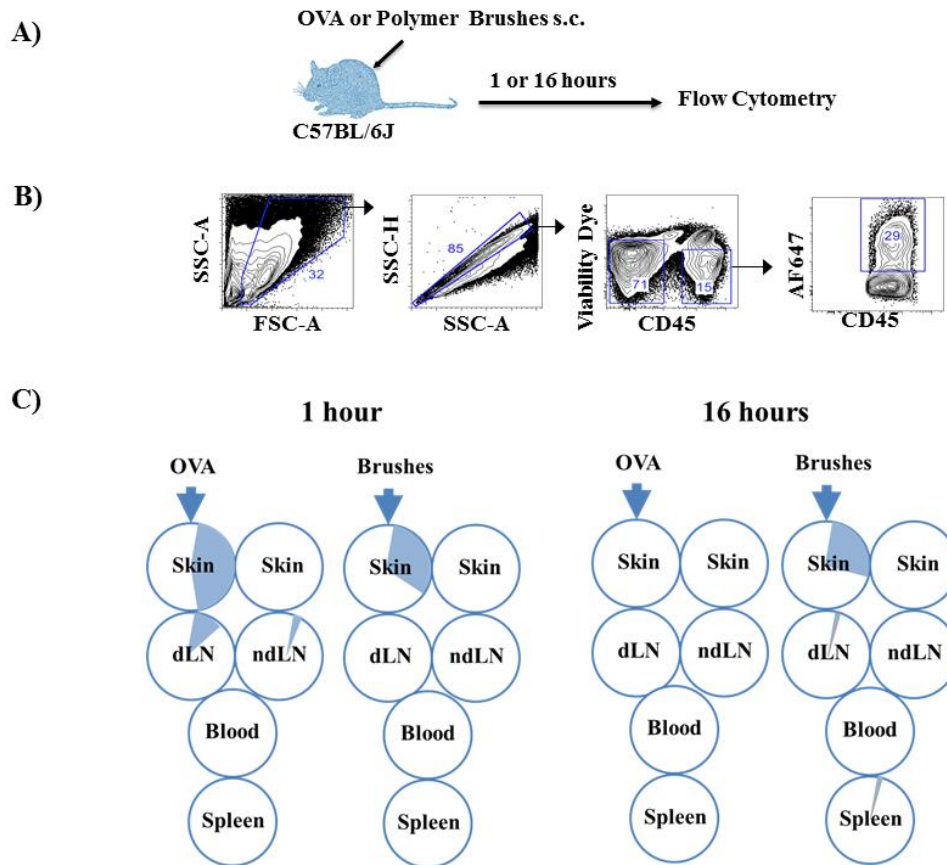
Figure 4.15 *In vivo* **tracking of polymer brushes**

A) Schematic representation of the experimental setup. C57BL/6J were subcutaneously (s.c.) injected at their right flank with Alexa Fluor 647 (AF647) labelled polymer brushes alone or coupled with ovalbumin (OVA), cytosine-phosphate-guanine (CpG) or OVA-CpG as well as commercially available Alexa Fluor 647 labelled OVA. The amount of particle used was calculated based on and normalized to the injection of 10 µg of OVA. Mice were sacrificed 1 or 16 hours after injection and the skin, blood, spleen, draining lymph node (dLN) and non-draining lymph node were (ndLN) harvested. Single cell suspensions were prepared and stained with CD45 while dead cells were excluded using Fixable Viability Dye. **B)** Gating strategy for the evaluation of Alexa Fluor 647 labelled OVA or polymer brushes associated with CD45+ cells. **C)** Graphic representation of the results from different time points of the body distribution of Alexa Fluor 647 labelled OVA or polymer brushes associated with CD45+ cells. FSC-A: Forward Scatter Area; pos: positive; SSC-A: Side Scatter Area; SSC-H: Side Scatter Hight.

Subsequently, *in vivo* T cell proliferation after immunization was evaluated to study the efficacy of OVA presentation using polymer brushes coupled with OVA in contrast to soluble OVA. Therefore, CTV or CFSE labelled spleens from OT-I and OT-II mice were adoptively transferred into C57BL/6J which shortly after were immunized with HBSS, soluble OVA, polymer brushes alone or coupled with OVA, CpG or OVA-CpG. Five days later the T cell response was investigated by Flow Cytometry (Figure 4.15 A). A response towards the vaccination in form of T cell proliferation in both the CD4+ (OT-I CD4+) and CD8+ (OT-II

CD8⁺) compartment was evident in the draining lymph node and the spleen of mice immunized with the polymer brush coupled with OVA or OVA-CpG, while it could only be observed in the spleen of mice immunized with OVA only (Figure 4.15 B). It appears that in contrast to soluble OVA, the polymer brushes coupled with OVA or OVA-CpG induce a lasting systemic response, whereby it stays unclear whether the adjuvant CpG adds towards the effectiveness of the vaccination. The results also correlate with the observations from the brushes body distribution where the polymer brushes prevented an immediate redistribution of the antigen and adjuvant, consequently promoting systemic distribution.
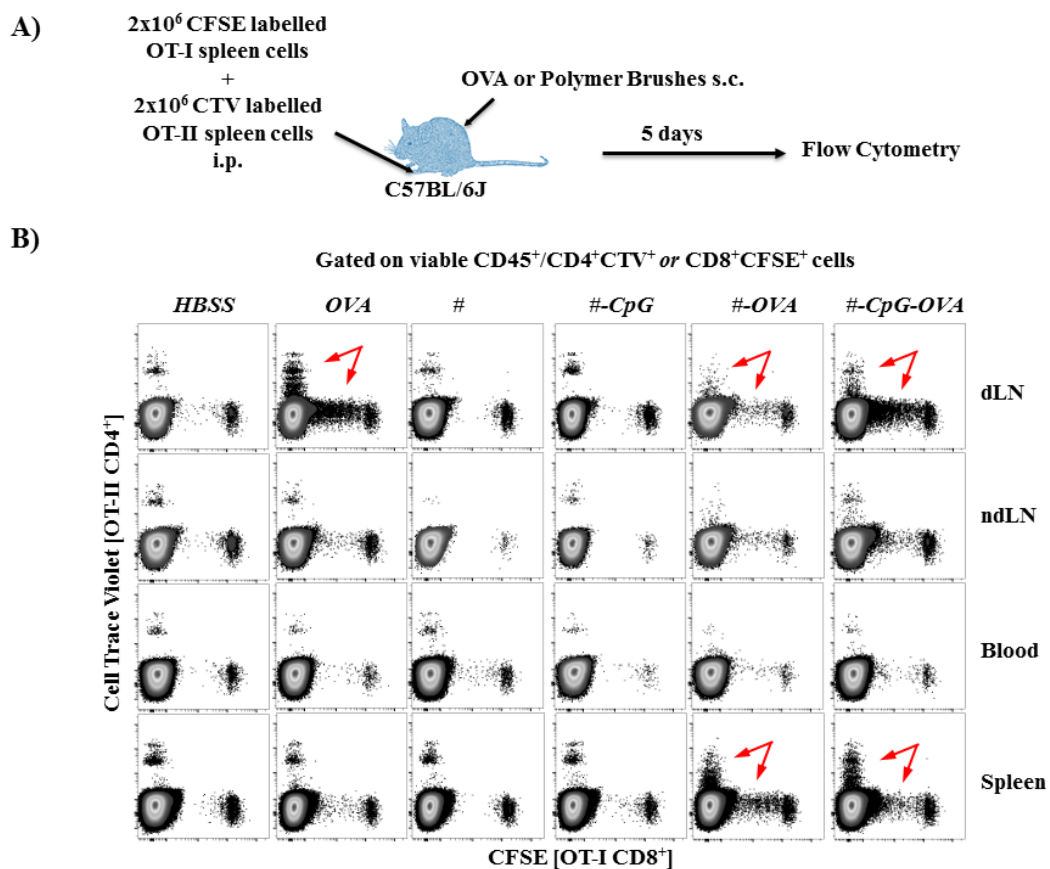
Figure 4.16 *In vivo* **T cell response to polymer brushes.**
A) Schematic representation of the experimental setup. Single cell suspensions of the spleens of OT-I and OT-II mice were prepared and labelled with 1 µM Carboxyfluorescein Succinimidyl Ester (CFSE) and 0.5 µM Cell Trace Violet (CTV) respectively. 2x10⁶ labelled OT-I and OT-II cells were each intraperitoneally (i.p.) injected into C57BL/6J mice. Mice were then subcutaneously (s.c.) injected at their right flank with Hank's Balanced Salt Medium (HBSS), ovalbumin (OVA), polymer brushes (#) alone or coupled with OVA, cytosine-phosphate-guanine (CpG) or OVA-CpG. The amount of particle used was calculated based on and normalized to the injection of 10 µg of OVA. Five days later mice were euthanized and the spleen, blood and draining lymph nodes (dLN) and non-draining lymph nodes (ndLN) were harvested. Single cell suspensions were prepared and stained with fluorescently labelled antibodies against CD45, CD4 and CD8. Flow Cytometry was employed to determine the proliferative capacity of OT-I (CD45⁺CD4⁺CTV⁺) and OT-II (CD45⁺CD8⁺CFSE⁺) cells. Dead cells were excluded

using Fixable Viability Dye. **B)** Representative contour plots of adoptively transferred OT-II CD4$^+$CTV$^+$ and OT-I CD8$^+$CFSE$^+$ cells from the blood, spleen, draining lymph node and non-draining lymph node upon treatment with HBSS, OVA alone, brushes only and coupled with CpG, OVA and CpG-OVA.

The effectiveness of the polymer brushes as a protective vaccine were subsequently tested in the context of the B16F10-OVA model. Therefore, polymer brushes alone or coupled with OVA, OVA-CpG, were subcutaneously injected in C57BL/6J on three consecutive weeks. One week later, mice were challenged with B16F10-OVA and tumour growth progression was monitored (Figure 4.17 A). No significant difference in the tumour growth rate was observed between the control group and the mice vaccinated with the polymer brushes only. The use of polymer brushes coupled with OVA or CpG-OVA as a protective vaccine did however result in a complete prevention of tumour growth (Figure 4.17 B). Once again as already demonstrated while investigating the T cell response towards the polymer brushes it could be concluded that the polymer brushes themselves do not cause any notable adverse reactions when compared to these coupled with a suitable antigen or adjuvant.
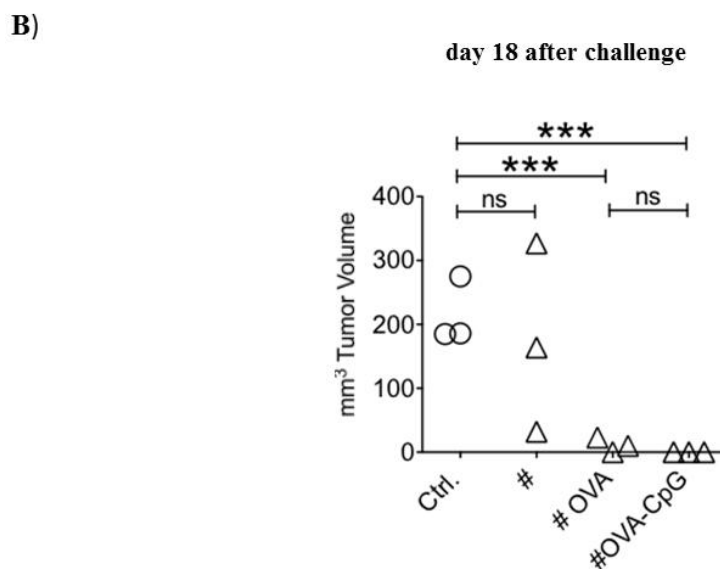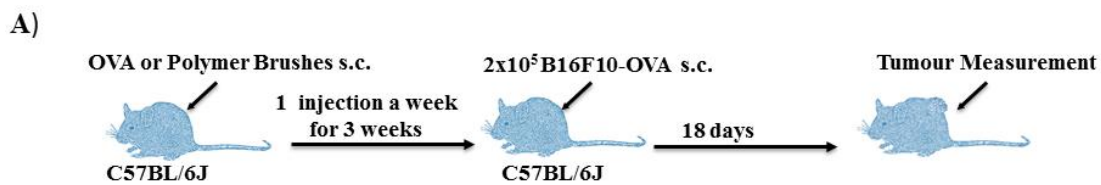
Figure 4.17   The effect of immunization using polymer brushes on the growth of B16F10-OVA.

A) Schematic representation of the experimental setup. C57BL/6J were subcutaneously (s.c.) injected on three consecutive weeks at their right flank with 1x Hank's Balanced Salt Solution (HBSS) (Ctrl.); polymer brushes (#) alone or coupled with ovalbumin (OVA), OVA-cytosine-phosphate-guanine (CpG) or OVA alone. The amount of particle used was calculated based on and normalized to the injection of 10 µg of OVA. One week after the last injection mice were subcutaneously inoculated at the left flank with $2x10^5$ B16OVA-F10. Tumour growth was monitored for two weeks. Mice were sacrificed due to poor health or upon the tumour reaching or passing the maximum tumour dimensions of $1cm^2$. **B)** Graphic representation and statistical evaluation (t-test) of tumour volume following protective treatment with 1xHBSS, polymer brushes alone and coupled with OVA and OVA-CpG. Results are shown as mean±SEM *$P<0.05$, **$P<0.01$, ***$P<0.001$, ****$P<0.0001$. ns: not significant.

Since the polymer brushes coupled with OVA only or in combination with CpG did prove to be effective in preventing tumour outgrowth in a protective vaccination strategy, they were once again tested in the contest of the B16F10-OVA model in a therapeutic vaccination regiment. Upon the inoculation of B16F10-OVA into C57BL/6J mice, soluble OVA, polymer brushes alone or with and without OVA or OVA-CpG were subcutaneously injected at days 3 and 6 after tumour inoculation (Figure 4. 18A). Observation of the tumours treated with soluble OVA or polymer brushes only revealed their inability to supress tumour growth. Polymer brushes coupled with OVA or OVA-CpG were however able to significantly halt tumour outgrowth. When considering the outcome of the therapeutic vaccination using polymer brushes coupled with OVA or OVA-CpG, no obvious benefit could be attributed to the use of the adjuvant in combination with the antigen over the use of just the antigen in the context of the B16F10-OVA model (Figure 4. 18 B). While these results were generated using a highly artificial model, they do still give the incentive to further investigate the azide functionalized polysarcosine brushes with polylysine backbone and polysarcosine side chains and to combine this strategy possibly even with the reduction of cAMP by intervening at the cAMP pathway.

A)

B)
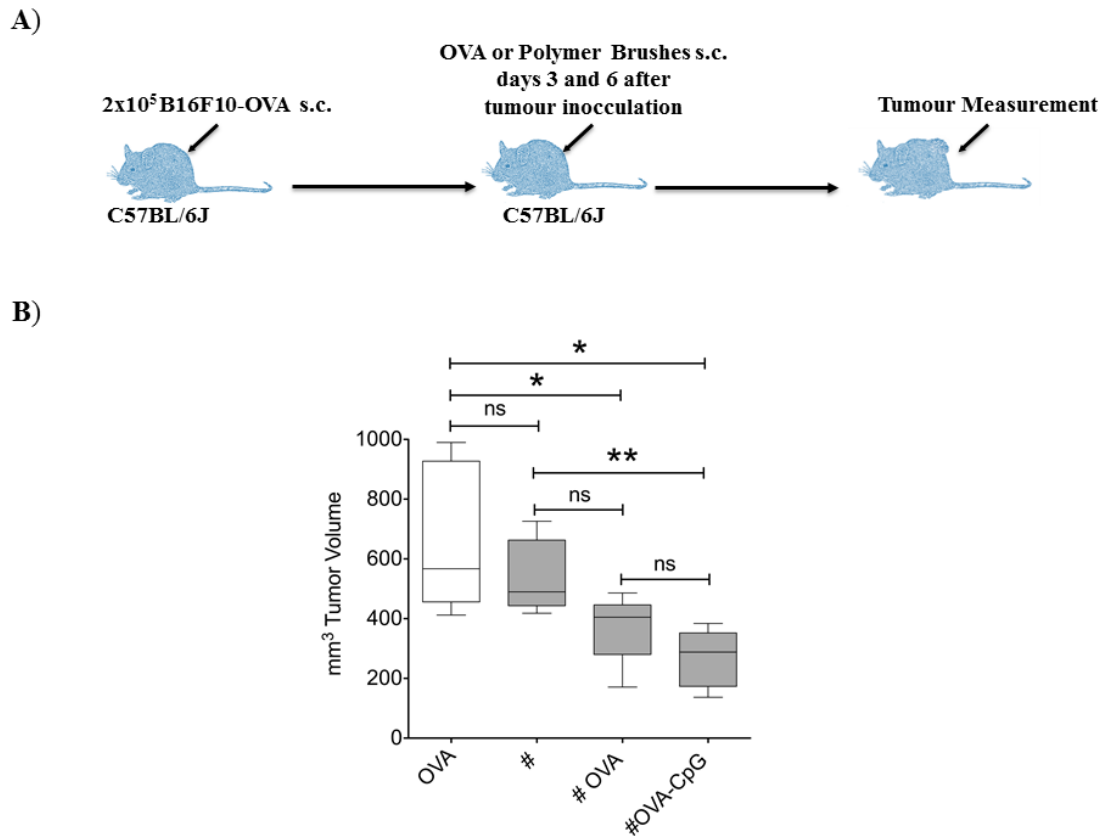
Figure 4.18   The effect of therapeutic treatment using polymer brushes on the growth of B16F10-OVA.

A) Schematic representation of the experimental setup. 2×10^5 B16F10-OVA were subcutaneously injected at the right flank of C57BL/6J. At days 3 and 6 after tumour inoculation, ovalbumin (OVA) alone and polymer brushes (#) alone with and without OVA or OVA-cytosine-phosphate-guanine (CpG) were subcutaneously (s.c.) injected at the left flank of a mouse. The amount of particle used was calculated based on and normalized to the injection of 10 µg of OVA. Tumour progression was monitored. Mice were sacrificed due to poor health or upon the tumour reaching or passing the maximum tumour dimensions of $1cm^2$. **B)** Graphic representation and statistical evaluation (t-test) of tumour volume after therapeutic treatment with polymer brushes alone and coupled with OVA and OVA-CpG. Results are shown as mean±SEM *P<0.05, **P<0.01, ***P<0.001, ****P<0.0001.

5. Discussion

5.1   The Relationship between cAMP and Melanoma

Alteration in metabolic pathways have only recently been recognized as a hallmark of cancer (Hanahan, D. & Weinberg, R.A., 2011; Pavlova, N.N. & Thompson, C.B., 2016) and have been characterized by features which include the deregulated uptake of glucose and amino acids, the use of opportunistic modes of nutrient acquisition, the use of glycolysis/tricarboxylic acid (TCA) cycle intermediates for biosynthesis and nicotinamide adenine dinucleotide phosphate (NADPH) production, increased demand for nitrogen, alterations in metabolite-driven gene regulation and metabolic interactions with the microenvironment. While the minority of tumours rely on the whole set of these characteristics, most feature only a selected few (Pavlova, N.N. & Thompson, C.B., 2016). Malignant melanoma has for example been shown to be highly dependent on glycolysis and to be closely associated with the MAPK pathway (Fischer, G.M. *et al.*, 2018).

Metabolites in general, but also those specifically pertaining to glycolysis have been investigated and related to certain types of cancer. This includes serum lactate dehydrogenase (LDH), a ubiquitously expressed enzyme investigated in a great variety of cancers which catalyses the conversion of lactate to pyruvic acid as well as nicotinamide adenine dinucleotide, oxidized form (NAD^+) to nicotinamide adenine dinucleotide, reduced form (NADH) and back (Miao, P. *et al.*, 2013). In general, elevated LDH levels have been associated with an unfavourable survival (Zhang, J. *et al.*, 2015). In relation to melanoma, LDH has been recognized as a valid prognostic marker regarding Stage IV melanoma patients (Balch, C.M. *et al.*, 2009). Its inhibition in the context of the B16F10 melanoma model, ultimately provoking a shift from glycolysis to glucose oxidation, seems favourable since *in vitro* it initiates decreased cellular viability, invasion as well as by angiogenesis affected metabolic pathways such as the PKA/cAMP pathway while *in vivo* it resulted in smaller tumours and the lack of metastasis (Franco-Molina, M.A. *et al.*, 2012). cAMP, another ubiquitously expressed glycolysis dependent metabolite, which is closely linked to processes involved in skin pigmentation, protection from UV radiation and ultimately also skin cancer (Costin, G.E. & Hearing, V.J. , 2007; Rodriguez, C.I. & Setaluri, C., 2014) has been noted to be elevated in melanoma and to correlated with a heightened metastatic potential in both a human and murine setting (Shepard, J.R. *et al.*, 1984; Ito, A., et al., 2000; Raskovalova, T., *et al.*, 2007; Villares, G.J., *et al.*, 2009). Its repression with the help of the adenylyl cyclase inhibitor MDL-12, 330A hydrochloride has

previously been confirmed in the human melanoma cell line MaMel91 (Birke, A. *et al.*, 2014) and was reported to revoke Treg induced immunosuppression (Klein, M. *et al.*, 2012). Furthermore, IFN-α, an agent commonly used in melanoma therapy, has been reported to alter cAMP production (Bacher, N.*et al.*, 2013).

Intervention at different metabolic levels, lactate and cAMP, in the context of melanoma have in the past shown favourable results and have been advocated as adequate points of intervention (Farnco-Molina, M.A. *et al.*, 2012; Miao, P. *et al.*, 2013; Muller-Haegele, S. *et al.*, 2014). As LDH is regulated by cAMP (Miles, M.F. *et al.*, 1981; Valvona, C.J. *et al.*, 2016), intervention at the cAMP level, namely at the phosphodiesterases, adenylyl cyclases or any of its five target proteins, seems reasonable (Amunjela, J.N. & Tucker, S.J., 2016). As it has been suggested that immunosuppression in the tumour microenvironment is promoted by a subtle interplay between the metabolites adenosine, prostaglandin E2 (PGE2) and signalling of adenosine and E prostaglandin receptor (EPR) which all ultimately converge on the adenylyl cyclase/3'5'-cAMP axis, intervention at the adenylyl cyclase presents as an adequate option (Muller-Haegele, S., *et al.*, 2014). MDL-12, 330A hydrochloride, a cell-permeable non-nucleotide-based adenylyl cyclase inhibitor previously used when studying the effects of cAMP on the suppressive capacity of Treg, which irreversibly blocks all ten known adenylyl cyclases, represents a valid choice (Seifert, R. *et al.*, 2012; Klein, M. *et al.*, 2012). In contrast to traditionally used nucleotide-based structures such as SQ22, 536, long-term effects due to interference with DNA synthesis or the purine metabolism can be avoided. Furthermore, ATP mimetics could be considered as options, since they are however too hydrophilic to be absorbed by intact cells, they are unsuitable for the intended use (Seifert, R. et al., 2012). Besides its ability to block all adenylyl cyclases it represents an essential feature as their individual contribution and spatiotemporal distribution across signalling compartments represented by lipid rafts has so far not been resolved (Cooper, D.M.F. *et al.*, 2005; Seifert, R. *et al.*, 2012).

While MDL-12, 330A hydrochloride is well able to *in vitro* reduce the cAMP content of the human melanoma cell line (Birke, A. *et al.*, 2014), it is also capable to *in vitro* and presumably also *in vivo* decrease cAMP levels in its murine counterpart, the extensively studied B16F10-OVA cell line (Figure 4.2 A, Figure 4.2 C), without affecting its proliferative capacity (Figure 4.2 A, Figure 4.2 D). Its repeated local *in vivo* application towards a subcutaneously growing B16F10-OVA tumour leads to a significant reduction of the tumour burden (Figure 4.3 A, Figure 4.3 B) most likely as a result of the resolution of immunosuppression due to significant changes in the tumour microenvironment but also its immune cell content. In stark contrast

MDL-12, 330A hydrochloride has no effect on the tumour burden of the subcutaneously growing adenocarcinoma MC-38 (Figure 4.3 A, Figure 4.3 B), a tumour virtually devoid of cAMP (Figure 4.1 A, Figure 4.1 C). These results show that MDL-12, 330A hydrochloride exclusively affects cAMP, but also demonstrate that the outcome of mechanisms shared by two types of cancer are highly influenced by subtle mechanistic differences. While for example in melanoma glycolysis is mainly associated with the MAPK pathway (Fischer, G.M. *et al.*, 2018), in colon carcinoma it has been linked to micro ribonucleic acids (miRNAs) (Fang, S. & Fang, X. et al., 2016) but also to the presence of glutaminase which not only via the regulation of glycolysis but also glutaminolysis sustains cell survival (Song, Z. *et al.*, 2017).

5.2   Successful Application of novel MDL-12, 330A hydrochloride loaded Micelles

Nanoparticle-based drug delivery has successfully been introduced into the clinic and represents a strategy with which one anticipates to achieve a prolonged and selective delivery of increased drug doses. Furthermore, it presents a platform to circumvent unfavourable physiochemical and biopharmaceutical properties of potential therapeutics (Berciano-Guerrero, M.A., *et al.*, 2014). To secure continuous inhibition of all adenylyl cyclases, to achieve a tolerable delivery of higher drug doses but also to bypass the use of hydrophilic polar solvents such as DMSO to avail of MDL-12, 330A hydrochloride, a micellar nanoparticle-based delivery was considered.

Amphiphilic block copolymers such as PEG (poly(ethylene glycol))-*block*-polypeptides, which allow for the decoupling of the hydrophobic inner core by a hydrophilic outer corona, have previously been employed to solubilize hydrophobic agents in micellar drug formulations (Huesmann, D. *et al.*, 2015; Klinker, K. & Barz, M., 2015). For the nanoparticle-based delivery of the hydrophobic adenylyl cyclase inhibitor MDL-12, 330A hydrochloride, it was made available by its encapsulation with the novel amphiphilic polypeptoid-*block*-polypeptide copolymer polysacrcosine-*block*-polyglutamatic acid bezylester (PSar-b-PGlu(OBn)). While the functional inner block, made from the water stable polypeptide polyglutamatic acid benzylester (PGlu(OBn)), entrapped the drug, the hydrophilic polypeptoid polysacrcosine (PSar) shields the micelles core from their surrounding and prevents interactions with proteins and immune cells (Figure 4.4 A). In addition, the protein resistant polypeptoid is mainly responsible for a prolonged *in vivo* circulation time of particles made from polypeptoid-*block*-polypeptides (Birke, A. *et al.*, 2014; Klinker, K. & Barz, M., 2015). The replacement of PEG by PSar, entities with very similar chemical and physicochemical properties, allows to avoid

recently uncovered drawbacks of the protein resistant but hardly degradable PEG (Huesmann, D. *et al.*, 2015; Klinker, K. & Barz, M., 2015). While the efficacy of PEG-based nanoparticles has been reported to be reduced due to accelerated blood clearance because of the presence of IgM antibodies against PEG (Ishida, T. *et al.*, 2006; Wang, X. *et al.*, 2007; Garay, R.P. *et al.*, 2012; Klinker, K. & Barz, M., 2015) or complement activation (Hamad, I. *et al*., 2008a; Hamad, I. *et al.*, 2008b; Moghimi, S.M. *et al.*, 2010; Klinker, K. & Barz, M., 2015), PEG has also been reported to contribute to storage disease which eventually affects kidney, spleen, and liver function as well as high dose therapy (Young, M.A. *et al.*, 2007; Webster, R. *et al.* 2009; Klinker, K. & Barz, M., 2015).

MDL-12, 330A hydrochloride loaded micelles made from PSar-b-PGlu(OBn) were able to successfully release the adenylyl cyclase inhibitor as could be evaluated by a dose dependent decrease of the intracellular cAMP content (Figure 4.5 A, Figure 4.5 B). Processes associated with particle formulation (Figure 4.4 B, Figure 4.4 C) did not alter the function of MDL-12, 330A hydrochloride. Also, the amphiphilic block copolymer, PSar-b-PGlu(OBn), did as expected not interfere with cellular functions or display any toxic side effects (Figure 4.5 A, Figure 4.5 B, Figure 4.5 C). Hydrophilic synthetic polypeptides such as PGlu(OBn) represent biocompatible, nontoxic as well as degradable entities which risk activating the immune system due to the presence of charged or hydrophobic residues. The polypeptoid PSar, which naturally is a part of muscle metabolism and has previously been found to have negligible immunogenicity, does however prevent such interactions as it shields the polypeptide. Next to this it also influences the circulation time of nanoparticle-based formulations (Klinker, K. & Barz, M., 2015).

As cancer therapeutics are generally administered systemically in high doses by intravenous injections and packaging of therapeutics into nanoparticular formulations extends a drugs availability but also alters their distribution (Berciano-Guerrero, M.A., *et al.*, 2014), the distribution of empty and MDL-12, 330A hydrochloride loaded micelles was investigated upon systemic venous application on tumour bearing mice. Therefore, MDL-12, 330A hydrochloride loaded micelles coupled with the fluorophore Oregon Green were introduced by the iliac or jugular vein by intravenous or retro-orbital injection and followed by Flow Cytometry (Figure 4.6 A). Intravenous injection of MDL-12, 330A hydrochloride loaded or empty micelles did not result in preferential accumulation of the particles at the tumour site (Figure 4.6 B), therefore modifications to the particle or alternative forms of administration would have to be taken into consideration. Such modifications could for example include surface modifications of the

particle to promote accumulation at the tumour site based on an increased expression of an entity by a tumour such as for example in case of melanoma SPARC or the CD13/aminopeptidase N (APN) receptor isoform (Hersh, E.M. *et al.*, 2015; Mundra, V. *et al.*, 2015; Enyedi, K.N. *et al.*, 2017).

Since in contrast to other cancers, melanomas are easily accessible, the body distribution of MDL-12, 330A hydrochloride loaded and empty particles was investigated at 1 or 16 hours upon peritumoral injection of the particles on tumour bearing mice. Upon injection at the tumour site, micelles preferentially associated with viable $CD45^-$ and $CD45^+$ cells and would accumulate at the tumour site. While initially insignificant numbers of cells had not associated with any other tissue, over time a significant number of micelles did associate with the kidney (Figure 4.6 B). Since there was no indication for particle excretion 1 hour after intravenous injection, it can be assumed that the micelles favourable size, shape and the hydrophilic PSar was responsible for advantageous conditions for prolonged blood circulation and the prevention of the drugs immediate clearance (Choi, H.S., *et al.*, 2007; Liu, J. *et al.*, 2013). Furthermore, it can be suspected that upon peritumoral injection micelles could avoid being captured by the reticuloendothelial system (RES), as over time micelles primarily associated with the tumour or the kidney. It can also be assumed that prior to the micelles degradation and the materials clearance via the kidney, micelles must have been intact for at least 6 hours for accumulation at the tumour site for the EPR effect to properly function (Iyer, A.K. *et al.*, 2006; Liu, J. *et al.*, 2013). It however must be taken into consideration that site specific accumulation of particles believed to have taken place solely based on the EPR effect may not well translate into the clinical setting as the animal models used when studying the EPR effect differ quite drastically in several key aspects from clinically relevant tumours. Amongst others such key differences have been described to be represented by the tumours rate of development, its size relative to the host, differing metabolic rates as well as a deviant architecture of the tumour microenvironment. With the intention to reflect clinically relevant tumours more accurately, the use of patient-derived tumour explant *in vivo* tumour models has been suggested (Matsumura, J. & Maeda, H., 1986; Nichols, W. & Bae, Y.H., 2014; Danhier, F., 2016; Din, F. et al., 2017).

The MDL-12, 330A hydrochloride loaded or empty micellar formulation, made from PSar-b-PGlu(OBn), did previously not show any adverse effects *in vitro* (Figure 4.5 A, Figure 4.5 B, Figure 4.5C) and were found to preferentially accumulate at the tumour site upon peritumoral administration (Figure 4.6 A, Figure 4.6B). Therefore, its effect on an established experimental

regiment of *in vivo* tumour reduction upon peritumoral melanoma treatment with the adenylyl cyclase inhibitor MDL-12, 330A hydrochloride was tested (Figure 4.7 A). As previously established, treatment of B16F10-OVA with MDL-12, 330A hydrochloride did result in significantly reduced tumour volumes, however when compared to tumour volumes upon treatment with free or encapsulated MDL-12, 330A hydrochloride no significant differences could be observed. While encapsulation of MDL-12, 330A hydrochloride did not improve tumour reduction, treatment of tumours with empty micelles did however also not seem to cause any adverse or toxic side effects (Figure 4.7 B, Figure 4.7 C). The failure to further reduce tumour burden upon nanoparticle-based adenylyl cyclase inhibitor delivery might indicate that this strategy alone, the continuous delivery of increased doses of the inhibitor, is in general not suitable to effectively eliminate tumour burden. Instead it might need to be considered to combine cAMP repression with other strategies previously shown to convey at least partial effectiveness.

5.3 Effect of cAMP Repression on the Immune Cell Content of B16F10-OVA

Spontaneous melanoma regression, a sporadically observed phenomena, is associated with dermal lymphocyte infiltration, also referred to as tumour infiltrating lymphocytes (TILs) which were first described in 1863 by Rudolf Virchow. The heterogenous group of TILs, which amongst others includes effector, tolerogenic, regulatory or functionally exhaust T cells, natural killer (NK) cells, macrophages, dendritic cells, or myeloid-derived suppressor cells (MDSCs), represents an essential part of the host's response against melanoma (Lee, N. *et al.*, 2016). TILs, which in *in vitro* studies were found to display cytolytic activity against autologous melanoma (Hersey, P. *et al.*, 1981; Lee, N. *et al.*, 2016), have not only been identified in the primary tumour of numerous cancers but also in affected lymph nodes and visceral metastases (Azimi, F. *et al.*, 2012; Lee, N. *et al.*, 2016). Recruitment occurs during the tumours radical growth phase (Clark Jr., W.H., *et al.*, 1969; Lee, N. *et al.*, 2016) and their presence during the vertical growth phase has been associated with a higher likelihood of survival and fewer metastases (Clark Jr., W.H., *et al.*, 1989; Lee, N. *et al.*, 2016).

From the late 1970th on, except for few, numerous studies corroborated indications of an increased survival and better prognosis for patients with moderate to marked melanoma infiltrating lymphocytes (Schatton, T. *et al.*, 2014; Lee, N. *et al.*, 2016). Patterns of TILs in melanoma were first classified by Clark and colleagues in 1989 where the three categories, absent, non-brisk (focal TIL infiltrate) or brisk (infiltrate at the base or diffuse of the entire

vertical growth phase), were described (Clark Jr, W.H. *et al.*, 1989; Lee, N. *et al.*, 2016). The Melanoma Institute of Australia (MIA) recently proposed a novel TIL grading system (grades 0-3) which is based on their density and location in the dermis (Azimi, F. *et al.*, 2012). Efforts are currently underway for the introduction of a cancer classification system, the Immunoscore, a TIL grading system based on the immune context and the enumeration of lymphocyte populations (CD3/CD45RO, CD3/CD8 or CD8/CD45RO) currently developed for colorectal cancer but ultimately also applicable to melanoma (Galon, J. *et al.*, 2014). Based on the emerging prominence of T cell infiltrates in the diagnosis of melanoma but also due to reports that cAMP repression with the help of the adenylyl cyclase inhibitor MDL-12, 330A hydrochloride revokes Treg induced immunosuppression (Klein, M. *et al.*, 2012), the effect of cAMP inhibition on the immune cell content of the B16F10-OVA murine melanoma model was studied.

cAMP reduction as a result of the application of MDL-12, 330A hydrochloride loaded, or empty micelles revealed that inhibition of the adenylyl cyclases resulted in a significant increase of T and NKT cells infiltrating the tumour (Figure 4.8 A, Figure 4.8 B, Figure 4.8 C, Figure 4.8 D). The positive correlation of increased survival upon TIL infiltration (Galon, J. *et al.*, 2014), could be corroborated for the intervention with the cAMP reducing strategy of adenyl cyclase inhibition. While no numerical changes were observed in terms of NK cells (Figure 4.8 A, Figure 4.8 B, Figure 4.8 E), it remains to be investigated weather subpopulations of NK cells had not been affected by the treatment. In contrast to the prominent increase in T cells (Figure 4.8 A, Figure 4.8 B, Figure 4.8 C), a significant decrease of Tregs was noted in the tumour tissue upon its treatment with MDL-12 330A, hydrochloride loaded micelles (Figure 4.8 A, Figure 4.8 B, Figure 4.8 F). The reduction of Tregs in treated tumours too correlates with a better survival (Galon, J. *et al.*, 2014). It also comes with the resolution of immunosuppression, a state provoked by signalling of adenosine through the adenosine receptors $A_{2a}R$ and $A_{2b}R$ which leads to engagement of the adenylyl cyclases and consequently production of cAMP. The dampening of immunosuppression is however also helped by the reduction in the number of Tregs which upon the expression of CD39 and CD73 can generate adenosine (Muller-Haegele, S. *et al.*, 2014). Furthermore, it is known that cAMP repression by MDL-12, 330A hydrochloride leads to the re-expression of nuclear factor of activated T cells, cytoplasmic 1 (NFATc1) expression which subsequently induces expression of an isoform of NFATc1, namely NFATc1/αA (Klein, M. *et al*., 2012). In a glucose deficient environment such as in tumours, the diminished anti-tumour response has been linked to a lack of the glycolytic

metabolite phosphoenolpyruvate (PEP) which in a well glycosylated environment blocks sarco/ER Ca^{2+}-NFAT signalling (SERCA) to sustain T cell receptor-mediated Ca^{2+}-NFAT signalling (Ho, P.C. *et al.*, 2015). NFATc1 has also been linked to cytotoxic T lymphocyte exhaustion in the context of chronic infection (Agnellini, P., *et al.*, 2007).

The functional state of $CD4^+$ and $CD8^+$ cells upon cAMP repression was investigated by assessing the production of IFN-γ and KLRG-1 (Figure 4.9 A). While IFN-γ production in $CD4^+$ cells was not affected, it was significantly decreased in $CD8^+$ cells (Figure 4.9 B). The expression of KLRG-1 was however greatly reduced in both the $CD4^+$ and $CD8^+$ compartment upon treatment with MDL-12, 330A hydrochloride (Figure 4.9 C). Decreased expression of KLRG-1 on both $CD4^+$ and $CD8^+$ cells revoked T cell exhaustion, a state marked by an increased expression of KLRG-1 and a decrease in the number of $CD4^+$ cells (Wherry, E.J. *et al.*, 2003; Gholami, M.D. *et al.*, 2017). It is furthermore associated with an expression of surface markers CD57, CD95, PD-1, CTLA-4, T cell immunoglobulin and mucin-domain containing-3 (TIM-3), LAG-3 or B and T lymphocyte attenuator (BTLA), the transcription factors NFAT, PR domain zinc finger protein 1 (Blimp-1), basic leucine zipper transcription factor, ATF-like (BATF) and FoxP3 (Gholami, M.D., *et al.*, 2017) as well as $CD8^+$ cells origining from the $CD127^+$ subset of memory precursors (Angelosanto, J.M., *et al.*, 2012; Wherry, E.J. & Kurachi, M., 2016). Exhausted $CD8^+$ have been further defined by the differential expression of the T cell associated transcription factor T-box transcription factor TBX21 (T-bet) and Eomesodormin (Eomes), a marker for immunosuppression. $Tbet^{high}Eomes^{low}PD-1^{int}$ $CD8^+$ which proliferate and produce cytokines convert upon antigen exposure to $Tbet^{low}Eomes^{high}PD-1^{hi}CD8^+$, a population expressing multiple inhibitory receptors with decreased proliferative and cytokine producing capacity which displays lytic functions and accumulates in the periphery (Paley, M.A. *et al.*, 2012; Zarour, H.M., 2016). The ability to produce IFN-γ by $PD-1^-CD8^+$ in contrast to $PD-1^+CD8^+$ has previously been reported in a study based on human melanoma tissue (Inozume, T., *et al.*, 2010).

Next to the T cell compartment, the effect of MDL-12, 330 A hydrochloride on the myeloid compartment was probed. As the number of neutrophils/granulocytes significantly decreased upon cAMP repression (Figure 4.10 A, Figure 4.10 B, Figure 4.10 C), the functional state of these myeloid TILs was determined. cAMP interference resulted in a shift from patrolling monocytes ($CD45^+Lin(CD3, CD45R/B220, NK1.1, Ly6G)^-CD11b^+CD115^+Ly6C^{low}Nur77^+$) in untreated tumours to an increase in the number of inflammatory monocytes ($CD45^+Lin$ (CD3, $CD45R/B220, NK1.1, Ly6G)^-CD11b^+CD115^+Ly6C^{high}Nur77^-$) (Figure 4.11 A, Figure 4.11 B,

Figure 4.11C). It has previously been acknowledged that myeloid-derived suppressor cells (MDSCs), which are subdivided into monocytic (CD11b$^+$Ly6G^{low}Ly6C^{high}) and granulocytic/neutrophil-like (CD11b$^+$Ly6G^{high}Ly6C^{low}) cells, promote carcinogenesis, induce T cell exhaustion, and supress T cell activation (Jiang, Y. *et al.*, 2015). Their suppressive activities, provoked by the accumulation of cAMP, is due to the adenosine receptor A$_{2b}$R expressed on MDSC. These are further promoted by an increase of both CD39 and CD73, needed for the generation of adenosine on granulocytic MDSCs (Ryzhov, S. *et al.*, 2011; Muller-Haegele, S. *et al.*, 2014).

cAMP interference using the adenylyl cyclase inhibitor MDL-12, 330A hydrochloride revealed previously described favourable changes in the tumour microenvironment which includes a number of different immune cell subpopulations. These alterations can be explained and correlated to findings in the context of the glucose metabolism in general and the cAMP pathway in particular. In addition, these observations demonstrate the close interlink between the different cell populations. While cAMP interference can interfere with T cell exhaustion, the expression of NFATc1 by Tregs upon cAMP repression has been linked to cytotoxic T cell exhaustion (Agnellini, P. *et al.*, 2007), in addition MDSCs have been described to induce T cell exhaustion and supress T cell activation (Jiang, Y. *et al.*, 2015). As these observations represent an explanation for the repression of the tumour growth upon decrease of the cAMP content, functional studies as well as the use of more markers would be needed to extend our understanding of the mechanisms contributing towards the reduction of the tumour burden. Furthermore, it would be interesting to study the impact of cAMP interference not only with regard to immune cells but also the greater tumour microenvironment.

5.4 Combination of cAMP Repression and Cell Depletion Strategies for Melanoma Therapy

Reduction of the tumour size of the murine B16F10-OVA model upon intervention with the adenylyl cyclase inhibitor MDL-12, 330A hydrochloride (Figure 4.3 A, Figure 4.3 B) the detailed insight gained regarding the provoked changes of the immune cell infiltrate (Figure 4.8, Figure 4.9, Figure 4.10, Figure 4.11) as well as propositions to move towards a combination of different approaches to ultimately reach an effective therapeutic regiment (Koller, K.M. *et al.*, 2016), led to the idea of combining cAMP interference with the depletion of immune cell subsets. The drastic changes in the myeloid compartment (Figure 4.10, Figure 4.11) and previous reports indicating a reduction of the tumour size upon depletion of the myeloid

compartment (Jablonska, J. *et al.*, 2010) initiated the combination of both cAMP reduction and granulocyte depletion. Further reduction of the number of granulocytes, in particular neutrophils, by their depletion while interfering with the accumulation of cAMP by treatment with the adenylyl cyclase inhibitor MDL-12, 330A hydrochloride did not result in a further reduction of the tumour burden (Figure 4.12 A, Figure 4.12, B) indicating that granulocytes are either indispensable for the working of MDL-12, 330A hydrochloride or that their depletion alters other mechanisms of tumour defence.

The drastic reduction of Treg in the tumour microenvironment upon cAMP interference (Figure 4.13 B), the presumably resulting resolution of immunosuppression as well as studies pointing towards the initiation of a beneficial anti-tumour response upon transient Treg depletion (Klages, K.*et al.*, 2010) promoted the efforts to try to combine cAMP interference and Treg depletion to fully abolish tumour growth. MDL-12, 330A hydrochloride treatment and non-therapeutic punctual Treg depletion (Figure 4.13 C) resulted in a complete tumour abolishment (Figure 4.13 D), survival (Figure 4.13 E) and a later persisting protection (Figure 4.13 F) demonstrating that the MDL-12, 330A hydrochloride driven tumour tissue reprogramming efficiently combines with the removal of Tregs. Regrettably, so far it has not been possible to convincingly translate Treg depletion regiments successfully established in mice into the clinical setting (Jacobs, F.M. *et al.*, 2012). This is mainly due to the lack of a sole and specific Treg marker in humans. While in mice the transcription factor FoxP3 has been recognized as a reliable marker, it cannot be used as such for human Tregs since it can also be expressed by activated $CD4^+$ T effector or tissue cells and might not be expressed in selected activated Tregs. Instead the expression level of CD25 has commonly been used to identify activated Tregs ($CD4^+CD25^+$). The expression of molecules such as CTLA-4, glucocorticoid-induced TNFR-related protein (GITR), PD-1, inducible T cell costimulator (ICOS), Chemokine Receptor (CCR) 4, CCR6 or CCR7 is commonly used to ascribe further functional characteristics to Tregs (Whiteside, T.L. & Jackson, E.K., 2013). Cyclophosphamide, Denileukin diftitox, anti-CD25 (Clone: PC61), daclizumab, immunotoxin as well as FoxP3 vaccination have been studied both in the murine and human setting. Variable responses in terms of Treg ablation, tumour reduction and immunological responses have been observed. It has however been suggested that further studies into the timing, dosage and possibly also trials in patients prior to stage IV might reveal a route to successfully establish Treg ablation as a therapeutic option (Jacobs, F.M *et al.*, 2012)

5.5 Protective and Therapeutic Intervention of B16F10-OVA with Polymer Brushes

Another therapeutic strategy ventured in the fight against cancer are protective and therapeutic vaccination strategies (Fan, Y. & Moon, J.J., 2015). Since the first effort by Dr. William Coley in 1891 to cure cancer by the intratumoral administration of Coley's Toxin (inactivated *Streptococcus pyogenes* and *Serratia marsescenses*), the FDA has approved two prophylactic and one therapeutic cancer vaccine. While since 1981 potential liver cancer caused by hepatitis B can be prevented, protective measures against cervical cancer were introduced in 2006 with a vaccination regiment against human papillomavirus (HPV) (Guo, C. *et al.*, 2013). In 2010, Sipuleucel-T also referred to as Provengen, a vaccine made from endogenous DCs incubated with a genetically engineered fusion protein made from granulocyte-macrophage colony stimulating factor (GM-CSF) and prostate-specific phosphatase (PAP), was approved by the FDA for the therapeutic treatment of prostate cancer (Cheever, M.A. & Higano, C.S., 2011; Guo, C. *et al.*, 2013). Since then extensive efforts have been made to expand on the already existing cancer vaccines, with the help of numerous strategies which include: autologous and allogenic tumour whole cell vaccines, DC vaccines as well as subunit antigen specific protein, peptide, DNA, ribonucleic acid (RNA) and viral based vaccines and the use of adjuvants and other immune modulating agents (Guo, C. *et al.*, 2013).

Next to the lack of suitable antigens, traditional vaccine delivery systems are unable to efficiently present tumour antigens or adjuvants to APCs and intracellular compartments (Fan, Y. & Moon, J.J., 2015). Nanoparticle-based systems in the form of for example emulsions, self-assembled proteins, virus-like particles, liposomes, immune-stimulating complexes and inorganic or polymeric nanoparticles have been developed to improve the efficacy of protective and therapeutic tumour vaccination strategies (Zhao, L. *et al.*, 2014). Novel azide functionalized polysarcosine brushes with polylysine backbone and polysarcosine side chains labelled with the fluorescent dye Alexa Fluor 647 and functionalized with the model antigen OVA and the nucleic-acid-based immune modulator CpG (Figure 4.14 A, Figure 4.14 B, Figure 4.14 C) were characterized and compared to soluble OVA. In contrast to soluble OVA, the nanoparticle-based system was able to delay and significantly alter the body distribution of the nanoparticle bound antigen and adjuvant (Figure 4.15 A, Figure 4.15 B, Figure 4.15 C). These results indicate that the intermediate sized polymer brushes with a hydrodynamic radius of 21 nm prevent a fast redistribution of the antigen and adjuvant but instead anchor these in the skin allowing them to efficiently drain to close by lymph nodes and for a prolonged exposition to APCs (Fan, Y. & Moon, J.J., 2015). The results also correlate with the observations when the

T cell response upon vaccination with brushes coupled with OVA or OVA-CpG was probed, which in contrast to soluble OVA resulted in a lasting systemic response (Figure 4.16 A, Figure 4.16 B).

Investigations into the potential of the polymer brushes as a protective cancer vaccine revealed favourable results as tumour onset could be prevented (Figure 4.17 A, Figure 4.17 B). When used in a therapeutic regiment, it was possible to significantly reduce tumour outgrowth (Figure 4.18 A, Figure 4.18 B). Unlike soluble OVA, the use of polymer brushes anchors the vaccine in the skin and allows for a steady redistribution and an extended contact of the antigen and adjuvant with professional APCs, such as B cells, macrophages, or DCs. Prolonged contact with APCs allows for cross presentation of exogenous materials resulting in activated cytotoxic CD8$^+$ T lymphocytes entering systemic circulation to, upon the encounter of a target cell, eradicate them by secreting granzymes and perforins. In stark contrast to traditional vaccines where the use of soluble antigens frequently leads to the favouring of the CD4$^+$ T cell response, which, determined by polarizing cytokines, leads to their conversion to distinctive helper T cell subtypes, it is essential to promote the CD8$^+$ T cell response in the context of cancer vaccines (Fan, Y. & Moon, J.J., 2015). While these results were generated using a highly artificial model, they do still give the incentive to further investigate the azide functionalized polysarcosine brushes with polylysine backbone and polysarcosine side chains and to possibly even combine this strategy with the reduction of cAMP by intervening the cAMP pathway. A similar approach, the administration of a cancer vaccine in combination with IFN-α, which leads to an optimized antitumor response by a concerted induction of immune stimulation of DCs and T cells as well as antagonized Treg mediated immune suppression, has previously been proposed (Pace, L., *et al.*, 2010; Guo, C. *et al.*, 2013). As IFN-α has extensively been used to, amongst others, treat cancer, considerable off target effects have however also been unravelled which include a contribution towards the breaking of peripheral tolerance through activation and differentiation of naïve autoreactive T cells as well as the onset of type I diabetes mellitus or systemic lupus erythematosus (Gogas, H. *et al.*, 2006; Guo, C. *et al.*, 2013).

6. Conclusion

In vivo evaluation of cAMP inhibition using the adenylyl cyclase inhibitor MDL-12, 330A hydrochloride in the context of the murine melanoma B16F10-OVA and the MC-38 murine adenocarcinoma model showcased its potential as a therapeutic in the context of the B16F10-OVA melanoma model as it was able to significantly reduce tumour burden. Its failure to effectively fight adenocarcinoma is not only justified by its lack of cAMP but also by metabolic mechanism divergent of malignant melanoma.

Encapsulation of the adenylyl cyclase inhibitor MDL-12, 330A hydrochloride into micellar structures made from the novel amphiphilic polypeptoid-*block*-polypeptide copolymer polysacrcosine-*block*-polyglutamatic acid bezylester (PSar-b-PGlu(OBn)) and its *in vitro* and *in vivo* application towards B16F10-OVA revealed that cAMP repression effectively reduces tumour growth. It is able to emulate its therapeutic effect without provoking any detectable adverse or toxic side effects. *In vivo*, peritumoral application was selected as in contrast to venous administration it permits the therapeutic to primarily accumulate at the tumour site, presumably due to the EPR effect, and is readily excreted via the kidney. Modification of the particle in form of for example surface modifications is warranted to improve peritumoral and allow for venous administration. It however must be kept in mind that possible improvements of therapy solely based on the EPR effect might not translate into the clinical settings as the animal model used for its study differs quite drastically from clinically relevant tumours.

A detailed investigation into the tumour immune cell content upon cAMP repression revealed significant quantitative and functional changes in terms of T cells and neutrophils/granulocytes congruent with observations by others. Based on these results but also due to a trend towards the combination of current and novel strategies a therapeutic regiment involving cAMP repression and punctual Treg ablation to abolish tumour growth was successfully probed. Translation of the proposed regiment into the clinic does however seem unlikely as regrettably, so far, mainly due to a lack of a sole and specific human Treg marker, it has not been possible to convincingly implement regiments involving Treg depletion in humans.

Azide functionalized polysarcosine brushes with polylysine backbone and polysarcosine side chains coupled with antigen and adjuvant revealed its potential as a protective and therapeutic cancer vaccine. In contrast to soluble OVA, polymer brushes allow for a prolonged contact of APCs with both antigen and adjuvant presumably resulting in cross presentation and activation

of cytotoxic CD8$^+$ T lymphocytes. To ultimately fully eradicate tumour growth in a therapeutic regiment, it would be interesting to try to combine this approach with cAMP repression.

7. References

Abrahamsen, H., Baillie, G., Ngao, J., Vang, T., Nika, K., Ruppelt, A., Mustelin, T., Zaccolo, M., Houslay, M., Tasken, K., 2004. TCR- and CD28-mediated Recruitment of Phosphodiesterase 4 to Lipid Rafts Potentiates TCR Signaling. Journal of Immunology, 173 (8): 4847-4858.

Agnellini, P., Wolint, P., Rehr, M., Cahenzli, J., Karrer, U., Oxenius, A., 2007. Impaired NFAT nuclear translocation results in split exhaustion of virus-specific CD8^{+} T cell function during chronic viral infection. Proceedings of the National Academy of Sciences of the United States of America, 104 (11): 4565-4570.

Akasaka, K., Maesawa, C., Shibazaki, M., Maeda, F., Takahashi, K., Akasaka, T., Masuda, T., 2009. Loss of class III beta-tubulin induced by histone deacetylation is associated with chemosensitivety to paclitaxel in malignant melanoma cells. Journal of Investigative Dermatology, 129 (6): 1516-1526.

Alvarez, E., 2002. Murine melanoma: Historical perspective on the development of a solid tumor model. Tumor Models in Cancer Research, Vol I, Chapter. 4, Page 73-89. Beverly A. Teicher, Humana Press Inc., New Jersey.

Amunjela, J.N., Tucker, S.J., 2016. POPDC proteins as potential novel therapeutic targets in cancer. Drug Discovery Today, 21 (12): 1920-1927.

Angelosanto, J.M., Blackburn, S.D., Crawford, A., Wherry, E.J., 2012. Progressive Loss of Memory T Cell Potential and Commitment to Exhaustion during Chronic Viral Infection. Journal of Virology, 86 (15): 8161-8170.

Australian National Industrial Chemical Notification and Assessment Scheme (NICAS) 2010. Adjustments to NICAS new chemicals processes for industrial nanomaterials. National Industrial Chemicals notification and Assessment Scheme, Chemical Gazette, 10: 14.

Azevedo, M.F., Faucz, F.R., Bimpaki, E., Horvath, A., Levy, I., de Alexandre, R.B., Ahmad, F., Manganiello, V., Stratakis, C.A., 2014. Clinical and molecular genetics of the phosphodiesterases (PDEs). Endocrine Reviews, 35 (2): 195-233.

Azimi, F., Scolyer, R.A., Rumcheva, P., Moncrieff, M., Murali, R., McCarthy, S.W., Saw, R.P., Thompson, J.F., 2012. Tumor-infiltrating lymphocyte grade is an independent predictor of sentinel lymph node status and survival in patients with cutaneous melanoma. Journal of Clinical Oncology, 30 (21): 2678-2683.

Bacher, N., Raker, V. Hofmann, C., Graulich, E., Schwenk, M., Baumgrass, R., Bopp, T., Zechner, U., Merten, L., Becker, C. Steinbrink, K., 2013. Interferon-α suppresses cAMP to disarm human regulatory T cells. Cancer Research, 73 (18): 5647-5656.

Bae, K.H., Chung, H.J., Park, T.G., 2011. Nanomaterials for cancer therapy and imaging. Molecules and Cells, 31 (4): 295-302.

Balch, C.M., Gershenwald, J.E., Soong, S.J., Thompson, J.F., Atkins, M.B., Byrd, D.R., Buzaid, A.C., Cochran, A.J., Coit, D.G., Ding, S., Eggermont, A.M., Flaherty, K.T., Gimotty,

P.A., Kirkwood, J.M., McMaster, K.M., Mihm Jr., M.C., Morton, D.L., Ross, M.I., Sober, A.J., Sondak, V.K., 2009. Final version of 2009 AJCC melanoma staging and classification. Journal of Clinical Oncology, 27 (36): 6199-6206.

Balijinnyam, E., Iwatsubo, K., Kurotani, R., Wang, X., Ulucan, C., Iwatsubo, M., Lagunoff, D., Ishikawa, Y., 2009. Epac increases melanoma cell migration by heperan sulfate-realted mechanism. America Journal of Physiology - Cell Physiology, 297 (4): C802-813.

Barnden, M.J., Allison, J., Heath, W., Carbone, F.R., 1998. Defective TCR expression in transgenic mice constructed using cDNA-based alpha- and beta-chain genes under the control of heterologous regulatory elements. Immunology and Cell Biology, 76 (1): 34-40.

Bellone, M., Cantarella, D., Castiglioni, P., Crosti, M.C., Ronchetti, A., Moro, M., Garancini, M.P., Casorati, G., Dellabone, P., 2000. Relevance of the tumor antigen in the validation of three vaccination strategies for melanoma. Journal of Immunology, 165 (5): 26651-2656.

Bender, A.T., Ostenson C.L., Giordano D., Beavo J.A., 2004. Differentiation of human monocytes in vitro with granulocyte-macrophage colony-stimulating factor and macrophage colony-stimulating factor produces distinct changes in cGMP phosphodiesterase expression. Cell Signalling, 16 (3): 365–374.

Berciano-Guerrero, M.A., Montesa-Pino, A. Castaneda-Penalvo, G., Munoz-Fernandez, L., Rodriguez-Flores, J., 2014. Nanopartciles in Melanoma. Current Medicinal Chemistry, 21 (32): 3701-3716.

Bertalanffy, F.D., McAskill, C., 1964. Rate of Cell Division of Malignant Mouse Melanoma B16. Journal of the National Cancer Institute, 32: 535-544.

Berthet, J., Rall, T.W., Sutherland, E.W., 1957. The relationship of epinephrine and glucagon to liver phosphorylase. IV. Effect of epinephrine and glucagon on the reactivation of phosphorylase in liver homogenates. Journal of Biological Chemistry, 224 (1): 463-475.

Birke, A., Huesmann, D., Kelsch, A., Weilbächer, M., Xie, J., Bros, M., Bopp, T., Becker, C., Landfester, K., Barz, M., 2014. Polypeptoid-block-polypeptide copolymers: synthesis, chracterization, and application of ampiphilic block Copolypept(o)ides in drug formulation and miniemulsion techniques. Biomaromolecules, 15 (2), 548-557.

Bossuyt, X., Marti, G.E., Fleischer, T.A., 1997. Comparative analysis of whole blood lysis methods for flow cytometry. Cytometry, 30 (3): 124-133.

Breslow, A., 1970. Thickness, cross-sectional areas and depth of invasion in the prognosis of cutaneous melanoma. Annals of Surgery, 172 (5): 902-908.

B16-F10 (ATCC® CRL-6475™). Available from: https://www.lgcstandards-atcc.org/products/all/CRL-6475.aspx?geo_country=de (Last accessed: April 2018).

Carbone, F.R., Bevan, M.J., 1989. Introduction of ovalbumin-specific cytotoxic T cells by in vivo peptide immunization. The Journal of Experimental Medicine, 169 (3): 603-612.

Carswell, R., 1838. Illustrations of the Elementary Forms of Disease. London: Longman, Orme, Brown, Green and Longman.

Chang, T.-S., 2012. Natural Melanogenesis Inhibitors Acting Through the Down-Regulation of Tyrosine Activity. Materials, 5 (9): 1661-1685.

Chartrain, M., Riond, J., Stennevin, A., Vandenberghe, I., Gomes, B., Lamant, L., Meyer, N., Gairin, J.E., Guilbaud, N., Annereau, J.P., 2012. Melanoma Chemotherapy Leads to the Selection of ABCB5-expressing Cells. PLOS ONE, 7(5): e36762.

Chattopadhyay, P.K., Gierahn, T.M., Roederer, M., Love, J.C., 2014. Single-cell technologies for monitoring immune systems. Nature Immunology, 15:128-135.

Chattopadhyay, P.K., Roederer, M., 2012. Cytometry: Today`s technology and tomorrow`s horizons. Methods, 57 (3): 251-258.

Cheever, M.A., Higano, C.S., 2011. PROVENGE (Sipuleucel-T) in prostatate cacner: the first FDA-approved therapeutic cancer vaccine. Clinical Cancer Research, 17 (3): 3520-3526.

Cheung, K.C., Di Berardino, M., Schade-Kampmann, G., Hebeisen, M., Pierzchalski, A., Bocsi, J., Mittag, A, Tarnok, A., 2010. Microfluidic impedance-based flow cytometry. Cytometry A, 77 (7): 648-666.

Chichorek, M., Wachulska, M., Stasiewicz, A., Tyminska, A., 2013. Skin melanocytes: biology and development. Postepy Dermatologii I Alergologii, 30 (1): 30-41.

Choi, H.S., Liu, W., Misra, P., Tanaka, E., Zimmer, J.P., Itty Ipe, B., Bawendi, M.G., Frangioni, J.V., 2007. Renal clearance of quantum dots. Nature Biotechnology, 25: 1165-1170.

Clark Jr., W.H., Elder, D.E., Guerry IV, D., Braitman, L.E., Trock, B.J., Schultz, D., Synnestvedt, M., Halpern, A.C., 1989. Model Predicting Survival in Stage I Melanoma Based on Tumor Progression. Journal of the National Cancer Institute, 81 (24): 1893-1904.

Clark Jr., W.H., From, L., Bernadino E.A., Mihm M. C., 1969. The histogenesis and biological behaviour of primary human malignant melanoma of the skin. Cancer Research, 29 (3): 705-727.

Cooper, D.M.F., 2005. Compartmentalization of adenylate cyclase and cAMP signalling. Biochemical Society Transactions, 33 (6): 1319-1322.

Corbett, T.H., Grisewold Jr., D.P., Roberts, B.J., Peckham, J.C., Schabel Jr., F.M., 1975. Tumor Induction Relationships in Development of Transplantable Cancers of the Colon in Mice for Chemotherapy Assays, with a Note on Carcinogen structure. Cancer Research, 35 (9): 2434-2439.

Costin, G.E., Hearing, V.J., 2007. Human skin pigmentation: melanocytes modulate skin color in response to stress. The FASEB Journal, 21 (4): 976-994.

Coulter, W.H., 1957. High speed automatic blood cell counter and cell size analyser. Proceedings of the National Electronics Conference, 12: 1034-1042.

Curnis, F., Sacchi, A., Corti, A., 2002. Improving chemotherapeutic drug penetration in tumors by vascular targeting and barrier alteration. Journal of Clinical Investigation, 110 (4): 475-482.

Danhier, F., 2016. To exploit the tumor microenvironment: Since the EPR effect fails in the clinic, what is the future of nanomedicine? Journal of Controlled Release, 244 (Pt A): 108-121.

Delghandi, M.P., Johanessen, M., Moens, U., 2005. The cAMP signalling pathway activates CREB through PKA, p38 and MSK1 in NIH 3T3 cells. Cell Signaling, 17 (11): 1343-1351.

Di Meglio, P., Perera, G.K., Nestle, F.O., 2011. The multitasking organ: recent insights into skin immune function. Immunity, 35 (6): 867-869.

Din, F., Aman, W., Ullah, I., Qureshi, O.S., Mustapha, O., Shafique, S., Zeb, A., 2017. Effective use of nanocarriers as drug delivery systems for the treatment of selected tumors. International Journal of Nanomedicine, 12 (17): 7291-7309.

Dittrich, W., Göhde, W., 1969. Notizen: Impulsfluorometrie bei Einzelzellen in Suspension. Zeitschrift für Naturforschung B, 24: 360-361.

Drexler, K.E., 1986. Engines of Creation: The Coming Era of Nanotechnology. Anchor Books, New York.

Emery, A.C., Eiden, M.V., Eiden, L.E., 2013. A New Site and Mechanism of Action for the Widely Used Adenylate Cyclase Inhibitor SQ22,536. Molecular Pharmacology, 83 (1): 95-105.

Enyedi, K.N., Toth, S., Szakacs, G., Mezo, G., 2017. NGR-peptide-drug conjugates with dual targeting properties. PLoS ONE 12 (6): e0178632.

Fan, Y, Moon, J.J., 2015. Nanoparticle Drug Delivery Systems Designed to Improve Cancer Vaccines and Immunotherapy. Vaccines, 3 (3): 662-685.

Fang, R.H., Zhang, L., 2016. Nanoparticle-Based Modulation of the Immune System. Annual Review of Chemical and Biomolecular Engineering, 7: 305-326.

Fang, S., Fang, X., 2016. Advances in glucose metabolism research in colorectal cancer. Biomedical Reports, 5 (3): 289-295.

Feynman, R.P., 1960. There`s Plenty of Room at the Bottom. Engineering and Science, 23 (5): 22-36.

Fidler, I.J., 1970. Metastasis: quantitative analysis of distribution and fate of tumor emboli labeled with 125I-5-ido-2´-deoxyuridine. Journal of the National Cancer Institute, 45 (4): 773-782.

Fidler, I.J., 1973a. The relationship of embolic homogeneity, number, size and viability to the incidence of experimental metastasis. European Journal of Cancer, 9 (3): 223-227.

Fidler, I.J., 1973b. Selection of Successive Tumour Lines for Metastasis. Nature: New Biology, 242: 148-149.

Fidler, I.J., Nicolson, G.L., 1976. Organ selectivity for implantation survival and growth of B16 melanoma variant tumor lines. Journal of the National Cancer Institute, 57 (5): 1199-1202.

Fischer, G.M., Vashisht Gopal, Y.N., McQuade, J.L., Peng, W., DeBerardinis, R.J., Davies, M.A., 2018. Metabolic strategies of melanoma cells: Mechanisms, interactions with the tumor microenvironment, and therapeutic implications. Pigment Cell Melanoma Research, 31 (1): 11-30.

Franco-Molina, M.A., Mendoza-Gambosa, E., Sierra-Rivera, C.A, Zapata-Benavides, P., Miranda-Hernandez, D.F., Chavez-Reyes, A., Rivera-Morales, L.G. Tamez-Guerra, R., Rodriguez-Padilla, C., 2012. *In vitro* and *in vivo* antitumoral activity of sodium dichloroacetate (DCA-Na) against murine melanoma. African Journal of Microbiology Research, 6 (22): 4782-4796.

Freitas Jr., R.A., 1999. Nanomedicine, vol. I: Basic capabilities. Lands Biosciences, Georgetown, TX, USA.

Friberg, S., Nyström, A.M., 2016. NANOMEDICINE: will it offer possibilities to overcome multiple drug resistance in cancer? Journal of Nanobiotechnology, 14: 17-32.

Fulwyler, M.J., 1965. Electronic separation of biological cells by volume. Science, 150 (3698): 910-911.

Gadea, A., Lopez, E., Lopez-Colome, A.M., 1999. The adenylate cyclase inhibitor MDL-12330A has a non-specific effect on glycine transport in Müller cells from the retina. Brain Research, 838 (1-2): 200-204.

Galon, J., Mlecnik, B., Bindea, G., Angell. H.K., Berger, A., Lagorce, C., Lugli, A., Zlobec, I., Hartmann, A., Bifulco, C., Nagtegaal, I.D., Palmqvist, R., Masucci, G.V., Botti, G., Tatangelo, F., Delrio, P., maio, M., Laghi, L., Grizzi, F., Asslaber, M., D`Arrigo, C., Vidal-Vanaclocha, F., Zavadova, E., Chouchane, L., Ohashi, P.S., Hafezi-Bakhtiari, S., Wouters, B.G., Roehrl, M., Nguyen, L., Kawakami, Y., Hazama, S., Okuno, K., Ogino, S., Gibbs, P., Waring, P., Sato, N., Torigoe, T., Itoh, K., Patel, P.S., Shukla, S.N., Wang, Y., Kopetz, S., Sinicrope, F.A., Scripcariu, V., Ascierto, P.A., Marincola, F.M., Fox, B.A., Pages, F., 2014. Towards the introduction of the 'Immunoscore' in the classification of malignant tumours. Journal of Pathology, 232 (2): 199-209.

Garay, R.P., El-Gewely, R., Armstrong, J.K., Garratty, G., Richette, P., 2012. Antibodies against polyethylene glycol in healthy subjects and in patients treated with PEG-conjugated agents. Expert Opinion in Drug Delivery, 9 (11): 1319-1323.

Garbe, C., Peris, K., Hauschild, A., Saiag, P., Middleton, M., Bastholt, L., Grob, J.J., Malvehy, J., Newton-Bishop, J., Stratigos, A.J., Pehamberger, H., Eggermont, A.M., 2016. Diagnosis and treatement of melanoma. European consensus-based interdisciplinary guideline – Update 2016. European Journal of Cancer, 63: 201-217.

Garcia-Borron, J.C., Abdel-Malek, Z., Jimenez, Cervantes, C., 2014. MC1R, the cAMP pathway, and the response to solar UV: extending the horizon beyond pigmentation. Pigment Cell Melanoma Research 27 (5): 699-720.

Gholami, M.D., Kardar, G.A., Saeedi, Y., Heydari, S., Garssen, J., Falak, R., 2017. Exhaustion of T lymphocytes in the tumor microenvironment: significance and effective mechanisms. Cellular Immunology, 322: 1-14.

Gogas, H., Ionnovich, J., Dafni, U., Stavropoulou-Giokas, C., Frangia, K., Tsoutsos, D., Panagiotou, P., Polyzos, A., Papadopoulos, O., Stratigos, A., Markopoulos, C., Bafaloukos, D., Pectasidies, D., Fountzilas, G., Kirkwood, J.M., 2006. Prognostic significance of autoimmunity during treatment of melanoma with interferon. New England Journal of Medicine, 354 (7): 709-718.

Green, E., 1968. Handbook of genetically standardized JAX mice. The Jackson Laboratory, Bar Harbour, M.E., pages 57-58.

Grupp, G., Grupp, I.L., Johnson, C.L., Matlib, M.A., Rouslin, W., Schwartz, A, Wallick, E.T., Wang, T., Wisler, P., 1980. Effect of RMI 12330A, a new inhibitor adenylate cyclase on myocardial function and subcellular activity. British Journal of Pharmacology, 70 (3): 429-442.

Guellaen, G., Mahu, J.L., Mavier, P., Berthelot, P., Hanoune, J., 1977. RMI 12330A, an inhibitor of adenylate cyclase in rat liver. Biochemica et Biophysica Acta (BBA) -Enzymology, 484 (2): 465-475.

Guo, C., Manjili, M.H., Subjeck, J.R., Sarkar, D., Fisher, P.B., Wang, X.Y., 2013. Therapeutic cancer vaccines: past, present and future. Advanced Cancer Research, 119: 421-475.

Hamad, I., Christy Hunter, A., Rutt, K.J., Liu, Z., Dai, H., Moein Moghimi, S., 2008a. Complement activation by PEGylated single-walled carbon nanotubes is independent of C1q and alternative pathway turnover. Molecular Immunology, 45 (14): 3797-3803.

Hamad, I., Hunter, A.C., Szebeni, J., Moghimi, S.M., 2008b. Poly(ethylene glycol)s generate complement activation products in human serum through increased alternative pathway turnover and a MASP-2-dependent process. Molecular Immunology, 46, (2): 225-232.

Hanahan, D., Weinberg R.A., 2011. Hallmarks of cancer: the next generation. Cell, 144 (5): 646-674.

Hanna, R.N., Carlin, L.M., Hubbeling, H.G., Nackiewicz, D., Green, A.M., Punt, J.A., Geissmann, F., Hedrick, C.C., 2012. The transcription factor NR4A1 (Nur77) controls bone marrow differentiation and survival of Ly6C- monocytes. Nature Immunology, 12 (8): 778-785.

Health Canada, 2011. Policy Statement on Health Canada`s Working Definition for nanomaterials. Available from: https://www.canada.ca/en/health-canada/services/science-research/reports-publications/nanomaterial/policy-statement-health-canada-working-definition.html (Last Accessed: April 2018).

Herraiz, C., Garcia-Borron, J.C., Jimenez-Cervantes, C., Olivares, C., 2017. MCR1 signaling. Intracellular partners and pathophysiological implications. Biochimica et Biophysica Acta, 1863 (10 Pt A), 2448-2461.

Hersey, P., Bindon, C., Edwards, A., Murray, E., Philips, G., McCarthay, W.H., 1981. Induction of cytotoxic activity in human lymphocytes against autologous and allogeneic melanoma cells in vitro by culture with interleukin 2. International Journal of Cancer, 28 (6): 695-703.

Hersh, E.M., Del Vecchio, M., Brown, M.P., Kefford, R., Loquai, C., Testori, A., Bhatia, S., Gutzmer, R., Conry, R., Haydon, A., Robert, C., Ernst, S., Homsi, J., Grob, J.J., Kendra, K.,

Agarwala, S.S., Li, M., Clawson, A., Brachmann, C., Karnoub, M., Elias, I., Renschler, M.F., Hauschild, A., 2015. A randomized, controlled phase III trial of nab-Pacitaxel versus dacarbazine in chemotherapy-naïve patients with metastatic melanoma. Annals of Oncology, 26 (11): 2267-2274.

Hiramoto, K., Murata, T., Shimizu, K., Morati, H., Inui, M., Manganiello, V.C., Tagawa, T., Arai, N., 2014. Role of Phosphodiesterase 2 in Growth and Invasion of Human Malignant Melanoma Cells. Cell Signaling, 26 (9): 1807-1817.

Ho, P.C., Bihuniak, J.D., Macintyre, A.N., Staron, M., Liu, X., Amezquita, R., Tsui, Y.C., Cui, G., Micevic, G., Perales, J.C., Kleinstein, S.H., Abel, E.D., Insogan, K.L., Feske, S., Locasale, J.W., Bosenberg, M.W., Rathmell, J.C., Kaech, S.M., 2015. Phosphoenolpyruvate Is a metabolic Checkpoint of Anti-tumor T cell Responses. Cell, 162 (6): 1217-1227.

Hofmeister, F., 1889. Über die Darstellung von krystallisirtem Eieralbumin und die Krystallisierbarkeit colloider Stoffe. Zeitschrift für Physiologische Chemie, 14: 165-172.

Hogquist, K.A., Jameson, S.C., Heath, W.R., Howard, J.L., Bevan, M.J., Carbone, F.R., 1994. T Cell Receptor Antagonist Peptides Induce Positive Selection. Cell, 76 (1): 17-27.

Hu, C.-M., Zhang, L., 2012. Nanoparticle-based combination therapy toward overcoming drug resistance in cancer. Biochemical Pharmacology, 83 (3): 1104-1111.

Huesmann, D., Sevenich, A., Weber, B., Barz, M., 2015. A head-to-head comparison of poly(sarcosine) and poly(ethylene glycol) in peptidic, amphiphilic block copolymers. Polymer - London, 67: 240-248.

Hunt, N.H., Evans, T., 1980. RMI 12330A, an inhibitor of cyclic nucleotide phophodiesterases and adenylate cyclase in kidney preparations. Biochemica et Biophysica Acta, 613 (2): 499-506.

Hulett, H.R., Bonner, W.A., Barrett, J., Herzenberg, L.A., 1969. Cell sorting: automated separation of mammalian cells as a function of intracellular fluorescence. Science, 166 (3906): 747-749.

Inozume, T., Hanada, K.., Wang, Q.J., Ahmadzadeh, M., Wunderlich, J.R., Rosenberg, S.A., Yang, J.C., 2010. Selection of CD8+PD-1+ lymphocytes in fresh human melanomas enriches for tumor-reactive T cells. Journal of Immunotherapy, 33 (9): 956-964.

International Organization for Standardization (ISO), 2015. Online Browsing Platform. Available from: https://www.iso.org/obp/ui/#iso:std:iso:ts:80004:-2:ed-1:v1:en (Last Accessed: April 2018).

Ishida, T., Ichihara, H., Wang, X., Yamamoto, K., Kimura, J., Majima, E., Kiwada, H., 2006. Injection of PEGylated liposomes in rats elicits PEG-specific IgM, which is responsible for rapid elimination of a second dose of PEGylated liposomes. Journal of Controlled Release, 112 (1): 15-25.

Ito, A, Katoh, F., Kataoka, T.R., Tsubota, N., Asada, H., Yoshikawa, K., Maeda, S., Kitamura, Y, Yamaski, H., Nojima, H., 2000. A role for heterologous gap junctions between melanoma and endothelial cells in metastasis. Journal of Clinical Investigation,105 (9): 1189-1197.

Iyer, A.K., Khaled, g., Fang, J, Maeda, H., 2006. Exploiting the enhanced permeability and retention effect for tumor targeting. Drug Discovery Today, 11 (17-18): 812-818.

Jablonska, J., Leschner, S., Westphal, K., Lienenklaus, S., Weiss, S., 2010. Neutrophis responsive to endogenous IFN-β regulate tumor angiogenesis and growth in a mouse tumor model. Journal of Clinical Investigation, 120 (4): 1151-1164.

Jacobs, J.F., Nierkens, S., Figdor, C.G., de Vries, J.M., Adema, G.J., 2012. Regulatory T cells in melanoma: the final hurdle towards effective immunotherapy? Lancet Oncology, 13 (1): e32-42.

Jahan-Tigh, R.R., Ryan, C., Obermoser, G., Schwarzenberger, K., 2012. Flow cytometry. Journal of Investigative Dermatology, 132 (10): 1-6.

Jiang, Y., Li, Y., Zhu, B., 2015. T-cell exhaustion in the tumor microenvironment. Cell Death and Disease, 6: e1792.

Kedl, R.M., Jordan, M., Potter, T., Marrack, P., Dow, S., 2001. CD40 stimulation accelaerates deletion of tumor-specific CD8$^+$ T cells in the absence of tumor-antigen vaccination. Proceedings of the National Academy of Sciences of the United States of America, 98 (19): 10811-10816.

Keilholz, U., Brossart, P., Mackensen, A., Peschel, C., Prizkuleit, R., Schadendorf, D., Schlaeppi, M., Wörmann, B.J., Gerger, A., 2014. Melanoma, Guidelines, Recommendation of the Specialist Society for the Diagnosis and Therapy of Haematological and Oncological Diseases. Available from: https://www.onkopedia.com/de/onkopedia/guidelines/melanom/ @@view/html/index.html, (Last Accessed: July 2017).

Klages, K., Mayer, C.T., Lahl, K., Loddenkemper, C., Teng, M.W., Ngiow, S.F., Smyth, M.J., Hamann, A., Huehn, J., Sparwasser, T., 2010. Selective depletion of Foxp3+ regulatory T cells improves effective therapeutic vaccination against established malenoma. Cancer Research, 70 (20): 7788-7799.

Klein, M., Vaeth, M., Scheel, T., Grabbe, S., Baumgrass, R., Berberich-Siebelt, F., Bopp, T., Schmitt, E., Becker, C., 2012. Repression of cyclic adenosine monophosphate upregulation disarms and expands human regulatory T cells. Journal of Immunology, 188 (3):1091-1097.

Klinker, K., Barz, M., 2015. Polypept(o)ides: Hybrid Systems based on Polypeptides and Polypeptoids. Macromolecular Rapid Communications, 36 (22): 1943-1957.

Koller, K.M., Wang, W., Schell, T.D., Cozza, E.M., Kokolus, K.M., Neves, R.I., Mackley, H.B., Pameijer, C., Leung, A., Anderson, B., Mallon, C.A., Robertson, G., Drabick, J.J., 2016. Malignent malnaoma - The cradle of anti-neoplastic immunotherapy. Critical Reviews in Oncology/Hematology, 106: 25-54.

Kondo, T., Hearing, V.J., 2011. Update on the regulation of mammalian melanocyte function and skin pigmentation. Expert review of Dermatology, 6 (1): 97-108.

Kreuter, J., 2007. Nanoparticles - a historical perspective. International Journal of Pharmaceutics, 311 (1): 1-10.

Krukemeyer, M.G., Krenn, V., Huebner, F., Wagner, W., Resch, R., 2015. History and Possible Uses of Nanomedicine Based on Nanoparticles and Nanotechnological Progress. Journal of Nanomedicine and Nanotechnology, 6: 336-342.

Kumar R.K., Herbert C., Foster P.S., 2008. The "classical" ovalbumin challenge model of asthma in mice. Current Drug Targets 9 (6): 485-494.

Laennec, R.T.H., 1812. Extrait au memoire de M Laennec, sur les melanoses. Bull L`Ecole Societe de Medicine, Vol. 1., p. 24

Lahl, K., Loddenkemper, C., Drouin, C., Freyer, J., Arnason, J., Eberl, G., Hamann, A., Wagner, H., Huehn, J., Sparwasser, T., 2007. Selective depletion of Foxp3+ regulatory T cells induces a scurfy-like disease. Journal of Experimental Medicine, 204 (1): 57-63.

Lahl, K., Sparwasser, T., 2011. In vivo depletion of FoxP3+ Tregs using the DEREG mouse model. Methods in Molecular Biology, 707: 157-172.

Lakhter, A.J., Naidu, S.R., 2017. Cyclic AMP-Epac signaling pathway contributes to repression of PUMA transcription in melanoma cells. Melanoma Research, 27 (5): 411-416.

Lee, N., Zakka, L.R., Mihm Jr., M.C., Schatton, T., 2016. Tumour-infiltrating lymphocytes in melanoma prognosis and cancer immunotherapy. Pathology, 48 (2): 177-187.

Lefkimmiatis, K. & Zaccolo, M., 2014. cAMP signalling in subcellular compartments. Pharmacology & Therapeutics, 143 (3): 295-304.

Lin, D.C., Xu, L., Ding, L.W., Sharma, A., Liu, Z.L., Yang, H., Tan, P., Vadgama, J., Karlan, B.Y., Lester, J., Urban, N., Schummer, M., Doan, N., Said, J.W., Sun, H., Walsh, M., Thomas, C.J., Patel, P., Yin, D., Chan, D., Koeffler, H.P., 2013. Genomic and functional characterization of phosphodiesterase subtype 4D in human cancer. Proceedings of the National Academy of Sciences of the United States of America, 110 (15): 6109-6114.

Lippe, C., Ardizzone, C., 1991. Actions of vasopressin and isoprenaline on the ionic transport across the isolated frog skin in the presence and the absence of adenyl cyclase inhibitors MDL12330A and SQ22536. Comparative Biochemistry and Physiology Part C: Comparative Pharmacology, 99(1-2): 209-211.

Liu, J., Yu, M., Zhou, C., Zheng, J., 2013. Renal clearable inorganic nanoparticles: a new frontier of bionanotechnology. Materials Today, 16 (12): 477-486.

Lyons, A.B., Parish, C.R., 1994. Determination of lymphocyte division by flow cytometry. Journal of Immunological methods, 171 (1): 131-137.

Malassez, L.C., 1873. De la numération des globules rouges du sang. I. Des méthodes de numération. II. De la richesse du sang en globules rouges dans les différentes parties de l'arbre circulatoire. Paris.

Mantovani, G., Bondiono, S., Lania, A.G., Rodolfo, M., Peverelli, E., Polentarutti, N., Veliz Rodriguez, T., Ferrero, S., Bosari, S., Beck-Peccoz, P., Spada. A., 2008. High expression of PKA regulatory subunit 1A protein is related to proliferation of human melanoma cells. Oncogene, 27(13): 1834-1843.

Matsumura, Y., Maeda, H., 1986. A New Concept for Macromolecular Therapeutics in Cancer Chemotherapy: Mechanism of Tumoritropic Accumulation of Proteins and the Antitumor Agent Smancs. Cancer Research, 46 (12 Pt 1): 6387-6392.

Mayer, C.T., Lahl, K., Milanez-Almeida, P., Watts, D., Dittmer, U., Fyhrquist, N., Huehn, J., Kopf, M., Kretschmer, K., Rouse, B., Sparwasser, T., 2014. Advantages of Foxp3(+) regulatory T cell depletion using DEREG mice. Immunity, Inflammation and Disease, 2 (3): 162-165.

Miao, P., Sheng, S., Sun, X., Liu, J., Huang, G., 2013. Lactate dehydrogenase A in cancer: A promising target for diagnosis and therapy. IUBMB Life, 65 (11): 904-910.

Miles, M.F., Hung, P., Jungmann, R.A., 1981. Cyclic AMP regulation of lactate dehydrogenase. Quantitation of lactate dehydrogenase M-subunit messenger RNA in isoproterenol-and N6,O2′-dibutyryl cyclic AMP-stimulated rat C6 glioma cells by hybridization analysis using a cloned cDNA probe. Journal of Biological Chemistry, 256 (23):12545–12552.

Moore, M.W., Carbone, F.R., Bevan, M.J., 1988. Introduction of soluble protein into the class I pathway of antigen processing and presentation. Cell, 54 (6): 777-785.

Moghimi, S.M., Andersen, A.J., Hashemi, S.H., Lettiero, B., Ahmadvand, D., Hunter, A.C., Andresen, T.L., Hamad, I., Szebeni, J., 2010. Complement activation cascade triggered by PEG-PL engineered nanomedicines and carbon nanotubes: the challenges ahead. Journal of Controlled Release, 146 (2): 175-181.

Moran, A.E., Holzapfel, K.I., Xing, Y., Cunningham, N.R., Maltzmann, J.S., Punt, J., Hogquist, K.A., 2011. T cell receptor signal strength in T_{reg} and iNKT cell development demonstrated by a novel fluorescent reporter mouse. Journal of Experimental Medicine, 208 (6): 1279-1289.

Morita, H., Murata, T., Shimizu, K., Okumura, K., Inui, M., Tagawa, T., 2013. Characterization of phosphodiesterase 2A in human malignant melanoma PMP cells. Oncology Reports, 29 (4): 1275-1284.

Muller-Haegele, S., Muller, L., Whiteside, T.L., 2014. Immunoregulatory activity of adenosine and its role in human cancer progression. Expert Review of Clinical Immunology, 10 (7): 897-914.

Mundra, V., Li, W., Mahato, R.I., 2015. Nanoparticle-mediated drug delivery for targeting melanoma. Nanomedicine, 10 (6): 2613-2633.

Musheshe, N., Schmidt, M., Zaccolo, M., 2017. cAMP: From Long-Range Second Messenger to Nanodomain Signalling. Trends in Pharmacological Sciences, 39 (2): 209-222.

Nardin, C.A., Fitzpatrick, L., Zippin, J.H., 2014. Diverse effects of cAMP signalling in melanoma support the role of distinct microdomains in melanogenesis, metastasis, and resistance to therapy. OA Dermatology, 2 (1): 5-8.

Nasti, T.H., Timares, L., 2015. MC1R, Eumelanin and Pheomelanin: their role in determining the susceptibility to skin cancer. Photochemistry and Photobiology, 91 (1): 188-200.

Nichols, J.W., Bae, Y.H., 2014. EPR: Evidence and fallacy. Journal of Controlled Release, 190: 451-464.

Nikalje, A.P., 2015. Nanotechnology and its Application in Medicine. Medicinal Chemistry, 5 (2): 81-89.

Norris, W., 1820. Case of Fungoid Disease. The Edinburgh Medical and Surgical Journal, 16, 562-565. Photochemistry and Photobiology, 9 (1): 188-200.

Norris, W., 1857. Eight cases of melanosis with pathologicaland therapeutical remarks on that disease. London: Longman.

Overwijk, W.W., Restifo, N.P., 2001, B16 as a Mouse Model for Human Melanoma. Current Protocols in Immunology, John Wiley and Sons Inc, Philadelphia, pages 20.21-20.1.29.

Pace, L., Vitale S, Dettori B, Palombi C., La Sorsa, V., Belardelli, F., Proietti, E., Doria, G., 2010. APC activation by IFN-alpha decreases regulatory T cell and enhances Th cell functions. Journal of Immunology, 184 (11): 5969-5979.

Paley, M.A., Kroy, D.C., Odozziri, P.M., Johnnidis, J.B., Dolfi, D.V., Barnett, B.E., Bikoff, E.K., Robertson, E.J., Lauer, G.M., Reiner, S.L., Wherry, E.J., 2012. Progenitor and terminal subsets of CD8+ T cells cooperate to contain chronic viral infection. Science, 338 (6111): 1220-1225.

Parish, C.R., 1999. Fluorescent dyes for lymphocyte migration and proliferation studies. Immunology and Cell Biology, 77 (6): 499-508.

Parish, C.R., Glidden, M.H., Quah, B.J., Warren, H.S., 2009. Use of the intracellular fluorescent dye CFSE to monitor lymphocyte migration and proliferation. Current Protocols in Immunology, 84: 4.9.1-4.9.13.

Pavlova, N.N., Thompson, C.B., 2016. The Emerging Hallmarks of Cancer Metabolism. Cell Metabolism, 23 (1): 27-47.

Quah, B.J., Parish, C.R., 2012. New and improved methods for measuring lymphocyte proliferation *in vitro* and *in vivo* using CFSE-like fluorescent dyes. Journal of Immunological Methods, 379 (1-2): 1-14.

Raskovalova, T., Lokshin, A., Huang, X., Su, Y., Mandic, M., Zarour, H.M., Jackson, E.K., Gorelik, E., 2007. Inhibition of cytokine production and cytotoxic activity of human antimelanoma specific CD8+ and CD4+ T lymphocytes by adenosine-protein kinase A type I signaling. Cancer Research, 67 (12): 5949-5956.

Raz, A., McLellan, W.L., Hart, I.R., Bucana, C.D., Hoyer, L.C., Sela, B.A., Dragsten, P., Fidler, I.J., 1980. Cell Surface Properties of B16 Melanoma Variants with Differing Metastatic Potential. Cancer Research, 40 (5): 1645-1651.

Rebecca, V.W., Sondak, V.K., Smalley, K.S.M., 2012. A Brief History of Melanoma: From Mummies to Mutations. Melanoma Research, 22 (2): 114-122.

Reibold, M., Paufler, P., Levin, A.A., Kochmann, W., Pätzke, N., Meyer, D.C., 2006. Materials: carbon nanotubes in an ancient Damascus sabre. Nature, 444 (7117): 286.

Reinhardt, R.L., Liang, H.E., Bao, K., Price, A.E., Mohrs, M., Kelly, B.L., Locksley, M., 2015. A novel model for IFN-γ-mediated autoinflammatory syndromes. Journal of Immunology, 194 (5): 2358-2368.

Reinhardt, R.L., Liang, H.E., Locksley, R.M., 2009. Cytokine-secreting follicular T cells shape the antibody repertoire. Nature Immunology, 10 (4): 385-393.

Rodriguez, C.I., Setaluri, V., 2014. Cyclic AMP (cAMP) signaling in melanocytes and melanoma. Archives of Biochemistry and Biophysics: 563, 22-27.

Ryan, S.M., Brayden, D.J., 2014. Progress in the delivery of nanoparticle constructs: Towards clinical translation. Current Opinion in Pharmacology, 18: 120-128.

Ryzhov, S., Novitskiy, S.V., Goldstein, A.E., Biktasova, A., Blackburn, M.R., Biaggioni, I., Dikov. M.M., Feoktistov, I., 2011. Adenosinergic regulation of the expansion and immunosuppressive activity of $CD11b^+Gr1^+$ cells. Journal of Immunology, 187 (11): 6120-6129.

Sadana, R., Dessauer, C.W., 2009. Physiological roles for G protein-regulated adenylyl cyclase isoforms: insights from knockout and overexpression studies. Neurosignals, 17 (1): 5-22.

Schatton, T., Scolyer, R.A., Thompson, J.F., Mihm Jr., M.C., 2014. Tumor-infiltrating lymphocytes and their significance in melanoma prognosis. Methods in Molecular Biology, 1102: 287-324.

Scherer, D., Kumar, R., 2010. Genetics of pigmentation in skin cancer - a Review. Mutation Research, 705 (2): 141-153.

Schmid, A., Meili, D., Salathe, M., 2014. Soluble adenylyl cyclase in health and disease. Biochimica et Biophysica Acta, 1842 (12 Pt B): 2584-2592.

Scientific Committee on Emerging and Newly Identified Health Risks (SCENIHR), 2010. Opinion on the scientific basis for the definition of the term "nanomaterial". Scientific Committee on Emerging and newly Identified Health Risks (SCENIHR). European Commission Brussels, Belgium.

Seifert, R., Lushington, G.H., Mou, T.C., Gille, A., Sprang, R.S., 2012. Inhibitors of membranous adenylyl cylases. Trends in Pharmacological Sciences, 33(2): 64-78.

Shepard, J.R., Koestler, T.P., Corwin, S.P., Buscario, C., Doll, J., Lester, B., Greig, R.G., Poste, G., 1984. Experimental metastasis correlates with cyclic AMP accumulation in B16 melanoma clones. Nature, 308: 544-547.

Siegel, B.W., Wiech, N.L., 1976. RMI 12 330A: An inhibitor of cholera toxin induced intestinal hypersecretion which also inhibits adenylate cyclase activity. Gastroenterology: 70-937.

Slominski, A., Tobin, D.J., Shibahara, S., Wortsman, J., 2004. Melanin Pigmentation in Mammalian skin and Its Hormonal Regulation. Physiological Reviews, 84 (4): 1155-1228.
Song, H.K., Hwang, D.Y., 2017. Use of C57BL76N mice on the variety of immunological researches. Laboratory Animal Research, 33 (2): 119-123.

Song, Z., Wei, B. Lu, C., Li, P., Chen, L., 2017. Glutaminase sustains cell survival via the regulation of glycolysis and glutaminolysis in colorectal cancer. Oncology Letters, 14 (3): 3117-3123.

Stadler, S., Weina, K., Gebhardt, C., Utikal, J., 2015. New therapeutic options for advances non-resectable malignant melanoma. Advances in Medical Sciences, 60 (1): 83-88.

Surdo, N.C., Berrera, M., Koschinski, A., Brescia, M., Machado, M.R., Carr, C., Wright, P., Gorelik, J., Morotti, S., Grandi, E., Bers, D.M., Pantano, S., Zaccolo, M., 2017. FRET biosensor unscovers cAMP domains at ß-adrenergic targets that dictate precise tuning of cardiac contractility. Nature Communications, 8: 15031.

Sznol, M., Kluger, H.M., Callahan, M.K., Postow, M.A., Gordon, R.A., Segal, N.H., Rizvi, N.A., Lesokhin, A.M., Atkins, M. B., Kirkwood, J.M., Burke, M.M., Ralabate, A.L., Rivera, A.L., Kronenberg, D.A., Agunwamba, B., Feely, W., Hong, Q., Krishnan, S., Gupra, A. K., Wolchok, J.D., 2014. Survival, response duration, and activity by BRAF mutation (MT) status of nivolumab (NIVO, anti-PD-1, BMS-936558, ONO-4538) and ipilimumab (IPI) concurrent therapy in advanced melanoma (MEL). Journal of Clinical Oncology, 368: 1365-1366.

Tang, J.Q., Hou, X.Y., Yang, C.S., Li, Y.X., Xin, Y., Guo, W.W., Wie, Z.P., Liu, Y.Q., Jiang, G., 2017. Recent developments in nanomedicine for melanoma treatment. International Journal of Cancer, 141(4), 646-653.

Tanigushi, N., 1974. On the basic concept of "nano-technology". Proceedings of the International Conference on Production Engineering, part II, Tokyo 1974. Japan Society of Precision Engineering, Tokyo.

United States Food and Drug Administration (US-FDA), 2014. Considering Whether an FDA-Regulated Product Involves the Application of Nanotechnology – Guidance for Industry. Available from: https://www.fda.gov/downloads/RegulatoryInformation/Guidances/UCM401695.pdf. (Last Accessed: April 2018).

Urteaga, O., Pack, G.T., 1966. On the antiquity of melanoma. Cancer, 19 (4): 607-610.

Valet, G., Endl, E., Müller, S., 2011. 20 Years of the German Society for Cytometry: Past and Future Concepts. Cytometry A., 79A (11): 891-893.

Van Dilla, M.A., Mullaney, P.F., Coulter, J.R., 1968. The fluorescent cell spectrometer: A new method for the rapid detection of biological cells stained with fluorescentdyes. Biological and Medical Research Group (H-4) of the Health Division - Annual Report, July1966 through June 1967, Los Alamos Scientific Laboratory Report LA-3848-MS, page 100-105.

Van Rossum, D.B., Petterson, R.L., Ma, H.T., Gill, D.L., 2000. Ca2+ entry mediated by store depletion, S-nitrosylation, and TRP3 channels. Comparison of coupling and function. Journal of Biological Chemistry, 275 (37): 28562-28568.

Villares, G.J., Dobroff, A.S., Wang, H., Zigler, M., Melnikova, V.O., Huang, L. Bar-Eli, M., 2009. Overexpression of protease-activated receptor -1 contributes to melanoma metastasis via regulation of connexin 43. Cancer Research, 69 (16): 6730-6737.

Wang, A.X., Qi, X.Y., 2013. Targeting RAS/RAF/MEK/ERK Signaling in Metastatic Melanoma. IUBMB Life, 65 (9): 748-758.

Wang, J., Siffert, M., Spiliotis, M., Gottstein, B., 2016. Repeated Long-term DT Application in the DEREG Mouse Induces a Neutralizing Anti-DT Antibody Response. Journal of I Immunology Research, 1450398.

Wang, X., Ishida, T., Kiwada, H., 2007. Anti-PEG IgM elicited by injection of liposomes is involved in the enhanced blood clearance of a subsequent dose of PEGylated liposomes. Journal of Controlled Release, 119 (2): 236-244.

Webster R., Elliott V., Park B.K., Walker D., Hankin M., Taupin P., 2009. PEG and PEG conjugates toxicity: towards an understanding of the toxicity of PEG and its relevance to PEGylated biologicals. In: Veronese F.M. (eds) PEGylated Protein Drugs: Basic Science and Clinical Applications. Milestones in Drug Therapy. Birkhäuser Basel.

Wellbrock, C., Arozarena, I., 2015. Microphtalmia-associated transcription factor in melanoma development and MAP-kinase pathway targeted therapy. Pigment Cell & Melanoma Research, 28 (4): 390-406.

Weston, S.A., Parish, C.R., 1990. New fluorescent dyes for lymphocyte migration studies. Analysis by flow cytometry and fluorescent microscopy. Journal of Immunological Methods, 133 (1): 87-97.

Wherry, E.J., Blattman, J.N., Murali-Krishna, K., Van Der Most, R., Ahmed, R., 2003. Viral persistence alters CD8 T-cell immunodominance and tissue distribution and results in distinct stages of functional impairment. Journal of Virology, 77 (8): 4911-4927.

Wherry, E.J., Kurachi, M., 2016. Molecular and cellular insights into T cell exhaustion. Nature Reviews Immunology, 15 (8): 486-499.

Whiteside, T.L., Jackson, E.K., 2013. Adensosine and prostaglandin E_2 production by human inducible regulatory t cells in health and disease. Frontiers in Immunology, 4: 212-219.

Wolchok, J.D., Kluger, H., Callahan, M.K., Postow, M.A., Rizvi, N. A., Lesokhin, A.M., Segal, N.H., Aryan, C.E., Gordon, R.A., Reed, K., Burke, M.A., Caldwell, A., Kronenberg, S.A., Agunwamba, B.U., Zhang, X, Lowry, I., Inzunza, H.D., Feely, W., Horak, C.E., Hong, Q., Korman, A.J., Wigginton, J.M., Gupta, A., Sznol, M., 2013. Nivolumab plus Ipilimumab in Advanced Melanoma. New England Journal of Medicine, 369: 122-133.

World Medical Association (WMA), 2016. WMA Statement on Animal Use in Biomedical Research. Adopted by the 41st World Medical Assembly, Hong Kong, September 1989 revised by the 57th WMA General Assembly, Pilanesberg, South Africa, October 2006 and reaffirmed by the 203rd WMA Council Session, Buenos Aires, Argentina, April 2016. Available from: ttps://www.wma.net/policies-post/wma-statement-on-animal-use-in-biomedical-research/ (Last Accessed: April 2018).

Young, M.A., Malavalli, A., Winslow, N., Vandegriff, K.D., Winslow, R.M.., 2007. Toxicity and hemodynamic effects after single dose administration of MalPEG-hemoglobin (MP4) in rhesus monkeys. Translational Research - The Journal of Laboratory and Clinical Medicine,149 (6): 333-342.

Zarour, H.M., 2016. Reversing T-cell Dysfunction and Exhaustion in Cancer. Clinical Cancer Research, 22 (8): 1856-1864.

Zhang, J., Yao, Y.-H., Li, B.G., Yang, Q, Zhang, P.Y., Wang, H.T., 2015. Prognostic value of pretreatment serum lactate dehydrogenase level in patients with solid tumors: a systematic review and meta-analysis. Scientific Reports, 5: 9800.

Zhao, L., Seth, A., Wibowo, N., Zhao, C.X., Mitter, N., Yu, C., Middelberg, A.P.J., 2014. Nanoparticle vaccines. Vaccine, 32 (3): 327-337.

Zhu, M., Wang, R., Nie, G., 2014. Applications of nanomaterials as vaccine adjuvants. Human Vaccines & Immunotherapeutics, 10 (9), 2761-2774.

Zippin, J.H., Farrell, J., Huron, D., Kamenetsky, M., Hess, K.C., Fischmann, D.A., Levin, L.R., Buck, J., 2004. Bicarbonate-responsive „soluble" adenylyl cyclase defines a nuclear cAMP microdomain. The Journal of Cell Biology, 164 (4): 527-534.

Zippin, J.H., Chadwick, P., Levin, L.R., Buck, J., Magro, C., 2010. Soluble adenylyl cyclase defines a nuclear cAMP microdomain in keratinocyte hyperproliferative skin diseases. Journal of Investigative Dermatology, 130 (5): 1279-1287.

8. Appendix

8.1 List of Abbreviations

5´AMP	5´adenosine monophosphate-activated protein kinase
°C	degree Celcius
%	percent
#	polymer brushes
α-MSH	alpha-Melanocype-stimulating hormone
α/β TCR	alpha/beta T cell receptor
μCi	micro Curie, unit of radioactivity
μg	microgram
μg/ml	microgram per milliliter
μl	mirocliter
μM	micromolar
τ/ms	measurement of time in Fluorescent Correlation Spectroscopy (FCS)
$A_{2a}R$	adenosine A_{2a} receptor
$A_{2b}R$	adenosine A_{2b} receptor
ABC transporter	ATP-binding cassette transporter
AC	adenylyl cyclases
ACK Lysis	Ammonium-Chloride-Potassium Lysis
ACTH	adrenocorticotropic hormone
AF647	Alexa Fluor 647
AFM	Atomic Force Microscope
AG	Aktiengesellschaft
AJCC	American Joint Commission on Cancer
AMG	American Microscopy Groupe
ANOVA	analysis of variance
APC	Allophycocyanin
APC	antigen presenting cell
APN	aminopeptidase N
ATCC	American Type Culture Collection
ATP	adenosine triphosphate
Aqua dest.	aqua destillata, distilled water
B16F10-OVA	murine melanoma cell line expressing OVA
BAC	bacterial artificial chromosome
BATF	basic leucine zipper transcription factor, ATF-like
BC	before Christ
Blimp-1	PR domain zinc finger protein 1
BTAL	B and T lymphocyte attenuator
BRAF	serine/threonine-protein kinase B-Raf, proto-oncogene, also referred to as B-Raf or v-Raf murine sarcoma viral oncogene homolog B
BRAF V600E	serine/threonine-protein kinase B-Raf with a mutation at the location V600E, substitution of valine (V) for glutamate E (E) at codon 600, which hints towards a sensitivity towards proteasome inhibitors
BRAF V600K	serine/threonine-protein kinase B-Raf with a mutation at

	the location V600K, substitution of valine (V) for lysine (K) at codon 600, it occurs within the activation segment of the kinase domain
C	concentration
$C_{10}H_{14}N_2O_8Na_2 \cdot 2H_2O$	ethylenediaminetetraacetic acid disodium salt dihydrate
CA	California
Ca^{2+}	calcium ions
cAMP	cyclic adenosine monophosphate
CBP	CREB-binding protein, protein activating transcription
CCR	chemokine receptor
CD	cluster of differentiation
CFSE	carboxyfluorescin succinimidyl ester
cGMP	cyclic guanosine monophosphate
CKIT, c-KIT	mast/stem cell growth factor receptor (SCFR), also known as proto-oncogene c-Kit or tyrosine-protein kinase Kit or CD117, is a receptor tyrosine kinase protein that in humans is encoded by the KIT gene
cm^2	square centimeter
CNG	cyclic nucleotide-gated ion channel
Co.	company
CO_2	carbon dioxide
CPD	Cell Proliferation Dye
CpG	cytosine-phosphate-guanine
CRAF	RAF proto-oncogene serine/threonine-protein kinase, an enzyme also known as proto-oncogene c-RAF, c-Raf or Raf-1
CRE	cyclic adenosine monophosphate response element
CREB	cyclic adenosine monophosphate response element binding unit
CRIS	cyclic nucleotide receptor involved in sperm function
CSC	cancer stem cell
CTL	cytotoxic T lymphocyte
CTLA-4	cytotoxic lymphocyte associated antigen 4
Ctrl.	control
CTV	Cell Trace Violet
Cy	cyanine
d	day, days
DBCO	dibenzocyclooctyne
DC	dendritic cell
dd H_2O	double distilled water
DEC205	lymphocyte antigen 75 (LY 75), also known as CD205, an endocytic receptor highly expressed by cortical thymic epithelial cells and dendritic cells
DEREG	depletion of regulatory T cells
DF	dilution factor
dLN	draining lymph node
DMEM	Dulbecco's Modified Eagle Medium
DMH	dimethylhydrazine
DMSO	dimethyl sulfoxide
DNA	deoxyribonucleic acid
DNase	deoxyribonuclease

DOPAquinone	L-Dopaquinone
DT	diphtheria toxin
DTR	diphtheria toxin receptor
eGFP	enhanced green fluorescent protein
eGFP-hCre	enhanced green fluorescent protein /codon-optemized "humanized" Cre recombinase fusion protein
EDTR	ethylenediaminetetraacetic acid
ELISA	Enzyme-linked Immunosorbant Assay
Eomes	Eomesodormin
EPAC	exchange protein directly activated by cyclic adenosine monophosphate
EPR	E prostaglandin receptor
EPR effect	enhanced permeation and retention effect
ERK	extracellular signal-regulated kinases or classical mitogen activated protein (MAP) kinases, a widely expressed protein kinase intracellular signaling molecule
eYFP	enhanced yellow fluorescent protein
FC receptor	Fragment, crystallizable receptor
FCS	fetal calf serum
FCS	Fluorescent Correlation Spectroscopy
FDA	Food and Drug Administration
FITC	Fluorescein Isothiocyanate
FoxP3	transcription factor forkhead box P3
FSC-A	Forward Scatter Area
FSC-H	Forwards Scatter Hight
$G_1(t)$	autocorrelation function
g	gravitational constant
G	Birmingham Gauge, system to specify thickness or diameter of hypodermic needles and tube products
GB	Great Britain
GDP	guanosine diphosphate
GFP	green fluorescent protein
GITR	glucocorticoid-induced TNFR-related protein, also known as tumor necrosis factor receptor superfamily member 18 (TNFRSF18 or) activation-inducible TNFR family receptor (AITR)
GmbH	Gesellschaft mit beschränkter Haftung
GmbH & Co. KG	Gesellschaft mit beschränkter Haftung & Compagnie Kommanditgesellschaft
GM-CSF	granulocyte-macrophage colony stimulating factor
GPC	Gel Permeation Chromatography
GREAT	interferon-gamma reporter with endogenous polyA transcript
G_sPCR	G_s protein coupled receptor
GTP	Guanosine-5´-triphosphate
HBSS	Hank`s Balanced Salt Solution
HCL	hydrochloric acid
HEDGEHOG pathway	signaling pathway that transmits information to embryonic cells required for proper cell differentiation
HEPES	4-(2-hydroxyethyl)-1-piperazineethanesulfonic acid
HIV	human immunodeficiency virus

HMB45	Human Melanoma Black 45, monoclonal antibody that reacts against Pmel17, an antigen present in melanocytic melanomas
HPLC	High-performance liquid chromatography
HPV	human papillomavirus
HSA	human serum albumin, Human Albumin 20%, salzarm
hUBC9	ubiquitin-conjugated enzyme UBC9
i.p.	intraperitoneal
IDO1	Indoleamine 2,3-dioxygenase-1
ICOS	inducible T cell costimulator, also known as CD278
IFN-α	Interferon-alpha
IFN-γ	Interferon-gamma
Ig	Immunoglobulin
Il-10	Interleukin 10
IMDM	Iscove's Modified Dulbecco`s Medium
Inc.	Incorporation
IRES	internal ribosome entry site
ISO	International Organization for Standardization
JAX	The Jackson Laboratory
K^+-ATPase	potassium-ATPase, ATP driven proton pump
KGaA	Kommanditgesellschaft auf Aktien
$KHCO_3$	potassium hydrogen carbonate
KLRG-1	Killer cell lectin-like receptor subfamily G member 1
L-DOPA	levodopa
LAG-3	Lymphocyte-activation gene-3
LDH	lactate dehydrogenase
Lin	lineage
LLC	Limited Liability Company
LN	lymph node
Ltd.	Limited
MA	Massachusetts
MAPK pathway	mitogen-activated protein kinase, a type of protein kinase which is phosphorylated by mitogen-activated protein kinase kinase enzymes MEK1 and/or MEK2
MAMel91	human melanoma cell line
MC-38	murine colon adenocarcinoma cell line
MCR1	melanocortin-1 receptor
MDL	MDL-12, 330A hydrochloride, adenylyl cyclase inhibitor
MDL-12,330 A hydrochloride	adenylyl cyclase inhibitor
MDR	multidrug resistance
MDSC	myeloid-derived suppressor cells
ME	Maine
MEK1/2	mitogen-activated protein kinase kinase enzyme MEK1 and/or MEK2, a kinase enzyme which phosphorylates mitogen-activated protein kinase (MAPK)
Melan-A	protein melan-A or melanoma antigen recognized by T cells 1 (MART-1), a protein antigen found on the surface of melanocytes
mg	milligram
Mg^{2+}-ATPase	magnesium ATPase, ATP driven proton pump

MHC	major histocompatibility complex
MIA	Melanoma Institute of Australia
miRNA	micro ribonucleic acid
MITF	microphthalamia-associated transcription factor
ml	milliliter
mm	millimeter
mM	millimolar
mm^3	cubic millimeter
MMRRC	Mutant Mouse Resource & Research Centers
MO	Missouri
mRNA	messenger ribonucleic acid
Na^+-ATPase	sodium-ATPase, ATP driven proton pump
NaCl	sodium chloride
NAD^+	nicotinamide adenine dinucleotide, oxidized form
NADH	nicotinamide adenine dinucleotide, reduced form
NADPH	reduced form of nicotinamide adenine dinucleotide phosphate
$NaH_2PO_4 \cdot 2H_2O$	sodium phosphate monobasic dihydrate
NANOG	transcription factor critically involved with self-renewal of undifferentiated embryonic stem cells
NaOH	sodium hydroxide
ndLN	non-draining lymph node
neg	negative
NFAT	nuclear factor of activated T cells
NFATc1	nuclear factor of activated T cells, cytoplasmic 1
NFATc1/αA	isoform of nuclear factor of activated T cells, cytoplasmic 1
NH_4Cl	ammonium chloride
NICAS	Australian National Industrial Chemical Notification and Assessment Scheme
NJ	New Jersey
NK	Natural Killer Cells
NKT	Natural Killer T Cells
nm	nanometer
NOTCH pathway	highly conserved cell signaling pathway that occurs in most multicellular organisms
NP	nanoparticle
NP-MDL	nanoparticle loaded with MDL-12, 330A hydrochloride
NR	no remission
NRAS	neuroblastoma RAS viral oncogene homolog, one of three members of the Ras gene family
ns	not significant
Nur77	orphan nuclear receptor Nr4a1
NY	New York
OR	Oregon
OVA	ovalbumin
PA	Pennsylvania
PAGE	Polyacrylamide Gel Electrophoresis
PAP	prostate-specific phosphatase
PB	Pacific Blue
PE	Phycoerythrin

PEC	peritoneal exudate cell
PEG	poly(ethylene glycol)
PerCP	Peridinin-Chlorophyll-protein
PBS	phosphate buffered saline
PD	progressive disease
PD-1	Programmed Death Receptor-1
PD-1L	Programmed Death Receptor-1 Ligand
PDE	phosphodiesterase
PEP	phosphoenolpyruvate
PGE2	prostaglandin E2
PGlu(OBn)	polyglutamatic acid benzylester
PKA	protein kinase A
pmol	picomole
PMT	photomultiplier tube
POPDC	Popey domain-containing proteins
Pos	positive
PPi	proton-pump inhibitors
PSar	polysarcosine
PSar- b-PGlu(OBn)	polysacrosine-*block*-polyglutamatic acid benzylester
PTX	paclitaxel
RAS	family of related proteins which belong to a class of proteins referred to as small GTPases
Ras-Raf-MEK-ERK pathway	also referred to as the MAPK/ERK pathway, is a chain of proteins in the cell that communicates a receptor on the surface of the cell to the DNA in the nucleus
RES	reticuloendothelial system
RI	Rhode Island
RNA	ribonucleic acid
ROS	reactive oxygen species
rpm	rotations per minute
RPMI	Roswell Park Memorial Institute medium
RP-HPLC	Reverse Phase-High-Performance Liquid Chromatography
S-100 protein	family of at least 21 low-molecular-weight proteins characterized by two calcium-binding sites that have helix-loop-helix conformation which are also considered as damage-associated molecular pattern molecules (DAMPs)
s.c.	subcutaneous
sAC	soluble adenylyl cylases
SCENIHR	Scientific Committee on Emerging and Newly Identified Health Risks
SCF	stem cell factor, also referred to as KITligand, KL or steel factor, a cytokine which binds to CD117, the c-KIT receptor
SEM	standard error of the mean
SERCA	sacro/endoplasmic reticulum (ER) Ca^{2+}-nuclear factor of activated T cells (NFAT) signalling
SINFEKEL	H2K^b/chicken ovalbumin peptide 257-264
SPARC	secreted protein acidic and rich in cysteine also referred to as osteonectin or basement-membrane-protein 40

SSC-A	Side Scatter Are
SSC-H	Side Scatter Hight
STM	Scanning Tunnelling Microscope
SQ22, 536	adenylyl cyclase inhibitor
T-bet	T-box transcription factor TBX21
tAC	transmembrane adenylyl cylases
TARC	Translational Animal Research Center
TCA cycle	tricarboxylic acid cycle, also known as citric acid or Krebs cycle
TCR β	the beta chain of the alpha/beta T cell receptor
TEM	Transmission Electron Microscope
Treg	regulatory T cell
TGF-β	transforming growth factor beta
TIL	tumour infiltrating lymphocytes
TIM-3	T cell immunoglobulin and mucin-domain containing-3, also known as Hepatitis A virus cellular receptor 2 (HAVCR2)
TNF-α	tumour necrosis factor alpha
Trypsin-EDTA	trypsin-ethylenediaminetetraacetic acid
TUBB3	anti-apoptotic class III β-tubulin
TYRP1	tyrosine-related-protein-1
TYRP2	tyrosine-related-protein-2
U-U-MITF	ubiquinated microphtalamina-associated transcription factor (MITF)
UK	United Kingdom
USA	United States of America
US-FDA	United States Food and Drug Administration
UTR	untranslated region
UV	ultraviolet
UV-Vis	Ultraviolet-Visible Spectroscopy
V/V	volume percent
VT	Vermont
WI	Wisconsin
WMA	World Medical Association
WNT pathway	a group of three signal transduction pathways which pass signals into a cell through cell surface receptors
WT	C57BL/6J also referred to as wild type

8.2 List of Figures and Tables

8.2.1 List of Figures

8.2.2   List of Tables

8.3 Publications and Poster Presentations

8.3.1 Publications

8.3.1.1 Original Publications

1.) Prochaska, J.H., *Luther, N.*, Brähler, M., Schulz, A., Hermanns, I., Lackner, K.J., Espinola-Klein, C., Munzel, T., Wild, P.S., Becker, C., 2018. Acute deep vein thrombosis Suppresses peripheral T cell effector function. British Journal of Haematology, 2018 Mar 25. doi: 10.1111/bjh.15192. [Epub ahead of print].

2.) *Luther, N.*, Shahneh, F., Brähler, M., Krebs, F., Jäckel, S., Subramaniam S., Stanger, C., Schönfelder, T., Kleis-Fischer, B., Reinhardt, C., Probst, H.C., Wenzel, P., Schäfer, K., Becker, C., 2016. Innate Effector-Memory T-Cell Activation Regulates Post-Thrombotic Vein Wall Inflammation and Thrombus Resolution. Circulation research, 119 (12), 1286-1295.

8.3.1.2 Reviews

1.) Assil, S., Bolz, P.A., Boukhali, M., Cariou, C., Chauveau, L., Chuvi, N., Dhondt, K., Ducuing, A., Dupont, J.-B., Grandin, C., Jarre, G., Le Douce, J., Lebrun, D., Lechenet, F.-X., *Luther, N.*, Milivojevic, M., Peres, E., Plantamura, E., Sanlaville, A., Schwob, A., Seggio, M., Serre, J.-E., Thiebaut, P.A., Tirmarche, S., Tshileng, K.-T., Vandamme, C., Verlhac, P., Vinera, J., Mathieux, R., Journo, C., 2011. XMRV human retrovirus: the end of an appealing story? Virologie, 15 (4), 222-234.

8.3.2 Poster Presentations

1.) Grikscheit, K., *Luther, N.*, Wang, Y., Grosse, R., 2013. The formin FMNL2 regulates actin dynamics at cell-cell contact sites during spheroid development. Joint International Meeting of the German Society for Cell Biology (DGZ) and the German Society for Developmental Biology (GfE), March 20th - 23rd, 2013, Heidelberg.

8.4   Curriculum Vitae